©2009

Natasa Skific

CHANGES IN ARCTIC MOIST STATIC ENERGY TRANSPORT AND

MOISTURE CONVERGENCE IN THE 21ST CENTURY

by

NATASA SKIFIC

A dissertation submitted to the

Graduate School-New Brunswick

Rutgers, The State University of New Jersey

In partial fulfillment of the requirements

For the degree of

Doctor of Philosophy

Graduate Program in Atmospheric Sciences

Written under the direction of

Jennifer A. Francis

And approved by

_____ _____

_____ _____

_____ _____

_____ _____

New Brunswick, New Jersey

May, 2009

ABSTRACT OF THE DISSERTATION

CHANGES IN ARCTIC MOIST STATIC ENERGY TRANSPORT AND

MOISTURE CONVERGENCE IN THE 21ST CENTURY

By NATASA SKIFIC

Dissertation Director:
Jennifer A. Francis

This study explores processes that greatly affect the energy balance of the Arctic system: moisture convergence (net precipitation) and the poleward transport of moist static energy (MSE). Because Arctic temperature response to climate perturbations, particularly in the context of global climate change, is amplified compared to that of middle and lower latitudes, this work attempts to identify mechanisms that contribute to Arctic amplification, as well as the physical processes that govern them. The MSE is derived as a sum of latent heat flux (LH) and dry static energy flux (DSE) across an imaginary wall at 70°N latitude. I analyze changes in these variables over the next century by using output from a global climate-system model simulation by the Community Climate System Model, version 3 (CCSM3) that assumes greenhouse emissions will follow the trajectory of recent years. Although tropospheric DSE is

predicted to decrease by about 3.5% by the end of 21st century, it is offset by an increase in LH of about 20% from its 20th century average. These changes combine to result in a total increase in tropospheric MSE of about 1.6% by the late 21st century. Net precipitation in the central Arctic is projected to increase by 16% toward the end of the 21st century.

Modeled and observed sea level pressure fields are classified using a neural-network technique called self-organizing maps to create a set of characteristic circulation patterns over the region north of 60°N. By relating moisture transport and convergence to a particular circulation regime, future changes are attributed to varying atmospheric dynamics and/or thermodynamics. The model projects an increase in MSE in all seasons owing to more frequent occurrence of high-latitude cyclones, particularly in summer. The contribution from thermodynamic factors, related to an increased poleward moisture gradient and the consequent increase in LH, is offset by a decrease in the poleward temperature gradient and a decrease in DSE. An increase (decrease) in the thermodynamic effects is most pronounced in summer (winter). The projected increase in moisture convergence in mainly governed by thermodynamics, which explains over 70% of the total change in the Arctic region.

Preface

The main focus of this work is to gain understanding of mechanisms driving the observed and projected Arctic climate change. Processes with potential to strongly affect the Arctic energy balance, and consequently induce temperature perturbation are changes in moist static energy transport and moisture convergence (net precipitation). Each chapter of this dissertation consists of a manuscript prepared or submitted for publication in the Journal of Climate.

Acknowledgements

Dedication

To my parents and my sister - You have supported me in innumerable ways throughout my life and education. You have made me who I am today. Thank you for always believing in me. I owe all my accomplishments to you.

To my husband, Karl- You are a constant source of inspiration in my life. Thank you for encouraging me to and for standing by my side every step of the way. You bring out the best in me. You complete me. I love you deeply.

To my baby girl Karla- You are the light of my life, all my happiness and joy. I will cherish you and love you forever. This is for you.

To my friend Gordana- You always believed in me, supported me, and helped me to realize my potential. I am grateful for your kindness, and constant readiness to help in any way possible. I feel very lucky and also proud to have such an extraordinary person in my life.

Table of contents

List of illustrations

1. Introduction

The Arctic has captivated human imagination and motivated exploration for centuries. The land of the midnight sun -- a region of sensitive and often very complex climate interactions and feedbacks between the atmosphere, ocean, land and cryosphere -- is also very tightly coupled to the global climate system (Serreze and Barry 2005). It is therefore not surprising that the Arctic climate change has been a major focus of research in the modern era: era of supercomputers, satellites, and other technological achievements that help better understand and predict the climate. Although the fundamental physics behind general circulation models is basically sound, the question still remains of how much will the Arctic climate change, and when will these changes take place. Also, how will these changes affect the world as a whole.

1.1. How will the Arctic climate change in the future?

Instrumental records show that the Arctic has exhibited conspicuous fluctuations on interannual, decadal, and multidecadal scales. These fluctuations can be observed on **Fig. 1**, which shows the zonally-averaged time series of annual surface temperature anomalies for latitudes north of 30°N (Johanessen et al. 2004). This representation combines measurements from land stations, buoys, Russian meteorological stations on the sea-ice (1950-1991), and data from the European Centre for Medium Range Weather Forecasts reanalysis (ERA-40). The figure shows that the Arctic was cooler than average between 1890 and 1920. The warming episode between 1920 and 1940 is likely associated with changes in ocean circulation and sea-ice extent (Bengtsson et al. 2004).

However, the most recent warming signal is different in that it occurs at all latitudes, and it is stronger to the north into the Arctic Ocean. This feature is consistent with expected consequences of human-induced increased greenhouse gases, and a manifestation of global warming at high latitudes is usually referred to as the Arctic amplification (e.g., Serreze and Francis 2006).

Fig.1. Zonally-averaged time series of annual surface temperature anomalies (°C) from 1891-1999 north of 30°N (from Johanessen et al. 2004).
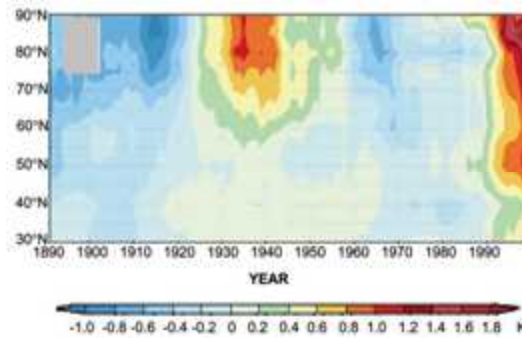
The most common explanation of Arctic amplification is that involving the ice-albedo feedback. In a climate warmed by increasing downward longwave radiation, a consequence of increased concentrations of anthropogenic greenhouse gases in the atmosphere, sea-ice and snow will melt, and that will expose dark surfaces to the solar radiation. Because darker surfaces (land and ocean) are better absorbers of solar radiation (unlike white surfaces, which reflect the incoming solar radiation), the increased absorption of solar radiation will lead to more warming, which will, in return, speed up the melting of snow and ice, thus amplifying the initial perturbation in temperature (positive feedback). Curry et al. (1995) and Grenfell and Perovich (2004) discuss

seasonal and spatial evolution of albedo in snow-ice-land-ocean environment. They point to the increase in snow grain size as the snow melts, or puddles of water forming on melting sea-ice, all of which decrease surface albedo and increase absorption of solar radiation. Serreze and Francis (2006) explain that if more ice is lost in summer, the ocean will absorb more heat. This will delay sea-ice growth in autumn and winter, and/or produce thinner ice. Some of the heat will escape through leads and polynyas, and the retained heat combined with thinner ice will result in earlier spring melt. This will result in even more solar absorption by the ocean and the cycle will continue. Some of the general circulation models predict ice-free Arctic to appear by about 2070, with most pronounced temperature changes expected to occur in autumn and winter (Walsh et al. 2002; Serreze and Barry 2005). The Arctic Climate Impact Assessment (ACIA 2005) reports that average annual temperatures in polar regions are projected to rise by 3 to 7°C by the end of the 21st century. However, more recent observations by Pielke et al. (2008) and Rahmstorf et al. (2007) underscore the concerns about the global climate change, revealing that previous projections, as summarized by the Intergovernmental Panel on Climate Change (IPCC), may have underestimated the change, in particular for sea-level. The observed rate of sea-level rise of about 3.3 mm yr^{-1} exceeds an IPCC best-estimate rise of less than 2 mm yr^{-1} (IPCC does not include contributions from ice-sheet melting in Greenland and Antarctica because they are too uncertain). The rate of rise during the past 20 years was 25% faster than the rate in any 20-year period in the preceding 115 years. The ACIA report also projects an increase in high latitude precipitation of between 10 and 20 % by the end of the 21st century. The general increase in high-latitude precipitation will occur in a warmer climate, as the atmosphere will support a higher

water vapor content. Although changes in evaporation are not as coherent, recent studies (e.g., Cassano et al. 2007; Skific et al. 2009) indicate that net precipitation, and presumably runoff to the Arctic Ocean, would also increase.

In recent years, studies of the Arctic amplification and its causes have revealed that ice albedo feedback may, in fact, not play a crucial role after all. Analyses by Graverssen and Wang (2009), and earlier work by Alexeev et al. (2005) showed that Arctic amplification existed in experiments with fixed ice albedo. It is found that an increase of water vapor and total cloud cover lead to a greenhouse effect, which is larger in the Arctic than at lower latitudes, and could explain a part of the Arctic surface-air temperature amplification.

1.2. What are the global implications of regional Arctic climate change?

Climate models, as well as paleoclimate records, reveal that there are many mechanisms linking the Arctic climate system with the rest of the globe.

One such mechanism, unveiled through experimenting with general circulation models (Manabe et al. 1991; Stouffer and Manabe 2003; Min et al. 2008), is the slowing of the oceanic thermohaline circulation in response to decreased high-latitude oceanic salinity, owing to increased runoff, ice melt, and enhanced high-latitude precipitation. Clark et al. (2001, 2002) propose that this mechanism could explain the Younger Dryas cold event that occurred from about 13 to 11.7 ka.

Lawrence and Slater (2005) demonstrate links between changes in Arctic hydrology and changes in vegetation distribution. In their modeling experiment, warmer and wetter Arctic soil results in northward expansion of shrubs and boreal forests, which

replace tundra and further lower the surface albedo, thus accelerating snow and ice melt. Sturm et al. (2001) and Chapin et al. (2005) establish connections between shrub abundance and trapping of drifting snow. The snow in shrub patches is thicker, thus better thermal insulator. As a consequence, winter soil surface temperatures are higher, which promotes decomposition and nutrient release the following summer, which in return promotes shrub growth. The snow-shrub interactions could lead to a widespread increase in the winter snow depth, which may increase spring runoff, as well as CO_2 emissions from the Arctic soil, thus contributing to the global increase in greenhouse gases.

Troubling projections are those of the future sea-level rise, owing to melting of the Greenland ice cap (Church and White 2006; Rahmstorf et al. 2007). The ACIA (2005) report reveals that of area of Greenland's surface that melts in summer has increased by about 16% between 1979 and 2002, an area roughly the size of Sweden. Climate models project that future temperature increases could eventually lead to a complete melting of Greenland Ice Sheet, with a resulting sea-level rise of about seven meters. While this is an extreme eventuality, even a fraction of this melting would have profound consequences for coastal communities worldwide. Based on the IPCC scenarios, sea level is projected to rise 10 to 90 cm by the end of the 21st century, accelerating through the time period (Meehl et al. 2007; Randall et al. 2007). Rahmstorf et al. (2007) argue that the sea-level rise may even be larger than that predicted by the IPCC, between 0.5 and 1.4 m by the end of the 21st century. The Arctic Ocean could experience the largest increases owing to an expected increase in freshwater input and the resulting decrease in salinity and density.

1.3. Are there feedbacks within the climate system that could slow the pace of Arctic warming?

As indicated in previous sections, many of the feedbacks within the Arctic emerging are positive, that is, they will amplify the initial Arctic temperature perturbation. Slowing of the thermohaline circulation in a response to freshwater input may have a dampening effect, but the time scales are too slow to have a substantial influence in the near-term climate (Manabe and Stouffer 1994). A great deal of uncertainty surrounds changes in high-latitude cloud properties such as cloud height, optical depth, cloud microphysical properties, and cloud fraction (Schweiger 2004; Garrett and Zhao 2006). Can negative feedback mechanisms involving lower latitudes offset widespread reductions in permanent ice and changes in physical and biological components? One of the more promising candidates is the transport of moist static energy (sensible heat, latent heat and geopotential energy) by the atmosphere, which in present climate conditions supplies approximately 98% of the energy annually lost to space in the high latitudes north of 70°N (Nakamura and Oort 1988). The intuitive argument is that if Arctic warming is enhanced in response to increasing greenhouse gas concentrations the lower-tropospheric poleward temperature gradient should relax, poleward advection of sensible heat should decrease, and Arctic warming should weaken. On the other hand, climate modeling experiments suggest that increases in advected latent heat will more than compensate for the reduction in sensible heat transport [S. Vavrus, pers. comm.]. Recent analyses by Graverssen et al. (2008) and earlier work by Alexeev et al. (2005) demonstrate that meridional energy transport, mainly in the form of latent heat, may enhance Arctic warming.

Some earlier studies by Hoerling et al. (2004) and Hurrell et al. (2004) discuss possible connections between high-latitude atmospheric circulation and tropical surface temperatures, although the mechanism itself remains unclear.

Understanding the behavior of advected moist static energy in the greenhouse-gas-forced world may shed light on the potential for this cog in the climate system to slow the pace of the shifting Arctic. Therefore, a large body of work presented here investigates this feedback mechanism, identified as a possible brake on the Arctic's rapid march toward an ice-free state. The results contributes to a system understanding by focusing on the primary energy source for the Arctic climate system, i.e., horizontal energy and moisture transport, diagnosing its behavior during recent decades, projecting its future trends, and understanding the atmospheric processes that govern future changes. In addition, the work also investigates recent and future behavior of net precipitation, a variable closely related to horizontal moisture transport and that is crucial to determining the nature of future Arctic change.

2. Background

The atmosphere and ocean work to balance the differential radiative heating between the equatorial regions and the Arctic through poleward energy transports, with the atmosphere playing the primary role (Serreze and Barry 2005). **Figure 2** shows a schematic of the energy balance for the north polar cap, as presented by Nakamura and Oort (1988).

Fig.2. Schematics of the energy balance for the north polar cap (from Nakamura and Oort, 1988).

Fwall is moist static energy flux:

$$Fwall = \iint c_p[\overline{vT}]dxdp\,/\,g + \iint L[\overline{vq}]dxdp\,/\,g + \iint g[\overline{vz}]dxdp\,/\,g$$

Sensible heat flux   Latent heat flux   Potential energy flux

2
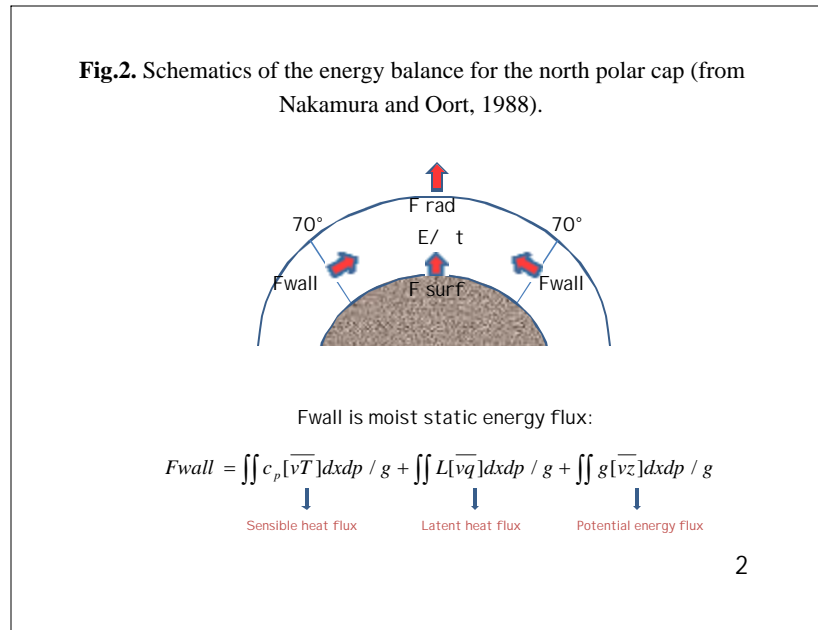
The budget of the north polar cap can be approximated as follows:

$$\partial E/\partial t = F_{rad} + F_{wall} + F_{surf}.$$

This equation shows that the change in the Arctic atmospheric storage of moist static energy ($\partial E/\partial t$) can be expressed as the sum of net radiation at the top of the atmosphere (F_{rad}), the net poleward energy flux across a hypothetical wall at 70°N extending from the surface to the top of the atmosphere (F_{wall}), and the net heat flux at the Earth's surface (F_{surf}). If the sum of all three terms is positive the system is gaining energy, and if it is negative, the system is losing energy. Although in the long-term annual mean the change in atmospheric storage is zero and the net surface flux is small, the annual cycle experiences significant variations.

Figure 3 shows the change in the atmospheric storage of moist static energy (top panel), and its components: F_{rad} (second panel), F_{wall} (third panel), and F_{surf} (bottom panel). The figure presents values from Trenberth and Caron (2001), who combine Earth Radiation Budget Experiment (ERBE) radiation data and atmospheric transports from the

National Center for Environmental Prediction/ National Center for Atmospheric Research (NCEP/NCAR) and European Centre for Medium Range Weather Forecasting (ECMWF) ERA-15 reanalyses.

The top panel shows that Arctic gains energy in spring, and loses in autumn. The annual cycle of moist static energy storage of the Arctic system is explained by Serreze and Barry (2005). In winter the incoming solar radiation is negligible, therefore there is a strong radiation deficit at the top of the atmosphere, owing to longwave cooling of the surface and the overlaying air column. The net loss is compensated for by large poleward atmospheric energy fluxes, but also by the surface fluxes, driven by the growth of sea ice, uptake of sensible heat from the ocean and snowfall.
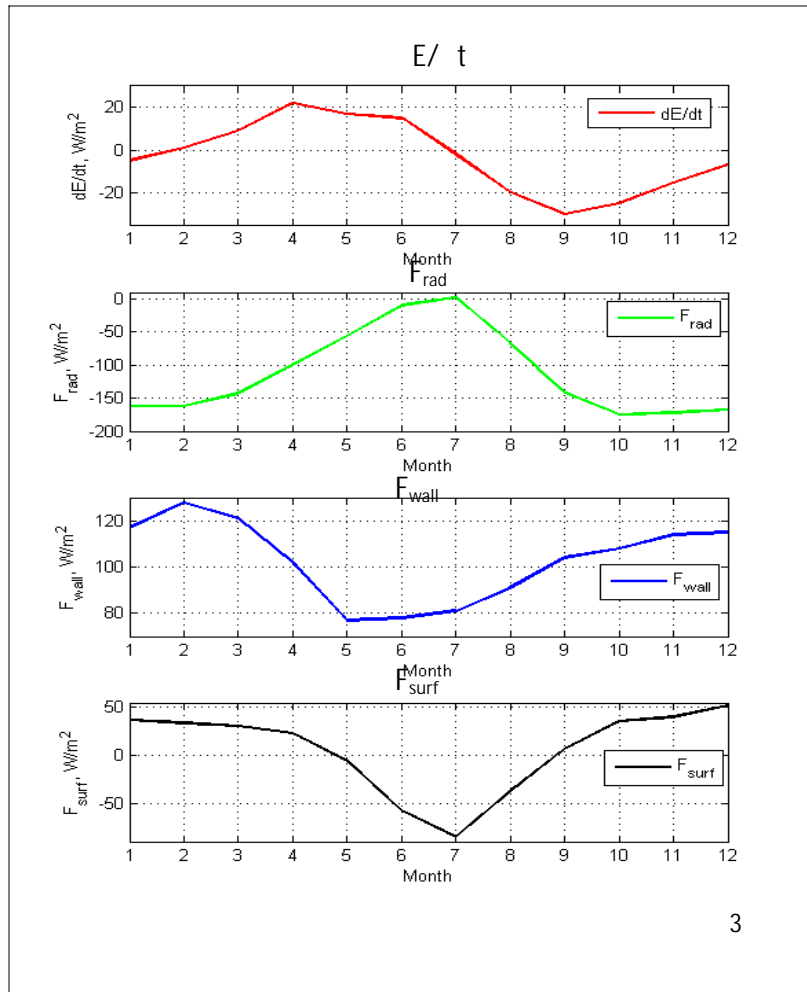
Fig. 3; Top: change in Arctic moist static energy storage; **second from top**: net radiation at top of the atmosphere; **third from top:** poleward moist static energy transport across 70°N; **bottom:** net surface flux. Units are Wm^{-2}. Based on data by Trenberth and Caron (2001).

Although the incoming solar radiation is strongest in the summer, it is offset by a seasonal maximum in longwave emission, so that net radiation at the top of the atmosphere is close to zero. Because the poleward temperature gradient relaxes in summer, the poleward energy transport is weaker in this season, and is almost equal to a negative surface flux, mostly due to the melt of sea ice and snow cover, and by a gain in sensible heat by the ocean (Serreze and Barry 2005). The third panel from the top shows the annual cycle of the poleward transport of moist static energy, which includes fluxes of sensible heat, geopotential energy and latent heat into the Arctic.

Figure 4 shows portions of the total annual moist static energy transport from each form of energy (after Overland et al. 1996). Sensible heat and geopotential energy flux together supply about 89% of the annual energy input into high latitudes, while only 11% is accounted for by the latent heat flux. Sensible heat is the energy associated with the temperature of a mass of atmosphere, and potential energy is the energy associated with the gravitational potential of air some distance above the surface (Hartmann 1994). Together they are usually referred to as a dry static energy. This energy is conserved during unsaturated vertical and horizontal motion.

Fig.4. Contribution of components of moist static energy transport to the annual mean transport across 70°N, from Overland et al. (1996).

Relative contributions of components of energy transport to total flux
across 70° N for various seasons

Winter

LH
8%

GP
36%

SH
56%

Summer

LH
20%

SH
25%

GP
55%

Fig.5. Contribution of components of moist static energy transport to the winter (left) and summer (right) mean transport across 70°N, after Overland et al. (1996).

Figure 5 represents relative contributions of the components of energy transport to the total flux across 70°N for winter and summer, based on the data provided by Overland et al. (1996). The total moist static energy transport peaks in the winter, mostly due to larger poleward temperature gradients and consequent large transport of sensible heat. In winter the moisture transport is small and only accounts for about 8% of the total transport. The situation is reversed in summer: the poleward temperature gradient relaxes, which weakens the meridional transport of sensible heat to about one third of its winter value. The latent heat flux peaks in summer, mostly due to the high water vapor content in the atmosphere.

An annual cycle of latent heat flux from the ERA-40 is shown in **Figure 6**. In summer the moisture flux is twice as large as the winter value, which reflects an exponential increase of saturation vapor pressure for a given temperature change. The latent heat flux accounts for 20% of the energy transport in summer, and is almost similar in magnitude to the sensible heat flux, which accounts for about 25% of the total summer

transport. Geopotential energy flux does not change much from the winter to the summer. However, because total energy transport decreases in the summer, the contribution of the geopotential flux to the moist static energy transport is larger than that in winter.

It is precisely this behavior of the three components of moist static energy transport in various seasons that intuitively helps anticipate their behavior in the greenhouse-gas-forced future. In other words, just as the change of season from winter to summer demonstrates an increase in the poleward latent heat flux and decrease in the sensible heat flux, the same tendency can be expected to occur in a future warmer climate. These questions remain, however: How much will each individual component change? How they will offset one another? In which season will the transports be most affected?
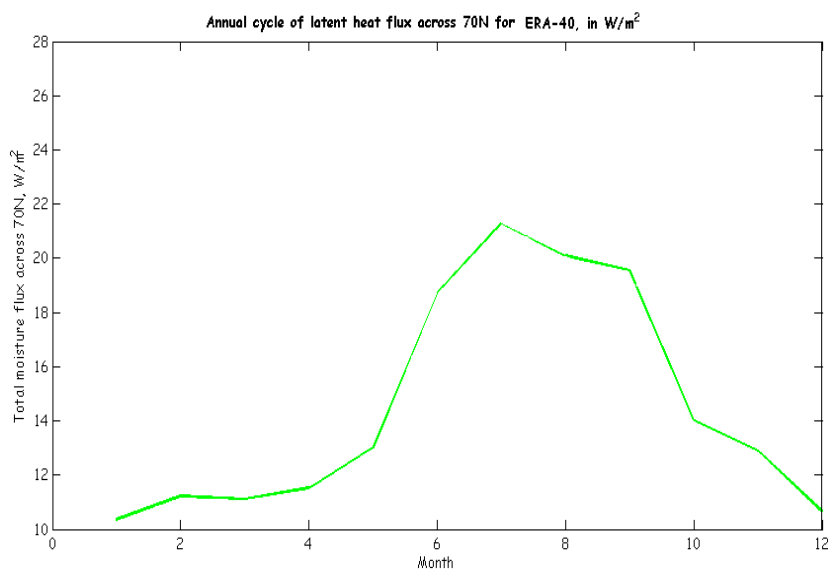
Fig.6. Annual cycle of the latent heat flux derived from European Centre for Medium Range Weather Forecasting (ECMWF) ERA-40 reanalysis, for period 1958-2001. Units are Wm^{-2}.

       The body of this dissertation consists of three separate manuscripts. Chapter 3 discusses projected changes in atmospheric moisture transport and is a paper in press in the Journal of Climate. Chapter 4 is a paper nearly ready for submission to Climate Dynamics and focuses on the changes in total poleward moist static energy transport. Chapter 5 is a paper accepted with major revision in the Journal of Climate, and explores changes of net precipitation in various regions of high latitudes.

Attribution of Projected Changes in Atmospheric Moisture Transport in the Arctic:

A Self –Organizing Map Perspective

Natasa Skific[1], Jennifer A. Francis[2], and John J. Cassano[3]

[1]Department of Atmospheric Sciences, Rutgers University

[2]Institute of Marine and Coastal Sciences, Rutgers University

[3]Department of Atmospheric and Oceanic Sciences, University of Colorado

and Cooperative Institute for Research in Environmental Sciences

Corresponding author: Jennifer A. Francis, IMCS, 71 Dudley Rd, Rutgers University, New Brunswick, 08901, e-mail: francis@imcs.rutgers.edu, tel: 732-708-1217, fax: 723-872-1586.

3. Attribution of projected changes in atmospheric moisture transport in the Arctic: A self-organizing map perspective

Abstract

We analyze meridonal moisture transport into the Arctic derived from one simulation of the National Center for Atmospheric Research Community Climate System Model (CCSM3) spanning the periods of 1960-1999, 2010-2030 and 2070-2089. The 21st century simulation incorporates the Intergovernmental Panel on Climate Change (IPCC) Special Report on Emission Scenarios (SRES) A2 scenario for CO_2 and sulfate emissions. Modeled and observed (from the European Centre for Medium-Range Weather Forecasting Reanalysis, ERA-40) sea level pressure (SLP) fields are classified using a neural-network technique called self-organizing maps to distill a set of characteristic atmospheric circulation patterns over the region north of 60°N. Model performance is validated for the 20th century by comparing the frequencies of occurrence of particular circulation regimes in the model to those from the ERA-40. The model successfully captures dominant SLP patterns, but differs from observations in the frequency with which certain patterns occur. The model's 20th century vertical mean moisture transport profile across 70ºN compares well in terms of structure but exceeds observations by about 12% overall. By relating moisture transport to a particular circulation regime, future changes in moisture transport across 70°N are assessed and attributed to changes in frequency with which the atmosphere resides in particular SLP patterns and/or to other factors, such as changes in the meridional moisture gradient. By

the late 21st century, the transport is projected to increase by about 21% in this model realization, with the largest contribution (32%) to the total change occurring in summer. Only about a quarter of the annual increase is due to changes in pattern occupancy, suggesting that majority is related to mainly thermodynamic factors. A larger poleward moisture transport likely constitutes a positive feedback on the system through related increases in latent heat release and the emission of longwave radiation to the surface.

3.1.   Introduction

The 4th Assessment Report of the Intergovernmental Panel on Climate Change (IPCC AR4, 2007) underscores previous striking and disturbing findings: The Arctic system appears to be heading toward a new state, and there are no apparent feedbacks within the Arctic that can arrest the cohesive change (Ferguson et al. 2004; Overpeck et al. 2005; Serreze and Francis 2006). Although there is a great deal of uncertainty related to feedbacks in the Arctic system, particularly involving cloud changes, it appears that the overwhelming majority of them are positive, i.e., they act to enhance changes (Serreze and Barry 2005).   The most often cited of these are the ice/snow-albedo feedback and water vapor feedback. The basic process in the former is that as high-latitude temperatures increase, additional sea ice and snow will melt, which will expose dark ocean and land surfaces that are more effective absorbers of solar radiation. This will increase the warming, leading to further melt of snow and ice, hence further warming. Because most of the Arctic surface is covered with ice and snow during spring, the effects will be most pronounced in high latitudes (Hartmann 1994). The water vapor feedback involves an increase in precipitable water in the atmosphere as warming raises

the saturation vapor pressure. Increased precipitable water enhances the emissivity of the atmosphere, which tends to increase the longwave flux to the surface, particularly in dry atmospheres like the polar regions (Soden and Held 2006). While these feedbacks seem straight-forward, the processes by which energy is sequestered in the system until the following year are not well understood. There are only a few known or suspected negative feedbacks within the Arctic system. The aerosol-dehydration feedback (Blanchet and Girard 1995) is a possibility, but it is likely too weak to have a discernible effect. Slowing of the thermohaline circulation in response to increased freshwater export to the N. Atlantic is likely to have a dampening effect, but the time scales are too slow to have substantial impact in the near-term (Fichefet et al. 2003).

In this study we investigate a potentially influential but poorly understood feedback that extends beyond the Arctic and involves the horizontal transport of moist static energy (sensible heat, latent heat, and geopotential energy) from low to high latitudes by the atmosphere. In the present climate, the moist static energy transport supplies approximately 98% of the energy annually lost to space by the Arctic north of 70ºN (Nakamura and Oort 1988). As the Arctic warms more than lower latitudes, one expects that the lower-tropospheric meridional temperature gradient should relax, poleward advection of sensible heat should decrease, and Arctic warming should weaken. Simulations with global climate models support this reasoning, but they also suggest that increases in moisture transport will more than compensate for the reduction in sensible heat transport [S. Vavrus, pers. comm.]. Recent analyses by Graverssen et al. (2008) and earlier work by Alexeev et al. (2005) and Held and Soden (2006) support the notion that meridional energy transport may enhance Arctic warming. Other studies reveal possible

linkages between high-latitude atmospheric circulation and tropical surface temperatures (e.g., Cassou and Terray 2001; Hoerling et al. 2004; Hurrell et al. 2004), but connections between tropical variations and poleward transport of moisture are unclear. It is also suggested that changing energy transport, perhaps in magnitude and/or in spatial distribution, may be partly responsible for observed reductions in Arctic sea ice extent (Rigor and Wallace 2004), increases in surface temperature (Comiso 2003), lengthening of the melt season (Belchansky et al. 2003), loss of permafrost (Osterkamp and Romanovsky 1999), and increases in river runoff (Peterson et al. 2002).

This study explores how moisture flux changes in a single run of the National Center for Atmospheric Research (NCAR) Community Climate System Model, version 3 (CCSM3) over the next 100 years forced with continually increasing anthropogenic greenhouse gases. We apply a neural network technique called self-organizing maps (SOMs) (Kohonen 2001) for this analysis because it distills voluminous fields of gridded values into representative, fundamental clusters organized in a matrix of 2D fields – geographic maps in this case -- that are expressed in a visual and intuitive rendering. The maps are situated in the matrix relative to one another according to their similarity. In this application, the fields of data are sea-level pressure (SLP) anomalies north of 60°N from both reanalyses and from the CCSM3. Each pattern in the SOM matrix is readily identifiable as having typical atmospheric features in a region, and inferences can be made about the weather generally associated with those features. The SOM can also be used to analyze other related variables, which is the approach taken in this study to assess patterns of moisture flux and moisture convergence, and ultimately to ascertain the causes of change in these variables in the future.

The data sets used and the data manipulation that precedes the actual application of the SOM algorithm are described in section 2, while section 3 provides a more in-depth description of the SOM method. Analysis of self-organizing maps of SLP and model validation using ERA-40 is summarized in Section 4. The analysis of the corresponding clusters of moisture transport across 70°N, fixed for a particular circulation regime, and its comparison to ERA-40 is given in Section 5. Future changes of moisture transport in the 21st century and derivation of contributions of dynamic, thermodynamic and combined fractions of change are provided in Section 6, followed by conclusions and future efforts in Section 7.

3.2.   Data sources and model output

Six-hourly, multi-level fields of specific humidity and meridional wind for a single run of the NCAR CCSM3 (version 3.0, T85 L26) were obtained from the Program for Climate Model Diagnostics and Intercomparison (PCMDI), at the Lawrence Livermore National Laboratory. CCSM3 simulations have been shown to reproduce the Arctic atmospheric hydrological cycle reasonably well (e.g. Holland et al. 2007; Finnis et al, 2008a,b). The atmospheric component of the model consists of 26 vertical levels, a top at 2.2 hPa, 13 layers above 200 hPa, and a horizontal resolution of about 1.4º. The atmospheric module is the CAM (Community Atmosphere Model) version 3.0 (Collins et al. 2006a). The 20th century experiment (20C3M) incorporates direct effect of sulfates (Smith et al. 2001, 2004a), with no indirect aerosol effects. The model is forced by observed concentrations of CO_2, CH_4, N_2O, CFCs, ozone (Kiehl et al. 1999), and solar fluxes (Lean et al. 2002). The effects of volcanic eruptions are parameterized (Ammann

et al. 2003). The 21st century simulation incorporates the Special Report on Emission Scenarios (SRES) A 2 scenario (Nakicemovic and Swart 2000), which assumes a continuously increasing population (15 billion by 2100), increasing greenhouse gases, and slow implementation of new technologies, appears to be most similar to the trajectory of the real world (Rahmstorf et al. 2007).

The original six-hourly PCMDI fields were interpolated from the hybrid sigma-pressure vertical coordinates to a pressure coordinate system and reduced in size by subsetting from global coverage to the region north of 60ºN, from 6-hourly time resolution to daily resolution (12 UTC only), and from 26 vertical levels to 10 levels (troposphere only). Moisture transport was calculated for five tropospheric layers (1000-850 hPa, 850-700 hPa, 700-500 hPa, 500-400 hPa, 400-300 hPa). The time slices used in this study span periods of 1960-1999 from the 20th century experiment (20C3M), as well as 2010-2030 and 2070-2089 from the SRES A2 scenario. The latter two periods were chosen to be consistent with results from the Arctic Climate Assessment Report (Huntington and Fox 2005; Serreze and Francis 2006), to represent the so-called emerging and mature greenhouse states. The SLP fields are also extracted for the same time periods and interpolated from the original 1.4º x 1.4º grid to a 200 km x 200 km Equal Area-Scalable Earth (EASE) grid (Armstrong et al. 1997), covering the area north of 60ºN and consisting of 51 x 51 grid points. The interpolation code was obtained from http://nsidc.org/data/ease/. Interpolation to an equal area grid avoids errors that might occur owing to equal weighting of the original latitude-longitude grid boxes in the self-organizing map algorithm, described in the next section.

Daily SLP fields from the European Centre for Medium-Range Forecasts (ECMWF) Reanalysis (ERA-40) (Upala et al. 2005) were used to validate the 20th century CCSM3 simulation. The fields from 1958 to 2001 were also interpolated to the same EASE grid prior to applying the SOM algorithm.

3.3. SOM methodology

Self-organizing maps (SOMs) provide a means to visualize the complex distribution of synoptic states (Hewitson and Crane 2002). This technique includes an unsupervised learning algorithm to reduce the dimension of large data sets by grouping similar multi-dimensional fields together and organizing them into a two-dimensional array (Kohonen 2001). In this study, the high-dimensional data subjected to SOM analysis are fields of daily SLP anomalies from CCSM3 for three time slices and the ERA-40 on a 51x51 EASE grid over the region north of 60°N.

The SOM consists of a 2D grid of nodes. Each node i corresponds to an n-dimensional weight or reference vector, m_i, where n is the dimension of the input data, treated as a vector created from the grid-points in each sample. The initial step of this routine is the creation of a first-guess array, which consists of an arbitrary number of nodes and corresponding reference vectors. In this study we use a grid of 35 nodes, creating a 7x5 array. Slightly smaller and larger SOM matrices were tested to determine a suitable number of nodes for this analysis. If the matrix is too small, some characteristic atmospheric patterns may not be represented; if it is too big, adjacent patterns will be too similar and visualization is unwieldy. The 7x5 matrix appears to capture and separate the important differences in pressure patterns. Moreover, the results are not affected by small

differences in the matrix size. The reference vectors are created at the beginning using linear initialization, which consists of first determining the two eigenvectors with the largest eigenvalues, then letting these eigenvectors span the two-dimensional linear subspace (Kohonen 2001). We use the covariance matrix of the input SLP dataset to determine the two eigenvectors. In this case the centroid of a rectangular array of initial reference vectors identified with array points corresponds to the mean of the sea level pressure values, and the vectors identified with the corners of the array correspond to the largest eigenvalues. By initiating a SOM in this way, the procedure starts with an already ordered set of weights, then training begins with the convergence phase. Linear initialization helps achieve faster convergence, which is an advantage of this procedure over other methods, but the SOM results are not sensitive to the selected initialization method. In the process of training, each data sample (i.e., one daily map of SLP) is presented to the SOM in the order it occurs in the original data set. The similarity between the data sample and each of the reference vectors is then calculated, usually as a measure of Euclidean distance in space. In this process, the "best match" node is identified as that with the smallest Euclidean distance between its reference vector and the data sample. Only the vectors for the best-matching node and those that are topologically close to it in the two-dimensional array are updated. The updating scheme is shown below

$$m_i(t + 1) - m_i(t) + h_{ci}(t) \cdot [x(t) - m_i(t)],$$

where t is a discrete-time coordinate, m_i is a reference vector, x is a data sample, and h_{ci} is a neighborhood function (Kohonen 2001), usually in the form of the Gaussian function,

$$h_{ci} = \alpha(t) \cdot \exp\left(-\frac{\|r_c - r_i\|^2}{2\sigma^2(t)}\right).$$

where   is the training rate function (usually an inverse function of time), r is the location vector in the matrix, the distance $\|r_c\text{-}r_i\|$ corresponds to the distance between the best-matching node (location r_c) and each of the other nodes (location r_i) in the two-dimensional matrix, and   defines the width of the kernel, or a relative distance between nodes, often referred to as the radius of training. The training procedure is controlled by the training rate   , the training radius r, and the duration of training, which is fixed at 20 times the number of data samples. The initial value of r is 4, and decreases linearly in time. The training scheme is repeated several times, with the training rate reduced by an order of magnitude each time. At the end of each trial the mean quantization error is calculated, defined as

$$mqe = \frac{\sqrt{\sum_{i=1}^{M}(x_i - m_c)^2}}{M},$$

where x_i is a data sample, M is the number of samples, and m_c is its best matching unit out of 35 reference vectors. A smaller mean quantization error indicates a closer resemblance between m_c and the daily SLP anomaly fields. The training is complete once the smallest mean quantization error is identified, as the reference vectors from that training best approximate the data space of interest. The final reference vectors are then mapped onto a 2D grid, with their locations in the matrix corresponding to their matching nodes. The maps in the resulting matrix represent the predominant patterns in which the atmosphere tends to reside, or alternatively the centroid of the particular data cluster.

Although the measure of similarity between the data and the reference vector is linear, it is this iterative training procedure that allows the SOM to account for the non-linear data distributions (Hewitson and Crane 2002). The non-linear approximation of the

data space is therefore a great advantage of the method compared to some other approaches, such as empirical orthogonal functions (EOFs) (Reusch et al. 2005).

3.4. SOM of CCSM3 and ERA-40 Arctic sea level pressure fields

3.4.1 20th Century Analysis

Daily sea-level pressure fields from ERA-40 (1958-2001), and CCSM3 for periods of 1960-1999, 2010-2030, and 2070-2089 for the region north of 60°N are used to create the master SOM. Daily SLP anomalies are derived by subtracting the gridpoint SLP from the domain-averaged SLP for each daily field (Cassano et al. 2007). The spatial distribution of the daily SLP anomalies represent the SLP gradient, and thus the circulation, but are not influenced by the absolute SLP values. Areas with elevation higher than 500 m are removed from the fields because pressure reduction to sea level can lead to unrealistic singularities emerging in the SOM training, which then obscure the realistic patterns.

Once a SOM of sea level pressure has been created from the combined sets of both ERA-40 and CCSM3 SLP anomalies – hereafter called the master SOM – all daily SLP anomaly fields may be mapped to the best-matching pattern in the master SOM to form clusters of daily maps. This is achieved by finding the trained reference vector associated with a node that minimizes the Euclidean distance, or the squared difference, between itself and the data sample. Once all the samples have been assigned to a node in the SOM, the frequencies of occurrence can be determined, i.e., the fraction of daily fields that reside in each cluster.

Ascribing a particular daily SLP sample to a specific circulation pattern in the SOM can also be useful for analyzing associated variables for the same days as those in each cluster. By mapping the new variable onto a particular SLP pattern, the new SOM representation can be used to describe the conditions associated with a specific circulation regime. In section 5 we apply this approach to fields of moisture flux across 70°N.

Figure 1 presents the master SOM for SLP anomalies north of 60°N derived using combined ERA-40 and CCSM3 SLP daily fields. These are the dominant circulation patterns in which the atmosphere tends to reside, according to these data sets. In the bottom right are patterns with a strong Icelandic low and a moderate-to-strong Aleutian low, with high pressure over the northern Eurasian continent. The upper right part of the map is dominated by pronounced low pressure in the Atlantic sector extending into Barents Sea, while the western central Arctic, continental regions, and the Pacific sector are dominated by high pressure. These patterns represent a moderate or strong Beaufort high in winter. The bottom left corner of the SOM is characterized by a pronounced low pressure area in the central Arctic with high pressure over northwestern Eurasia. Towards the upper left corner, a center of low pressure is located in the Kara and Laptev Seas, while high pressure is located over northeast N. America. The dominant feature in patterns near the middle of the SOM is high pressure in the central Arctic.

The frequency of occurrence of winter (DJF) patterns in CCSM3 is presented in **Fig. 2a**. Frequencies are expressed as a percent of days out of the total number of days in the data set that belong to a particular cluster. The highest winter frequencies occur in

patterns on the right side of the master SOM. Circulation patterns on the left side are more characteristic of summer (JJA) conditions (**Fig. 2b**).

The frequencies of occurrence of 20th century SLP patterns for the CCSM3 and ERA-40 are compared in **Fig. 3**. The bordering clusters characterized by more pronounced SLP gradients occur more frequently in the model than in the ERA-40 fields (**Fig. 3a**), while those positioned in the middle of the SOM occur less frequently. The distribution of frequencies of occurrence for the model fields does not reveal a preponderance of any particular group of clusters, while the real atmosphere (**Fig. 3b**) exhibits a preference for the regimes in the upper-middle and middle patterns in the SOM. These patterns tend to occur more often in summer, but not exclusively so.

The SLP anomalies averaged for an area north of 75°N for each individual cluster are presented in **Fig. 4**. The patterns in the middle, characterized by more pronounced high pressure over the central Arctic, also have higher SLP anomalies. Comparison of the mean SLP climatologies (**Figs. 5a and 5b**) confirms the conclusions resulting from the differences in the ERA40 and CCSM3 frequencies of occurrence shown in Figure 3. Compared to the ERA-40, mean model SLP anomalies (relative to the Arctic-mean SLP for each day) are lower in the central Arctic and in the Atlantic sector, along with higher pressure in northern Eurasia and northeastern American continent.

The differences in the distribution frequencies and SLP climatologies stem from the fact that the comparison is made between two single realizations of the 20th century climate. DeWeaver and Bitz (2006) analyzed the simulated Arctic atmospheric circulation in CCSM3 and found biases similar to those identified here, i.e., SLP in the Arctic is too low. They also found that the modeled wintertime Beaufort high is too

weak. Using a single model run clearly introduces uncertainty in future climate projections and attributions owing to natural variability, model physics and numerics, and uncertainty in emission projections. Nevertheless, as demonstrated in Section 5, despite the differences between the modeled and observed SLP, this model run realistically simulates 20th century moisture flux across 70°N. In addition, Cassano et al. (2007) analyzed 15 different IPCC AR4 models, including several realizations from CCSM, and found that the CCSM3 was one of the most realistic models in terms of adequately reproducing the observed Arctic hydrologic cycle. An assessment of the IPCC-4 set of models by Chapman and Walsh (2007) also identifies the CCSM3 model as one of the most realistic in simulating Arctic atmospheric behavior. Because the primary focus of this study is the changes projected from the 20th to the 21st century, the absolute accuracy of the simulated circulation patterns are not of central importance.

3.4.2. 21st Century Analysis

In this section we compare frequencies of occurrence for the distant–future (2070-2089) model simulations with those of the 20th century to investigate how circulation patterns are projected to change in the future (**Fig. 6**). Black solid (dashed) contours show areas of significantly (> 95% confidence) higher (lower) difference in frequency of occurrence. The range in a 95% confidence interval,

$$\pm 1.96 \sqrt{\frac{p_1(1-p_1)}{n_1} + \frac{p_2(1-p_2)}{n_2}},$$

where $p_1(1-p_1)/n_1$ and $p_2(1-p_2)/n_2$ are variances of two independent, random, binomial processes, p_1 and p_2 are the expected frequencies of occurrence for the two time periods (p=1/35), n_1 is the number of samples in the first data set, and n_2 is the number of

samples in the second data set (for more details see Cassano et al., 2007). Because this statistical test does not account for the effects of serial correlation in the daily SLP fields, and thus likely overestimates the degrees of freedom, we determine an approximation for the effective degrees of freedom by dividing the number of samples of the two data sets by 7. This value is determined from the serial correlation of the SLP time series, which indicates that the atmosphere tends to reside in a circulation regime for about one week. This procedure decreases the degrees of freedom, thus establishing a higher threshold for determination of a significance level.

A pronounced, statistically significant increase is apparent in patterns with low pressure over the central Arctic (left of the master SOM, **Figs. 1 and 4**), as well as those with strong high pressure across the western Arctic region and strong low pressure in the Atlantic sector and eastern Arctic (upper right of Fig. 1). The clusters in the middle, mostly dominated by a weak or a moderate high pressure over the central Arctic, decrease in frequency. Taken together these changes represent a decrease in pressure over the central Arctic in this greenhouse-gas-forced model projection. Indeed, differences in the mean SLP anomalies between 2070-2089 and 1960-1999 (**Fig. 7**) indicate reductions in SLP in the central Arctic, along with increases in SLP in the N. Atlantic and Pacific Oceans in the late 21st century. This tendency suggests that the Arctic Oscillation (Thompson and Wallace 1998) may reside in a positive phase more frequently in the future.

Cassano et al. (2007) formulated an equation that separates the factors contributing to a temporal change in a variable of interest into a portion caused by a change in the frequency of occurrence of daily maps in a cluster, a portion due to a change in the

cluster-mean physical variable, and a third due to a combination of the two effects. The equation is given as follows:

$$\Delta x = \sum_{i=1}^{N} (x_i + \Delta x_i)(f_i + \Delta f_i) - x_i f_i \qquad (1)$$

where x is the total change in a variable between two different time periods, x_i is the cluster-averaged variable in the initial time period, f_i is the frequency of occurrence of the daily maps in cluster i during the initial period, f_i is the change in cluster frequency between the two periods of interest, x_i is the change in the cluster-averaged variable between the two periods of interest, and N is the total number of clusters (N=35 in this study). Expanding (1):

$$\Delta x = \sum_{i=1}^{N} (x_i \Delta f_i + f_i \Delta x_i + \Delta x_i \Delta f_i), \qquad (2)$$

Previously we have observed and discussed the first term, x_i f_i, which relates changes in the pressure field to changes in the frequency of occurrence of circulation patterns. The second term, f_i x_i, relates to temporal changes in the variable of interest averaged over all days that belong to a cluster. In the case of cluster-averaged SLP anomalies, the values are non-zero because they are calculated for only a portion of the entire analysis domain, the area north of 75°N. Physically, a change in the cluster-averaged SLP may result from a general intensification or weakening of high/low pressure centers without a significant change in their spatial distribution. These changes are necessarily smaller than the differences in circulation between adjacent nodes. This assertion is supported by the nearly constant quantization error in time, indicating that the atmospheric circulation patterns represented by each cluster do not change significantly in the future, and that the change in frequency distribution for each cluster captures the important changes in atmospheric circulation.

The changes in frequency of occurrence from the 20th to 21st century are presented in **Fig. 6.** For this run of the CCSM3, patterns on the far left and right of the SOM that are dominated by low pressure will increase, while those characterized by relatively high pressure over the central Arctic will decrease in frequency. **Figure 7** shows the manifestation of this change in the difference in mean SLP between the end of the 21st century and the 20th century. The SLP is projected to decrease over most of the Arctic Ocean and increase over Arctic lands.

The three plots in **Figure 8** show the changes in the cluster-averaged SLP anomalies (i.e., x_i in Eq. 2) north of 75°N between 2010-2030 and 1960-1999, 2070-2089 and 2010-2030, and 2070-2089 and 1960-1999. These changes in SLP anomalies occur for the fixed circulation regimes of the SOM. The differences in cluster-averaged SLP anomalies generally reveal decreased pressure over the central Arctic, consistent with results from other GCMs (Chapman and Walsh, 2007), which contributes significantly to the total change.

3.5. Moisture fluxes across 70°N: 20th century analysis

The flux of moisture across the imaginary wall along the 70°N latitude is calculated for each daily field. The atmosphere is divided into five tropospheric layers: 300-400 hPa, 400-500 hPa, 500-700 hPa, 700-850 hPa and 850-1000 hPa. The flux in each layer is determined as $\bar{v} \cdot Q$, where

$$Q = \frac{1}{g} \int_{p_1}^{p_2} q \, dp$$

Q is the precipitable water in the layer (in kg m^{-2}), q is specific humidity, $\bar{v}$ is mean-layer meridional wind, g is gravity (9.8 ms^{-2}), and dp is the pressure differential in a layer between pressure levels p_1 and p_2. The moisture flux expressed in this way has the units of kg (ms)$^{-1}$. The total flux across the wall at 70°N is obtained by integrating around the latitude circle at each level and multiplying by the latent heat of evaporation (L=2.5 x 10^6 Jkg^{-1}). The values at each level are then summed vertically to obtain the total moisture transport into the Arctic, F$_q$, which has units of W. It is common to express this value as a flux per unit area of the Arctic region, so the flux is divided by the area of the polar cap north of 70°N to obtain units of W m^{-2}.

The 20th century mean, zonally averaged moisture flux profile, $L[\overline{vq}]$, across 70°N for CCSM3 (blue line) and ERA-40 (green line) is presented in **Fig. 9**. Greenland has been excluded from the calculations. The model reproduces the observed moisture flux remarkably well. Largest differences occur in the lower levels, which results in the model overestimating the 20th century moisture flux across 70°N by about 12%. The larger modeled fluxes in the lower levels are likely related to the generally lower Arctic SLP in the model than in ERA-40. Above 850 hPa however, the model profile is nearly indistinguishable from observed values.

Because each day of ERA-40 and model output can be ascribed to one of the SOM clusters, we can analyze poleward moisture fluxes corresponding to each atmospheric pattern in the SOM matrix. The cluster-averaged values of the flux across 70°N are presented in **Fig. 10** (Greenland has been excluded). Red areas in Fig. 10 correspond to patterns in the master SOM characterized by strong Icelandic lows and by pronounced low pressure over the central Arctic, both of which tend to advect large quantities of

moisture poleward. **Figure 11** presents a height-longitude view of moisture flux across 70°N mapped onto the circulation patterns in the master SOM, in units of kg (ms)$^{-1}$. The strongest moisture transport occurs in the lower and the middle troposphere, where the specific humidity is typically largest. Strong positive (poleward) moisture fluxes (red shading) are located east of low-pressure centers and west of high-pressure regions in the corresponding clusters in the master SOM. Correspondingly, negative equatorward moisture fluxes (blue areas) are found west of low-pressure systems and east of the high-pressure features. Features in the lower right portion of the SOM generate highest moisture transport. These patterns correspond to a positive North Atlantic Oscillation (NAO) index (Hurrell et al. 2003), with a pronounced Icelandic low in the Atlantic sector and high pressure over the Eurasian continent. The circulation patterns in the center of the SOM, related to weak or moderate high pressure over the central Arctic, generally show the weakest northward moisture transport. High pressure over the central Arctic, usually centered in the Beaufort Sea, generally indicates divergent flow and a stronger southward branch of moisture transport across the Canadian Arctic Archipelago. Strong low pressure over the central Arctic favors convergence and increased northward moisture transport (patterns in the lower left corner).

Seasonal-mean moisture fluxes across 70°N for the model's 20th century are presented in **Fig. 12**. Fluxes are strongest in summer primarily because of the increased depth of the moist layer and generally more poleward wind vectors (Groves and Francis 2002). A deeper moist layer also allows the stronger upper level winds to advect more moisture during summer. In winter fluxes are the weakest, as precipitable water values are lower, and the moist layer is shallow under a strong surface-based inversion. The

strongest fluxes in all seasons occur in the Atlantic sector, as this is the main pathway of moisture entering the Arctic. Temperature gradients are typically strongest in this area, and transports are driven by the primary storm track, i.e., the Icelandic low. Baroclinicity in this sector is associated with strong horizontal temperature gradients sharpened by coastal orography (Serreze and Barry 2005). Katabatic winds associated with the high Greenland plateau increase the temperature contrast in the region and help sustain a strong Atlantic baroclinic zone (Serreze and Barry 2005). In summer the meridional temperature gradient relaxes, but cyclonic activity is still high in the Arctic. Cyclones penetrate farther northward, with baroclinicity sustained by differential heating between the Arctic Ocean and snow-free land, and intensified by the coastal orography. Weak or moderate southward moisture flux occurs between $120°W$ and $60°W$. This area west of Greenland and across the Canadian Archipelago represents the main exiting branch of moisture out of the Arctic. The area of strong southward moisture flux just east of Greenland is most likely the result of high orography channeling the return flow of the Atlantic low pressure systems.

3.6. Attribution of changing moisture flux across 70°N in the 21st century

We now apply the same principle described in section 4.2 to provide insight into the causes for changes in the moisture flux across 70°N from the 20th century to the late 21st century. The first term in Eq. 2 represents the portion of the total change owing to shifts in the frequencies with which daily SLP fields reside in the patterns depicted in the SOM. A change in this distribution represents a change in the surface circulation, and thus we loosely refer to this contribution as the dynamic factor. The second term in Eq. 2

captures the fraction of the total change that is due to a change in the cluster-averaged value of the parameter of interest for each fixed SLP pattern. In the case of moisture flux, changes of this type are likely caused mainly by thermodynamic effects -- such as varying moisture gradients and the vertical distribution of water vapor -- thus we refer to this contribution as the thermodynamic factor. The third term in Eq. 2 represents the contribution from the interaction of both changing pattern frequency and the cluster-averaged variable. This term tends to be small.

The attribution of change is evaluated annually and seasonally between the three time slices (2010-2030 and 1960-1999, 2070-2089 and 2010-2030, and 2070-2089 and 1960-1999. It should be noted that these results are meant to provide insight into the causes of future change, not a quantitative accounting. The dynamic factor, x_i f_i, is obtained by multiplying the initial cluster-mean moisture flux values (shown in **Fig. 10**) by the change in the pattern frequency between each time slice, an example of which is shown in **Fig. 6**. The results for this contribution are shown in the top panels of **Figs. 14-16**. The thermodynamic factor, f_i x_i, is obtained by combining the initial distribution of frequencies of occurrence shown in Fig. 3a with the changes in cluster-mean moisture flux, x_i, presented in **Fig. 13** for each time slice. The thermodynamic factor is shown in the middle panels of **Figs. 14-16**. Finally, the combined term is x_i multiplied by f_i and is plotted in the bottom panels. To obtain the annual-mean contribution to the total change, the values for each contribution are summed over all clusters. The numerical results are summarized in **Table 1** along with a breakdown by season. It should be noted that these results are not sensitive to the size of the SOM used in this analysis. As shown in **Table 2**, the annual-mean contributions to the total change by the three terms are

virtually unchanged for varying sizes of the SOM matrix. The 7x5 array chosen for this study represents a balance between having enough nodes to capture the representative patterns in the Arctic atmosphere and the ability to present those patterns graphically.

In all three time comparisons, the thermodynamic factor clearly plays the most important role in the changing moisture transport in this model simulation, which is in turn driven by the change in the cluster-mean flux (**Fig. 13**). This quantity exhibits a positive temporal change in every node. Because the model is forced by a realistic estimate of increasing greenhouse gas composition through the 21st century, the most logical explanation for this result is the forcing. From the late 20th century to the near future, we find that over 80% of the increase in total northward moisture flux is due to the thermodynamic factor. A larger increase in the moisture transport of about 2.5 Wm^{-2} (16%) occurs later in the 21st century, from 2010-2030 to 2070-2089, compared to approximately 0.9 Wm^{-2} (5%) from 1960-1999 to 2010-2030. This results from the substantial warming, and the consequential increased water vapor content, by the end of the century. The increase in the later 21st century is also dominated by thermodynamic effects.

The dynamic term plays only a secondary role in driving projected moisture flux changes. As discussed in section 4, low-pressure anomalies over the central Arctic occur more frequently in the future in this simulation, while features showing weak or moderate high pressure occur less often. This also favors an increase in poleward moisture flux, but only explains about 15.5 % of the total projected change. The combined term contributes least to the total change, but its influence increases in the far future (2070-2089), accounting for about 7.7% of the total change.

The seasonal analysis also reveals the dominant contribution by the thermodynamic factor in governing increases in moisture flux by the 21st century CCSM3 (**Table 1**). The largest increases in moisture flux occur in summer: 0.3 Wm^{-2} (7%) between the near future and the 20th century and 0.8 Wm^{-2} (19%) between the near and the far future, with a total of 1.1 Wm^{-2} (26%) from the present to the far future. Summer increase in moisture transport accounts for about 32% of the total change by the late 21st century.

In summer the atmospheric moisture content, as well as the saturation vapor pressure, achieve their highest values. The increased meridional gradient in specific humidity can be explained by the exponential relationship between saturation vapor pressure and temperature. At the warmer low-latitude temperatures, a given increase in temperature will lead to a relatively larger increase in saturation vapor pressure than that at higher latitudes for the same warming, which likely results in an increased specific humidity gradient. High-latitude meridional temperature gradients are also sustained by land-ocean differential heating. While Arctic land areas warm as the snow and ice cover melts away, the Arctic Ocean's temperature is confined near the melting point. These factors contribute to the largest seasonal increase in poleward moisture fluxes. The thermodynamic factor play a dominant role in the summer, explaining about 79% of the moisture increase between the near future and the 20th century in this simulation, while the other effects account for a larger portion of the change between the near and far future. This can be explained by the increased frequency of occurrence in summer circulation patterns that favor convergence and thus an increase in the poleward moisture flux.

In spring the thermodynamic term dominates in all time intervals. Between the 20th century and the near future the flux increases about 0.3 Wm[-2] (8%), and between the near and far future the increase is 0.4 Wm[-2] (11%), resulting in a total change of 0.7 Wm[-2] (19%) between the 20th century and the far future. In the later period the role of the dynamic term decreases dramatically, resulting in the thermodynamic factor accounting for virtually all of the change in the moisture flux occurring between the near and far future. The spring increase in moisture transport accounts for about 23% of the total change by the late 21st century.

The change in the moisture flux in winter is small between the 20th century and the near future (approximately 0.1 Wm[-2], 4%), but increases between the near and far future (0.7 Wm[-2], 20%), resulting in a total change of 0.8 Wm[-2] (24%) between the 20th century and the late 21st century. The winter increase in moisture transport by the late 21st century accounts for 24% of the total change. While the thermodynamic term plays the leading role between the near and far future (accounting for 91% of the total change), between the 20th century and the near future the dynamic term dominates. In the early period dynamics explains about 46% of the total change in moisture flux, with the combined term playing a secondary role, accounting for 36%. The thermodynamic term accounts for only about 18% of the total change. This may be explained by a modest increase in frequency of occurrence of the winter patterns in the right of the SOM. Thermodynamic influences, mainly driven by the increased moisture content of the atmosphere, may be hampered by weakened temperature and humidity gradients that are expected in the near future (Serreze and Francis 2006). Delayed ice growth and the resulting thinner ice cover reduce the insulating effect of the sea ice. As the important

source of atmospheric heating of the polar atmosphere in cold seasons is the ocean, its effect may, in the emerging warming state, weaken the poleward moisture transport. Between the near and far future projections, the contributions by the dynamic and combined terms decrease, and the thermodynamic factor dominates. Weakening of winter dynamics in the late future can be explained by a decrease in the frequency of occurrence of the winter patterns in the lower right corner, corresponding to positive NAO-like patterns that generally bring more moisture into Arctic (Fig. 6).

The changes in autumn appear to be similar to those for winter, albeit smaller. Moisture flux increases by approximately 0.1 Wm^{-2} (2%) between the 20th century and the near future and 0.6 Wm^{-2} (14%) between the near and far future, resulting in a total change of 0.7 Wm^{-2} (16%) between the 20th century and the late 21st century. The autumn change represents about 21% of the annual-mean change. In the early period the largest contribution is from the dynamic term, which accounts for about 59% of the total change, followed by the combined term at 45%. Interestingly the thermodynamic term is negative, acting to weaken the poleward fluxes, which may be explained by the strong influence of decreased temperature and moisture gradients across 70°N as sea ice declines. This explanation is consistent with Serreze and Francis (2006), who found maximum autumn warming over the Arctic Ocean in four of five climate models analyzed, which reduced the meridional gradients. Later in the 21st century, thermodynamic effects dominate, accounting for 54% of the total change, followed by dynamics (28%), and finally the combined influence (18%). The general increase in the depth of the moist layer in the late 21st century during autumn allows stronger upper-level winds to play a greater role in moisture transport.

3.7. Discussion and conclusions

Changes in poleward moisture fluxes across 70°N in the 21st century and their relationships to surface circulation patterns have been analyzed using daily output from the NCAR CCSM3 and a neural-network technique called self-organizing maps (SOMs). The study focuses on changes in the moisture flux that are projected for the early (2010-2030) and late (2070-2089) 21st century, compared to the 1960-1999 period, based on a single model realization forced by the A2 SRES scenario.

Comparison of the modeled moisture fluxes for the 20th century with those derived from the ERA-40 indicates that the model realistically simulates the moisture flux across a wall at 70°N within about 12%. Based on a partitioning of the change into its components for fixed and varying circulation regimes, we find that approximately 75% of the change in moisture transport during the 21st century is attributed to factors related primarily to thermodynamic factors rather than changing circulation patterns. Poleward moisture flux across 70°N is projected to increase by approximately 0.9 Wm^{-2} (5%) between 1960-1999 and 2010-2030, and by about 2.5 Wm^{-2} (16%) between 2010-2030 and 2070-2089. These values are of similar magnitude to the increase in radiative forcing by anthropogenic greenhouse gases since the 1800s. Thermodynamic factors driving the enhanced moisture flux include increases in precipitable water and the meridional moisture gradient. The depth of the near-surface moist layer will also increase, allowing the typically stronger winds aloft to play a greater role in the transport. The modeled increase in northward moisture flux implicates further amplification of Arctic warming, as additional latent heat will be released through condensation of water vapor and the increased emissivity of the atmosphere. Increased warming may augment the already

rapidly declining permanent Arctic ice stores. The increased moisture content of the high-latitude atmosphere, particularly in summer, may also lead to an increase in cloud cover and precipitation, thus intensifying the hydrologic cycle. Skific et al. (2009) finds that for the same model simulation, Arctic net precipitation increases by about 20% and mean cloud fraction by about 10% by the late 21st century. They also find that the largest increase in net precipitation over the Arctic Ocean occurs in summer, with thermodynamic factors accounting for over 70% of the increase. The summer maximum in net precipitation is related to a seasonal maximum in moisture flux convergence (Serreze and Barry 2005), thus an increase in moisture flux in the future will likely lead to increased precipitation in the Arctic. This eventuality was demonstrated by Cassano et al. (2007), who find increases in high-latitude precipitation during the 21st century in ensemble output from 15 GCMs used for the 4th IPCC report. They also calculate that more than 75% of that change is due to atmospheric thermodynamics. According to Liu et al. (2007) the increase in winter moisture transport during the past few decades appears to be linked with more frequent cyclones and increased cloud amount in the Arctic.

Our results indicate that moisture fluxes are projected to increase in this model simulation. The future behavior of the other two components of the moist static energy flux -- geopotential and sensible heat advection -- are yet to be explored in terms of their behavior relative to moisture transport, their drivers and feedbacks within the Arctic system, and their roles in Arctic amplification. Linkages between the dramatic changes within the Arctic and the global system remain poorly understood in present conditions, thus the uncertainty regarding future changes will remain an important focus for global-change research.

References

Alexeev, V.A., P.L. Langen, and J.R. Bates, 2005: Polar amplification of surface warming on an aquaplanet in "ghost forcing" experiments without sea ice feedbacks. *Clim. Dynamics*, **24**,655-666.

Ammann, C. M., G. A. Meehl, W. M. Washington, and C. S. Zender, 2003: A monthly and latitudinally varying volcanic forcing dataset in simulations of 20th century climate. *Geophys. Res. Lett.,* **30**, 1657, doi:10.1029/2003GL016875.

Armstrong, R, M. J. Brodzik, and A. Varani, 1997: The NSIDC EASE-Grid: Addressing the need for a common, flexible, mapping and gridding scheme. *Earth System Monitor*, **7(3),** 3 pp.

Belchansky, G.I., D.C. Douglas, and N.G. Platonov, 2003: Duration of the Arctic melt season: Regional and interannual variability, 1979-2001. *J. Climate,* **17**, 67-80.

Blanchet, G.E. and J.P. Girard, 1995: Water vapor temperature feedback in the formation of continental Arctic air: implication for climate. *Sci.Total.Env.*, ***160/161***, 793-802.

Cassano, J.J, P. Uotilla, A.H. Lynch, E.N. Cassano, 2007: Predicted changes in Synoptic Forcing of Net Precipitation in Large Arctic River basins During the 21st century, *J. Geoph. Res- Biogeosciences*, **112**, G04S49, doi:10.1029/2006JG000332.

Cassou, C., and L. Terray, 2001: Dual influence of Atlantic and Pacific SST anomalies on the North Atlantic/Europe winter climate. *Geoph. Res. Lett*., **28,** 3195-3198.

Chapman, W.L. and J.E. Walsh, 2007: Simulations of Arctic temperature and pressure by global coupled models. *J. Clim*., **20**, 609-632.

Collins, W. D., C.M. Bitz, M.L Blackmon, G.B. Bonan, C.S. Bretherton, J.A. Carton, P. Chang, S.C. Doney, J.J Hack, T.B. Henderson, J.T. Kiehl, W.G. Large, D.S. McKenna, B.D. Santer, and R.D. Smith, 2006a: The Community Climate System Model Version 3 (CCSM3). *J. Climate,* **19**, 2122-2143.

Comiso, J. 2003: Warming trends in the Arctic from clear-sky satellite observations. *J. Climate,* **16,** 3498- 3510.

DeWeaver, E., and C.M. Bitz, 2006: Atmospheric circulation and Arctic sea ice in CCSM3 at medium and high resolution. *J. Climate*, **19,** 2415-2436.

Ferguson, D. and members of ARCSS Committee, 2004: Arctic system synthesis encourages program integration. *Witness the Arctic*, **11**, 8-9.

Fichefet, T., C. Poncin, and H. Goose, 2003: Implications of changes in freshwater flux from the Greenland ice sheet for the climate of the 21ˢᵗ century. *Geophy. Res. Lett.*, **30**, DOI:10.1029/2003GL017826.

Finnis, J., J.J. Cassano, M.M. Holland, M.C. Serreze, and P. Uotila, 2008: Synoptically forced hydroclimatology of major Arctic watersheds in general circulation models, Part 1: The MacKenzie River basin. *Int. J. Climatology*, accepted.

Finnis, J., J.J. Cassano, M.M. Holland, M.C. Serreze, and P. Uotila, 2008: Synoptically forced hydroclimatology of major Arctic watersheds in general circulation models, Part 2: Eurasian watersheds. *Int. J. Climatology*, accepted.

Graversen, R.G., T. Mauritsen, M. Tjernström, E. Källen and G. Svennson, 2008: Vertical structure of recent Arctic warming. *Nature*, **451**, 53-56.

Groves, D.G., and J.A. Francis, 2002: The moisture budget of the Arctic atmosphere from TOVS satellite data, *J. Geophy. Res.*, **107**(D19), 1-21.

Hartmann, D.L., 1994: *Global Physical Climatology*. Academic Press, 409 pp.

Held, I.M., and B.J. Soden, 2006: Robust responses of the hydrological cycle to global warming, *Annual Review of Energy and the Environment*, **25**, 441-475.

Hewitson, B.C., and R.G. Crane, 2002: Self-organizing maps: applications to synoptic climatology. *Clim. Res.*, **22**, 13-26.

Hoerling, M.P., J.W. Hurrell, T. Xu., T.G. Bates, and A. Phyllips, 2004: Twentieth century North Atlantic climate change. Part II: Understanding the effect of Indian Ocean warming. *Clim. Dynamics*, **23**, 391-405.

Holland, M.M., J. Finnis, and M.C. Serreze, 2007: Simulated Arctic Ocean freshwater budgets in the twentieth and twenty-first centuries. *J. Clim.,* **19,** 6221-6242.

Huntington, H., and S. Fox, 2005: The Changing Arctic: Indigenous Perspectives. *The Arctic Climate Impact Assessment (ACIA)*, Lelani Arris, Eds., Cambridge University Press, 61-98.

Hurrell, J.W., Y. Kushnir, G. Ottersen and M. Visbeck, 2003: An overview of the North Atlantic Oscillation. *The North Atlantic Oscillation: Climatic Significnace and Environmental Impact,* J.W. Hurrel, Y. Kushnir, G. Ottersen and M. Visbeck, Eds., Geophysical Monograph Series,1-36.

_____, M.P. Hoerling, and T. Xu, 2004: Twentieth century North Atlantic climate change. Part I: Assessing determination. *Clim. Dynamics,* **23**, 371-389.

Intergovernmental Panel on Climate Change, 2007: Climate Change 2007: The Physical Science Basis. Contribution of Working Group I to the Fourth Assessment Report of the Intergovernmental Panel on Climate Change [Solomon, S., D. Qin, M. Manning, Z. Chen, M. Marquis, K.B. Averyt, M. Tignor and H.L. Miller (eds.)]. Cambridge University Press, Cambridge, United Kingdom and New York, NY, USA, 996 pp.

Kiehl, J., T. Schneider, R. Portmann, and S. Solomon 1999: Climate forcing due to tropospheric and stratospheric ozone. *J. Geophys. Res.*, **104**, 31239-31254.

Kohonen, T., 2001:*Self-organizing maps*. 3d ed. Springer-Verlag, 501 pp.

Nakamura, N. and A.H. Oort, 1988: Atmospheric heat budgets of the polar regions. *J. Geophys. Res.,* **93***,* 9510-9524.

Lean, J., Y.-M. Wang, and N. R. Sheeley Jr., 2002: The effect of increasing solar activity on the sun's total and open magnetic flux during multiple cycles: Implications for solar forcing of climate. *Geophys. Res. Lett.,* **29**, 2224, doi:10.1029/2002GL015880.

Liu, Y., J. R. Key, J. A. Francis and X. Wang, 2007: Possible causes of decreasing cloud cover in the Arctic winter, 1982-2000, *Geophy Res Lett.*, **34**, L14705,doi:10.1029/2007GL030042 .

Nakicemovic, N. and R. Swart, 2000: *Intergovernmental Panel on Climate Change Special report on Emission Scenarios*. Cambridge University Press, 570 pp.

Osterkamp, T.E., and V.E. Romanovsky, 1999: Evidence for warming and thawing of discontinuous permafrost in Alaska. *Permafrost and Periglacial Processes,* **10**, 17-37.

Overpeck, J.T., M. Strum, J.A. Francis, D.K. Perovich, M.C. Serreze and 18 others, 2005: Arctic system on trajectory to new, seasonally ice‐free state. *EOS,* **86**, 309-313.

Peterson, B.J., Holmes, R.M., McClelland, J.W., Vorosmarty, C.V., Lammers, R.B., Shiklomanov, A.I., and S. Rahmstorf, 2002: Increasing river discharge to the Arctic Ocean. *Science,* **298**, 2171-2173.

Rahmstorf, S., A. Cazenave, J.A. Church, J.A. Hansen, R.F. Keeling, D.E. Parker, and R.J. Somerville, 2007: Recent climate observations compared to projections. *Science*, **316**, 709.

Reusch, D.B., R. Alley and B.C. Hewitson, 2005: Relative performance of self-organizing maps and principal component analysis in pattern. Extraction from synthetic climatologic. *Polar Geography*, **29,** 188-212.

Rigor, I.G., and J.M. Wallace, 2004: Variations in the age of Arctic sea‐ice and summer sea-ice extent. *Geophys. Res. Lett.* **31**, L09401, doi:10.1029/2004GL019492.

Serreze, M.C., and R.G. Barry, 2005: *The Arctic Climate System*. Cambridge University Press, 146 pp.

_____, and J.A. Francis, 2006: The Arctic on the fast track of change. *Weather,* **61**, 3.

Skific, N., J.A. Francis, and J. J. Cassano, 2009: Attribution of seasonal and regional changes in Arctic moisture convergence. *J. Climate*, submitted.

Soden, B.J., and I.M. Held, 2006: An assessment of climate feedbacks in coupled ocean-atmosphere models. *J. Climate*, **19(14)**, 3354-3360.

Smith, S.J., H. and T.M.L Wigley, 2001: Global and regional anthropogenic sulfur dioxide emissions. *Global and Planetary Change*., **29**, 99-119.

Smith, S.J., H. Pitcher, and T.M.L. Wigley, 2005: Future sulfur dioxide emissions. *Climatic Change*., **73(3),** 267–318.

Thompson, D.W.J. and M. Wallace, 1998: The Arctic oscillation signature in wintertime geopotential height and temperature fields. *Geophys. Res.Lett.,* **25**, 1297-1300.

Uppala, S.M., P.W. Kallberg, A. J. Simmons, U. Andrae, V.D. Bechtold, M, Fiorino, J.K. Gibson, J. Haseler, A. Hernandez, G. A. Kelly, X. Li, K. Onogi,S. Saarinen, N. Sokka, R. P. Allan, E. Andersson, K. Arpe, M. A. Balmaseda, A. C. M. Beljaars, L. Van De Berg, J. Bidlot, N. Bormann, S. Caires, F. Chevallier, A. Dethof, M. Dragosavac, M. Fisher, M. Fuentes, S. Hagermann, E. Holm, B.J. Hoskins, L. Isaksen, P.A.E.M. Janssen, A.P. McNally, J.F. Mahfouf, J.J. Morcreete, N.A. Rayner, R.W. Saunders, P. Simon, A. Sterl, K. E. Trenberth, A. Untch, D. Vasiljevic, P. Viterbo, and J.Wollen, 2005: The ERA-40 reanalysis. *Quart. J. Royal. Met. Soc*., **131**, 2961-3012.

Table 1.

Period observed	Dyn. term (W/m^2)	Thermodyn. term (W/m^2)	Comb. term (W/m^2)	Total (W/m^2)	Dyn. term (%)	Thermodyn. term (%)	Comb. term (%)
2010-2030 minus 1960-1999	0.15	0.72	0.07	0.90	17.4	81.8	0.8
2070-2089 minus 1960-1999	0.53	2.63	0.26	3.43	15.5	76.8	7.7
2010-2030 minus 1960-1999 winter	0.05	0.02	0.04	0.11	45.5	18.2	36.4
2070-2089 minus 1960-1999 winter	0.04	0.72	0.07	0.83	4.8	86.8	8.4
2010-2030 minus 1960-1999 spring	0.07	0.26	-0.03	0.34	22.3	78.6	-0.9
2070-2089 minus 1960-1999 spring	0.08	0.72	-0.03	0.78	11.1	92.4	-3.5
2010-2030 minus 1960-1999 summer	0.07	0.24	-0.01	0.3	23.7	79.6	-3.3
2070-2089 minus 1960-1999 summer	0.27	0.78	0.09	1.14	23.6	68.4	8.0
2010-2030 minus 1960-1999 fall	0.06	-0.004	0.05	0.11	58.8	-3.60	44.8
2070-2089 minus 1960-1999 fall	0.21	0.40	0.13	0.74	27.8	54.5	17.7

Table 1: Contributions of dynamic, thermodynamic and combined dynamic and thermodynamic change to a total change in moisture flux across 70°N (W/m^2), for various time frames of the 21st century. Changes are observed annually and seasonally. Changes between the 20th and the late 21st century are given in bold.

Table 2.

Size of map	Dynamic	Thermodynamic	Combined
20 (4x5)	0.34	2.68	0.40
30 (5x6)	0.36	2.66	0.40
35 (5x7)	0.43	2.63	0.36
40 (5x8)	0.38	2.67	0.37
48 (6x8)	0.45	2.65	0.32
56 (7x8)	0.46	2.65	0.31
80 (8x10)	0.42	2.65	0.35
120 (10x12)	0.39	2.68	0.35
240 (10x24)	0.41	2.63	0.38

Table 2: Dynamic, thermodynamic and combined dynamic/thermodynamic annual change in moisture flux across 70°N (W/m^2), between the late 21st century and the 20th century, for various map sizes.
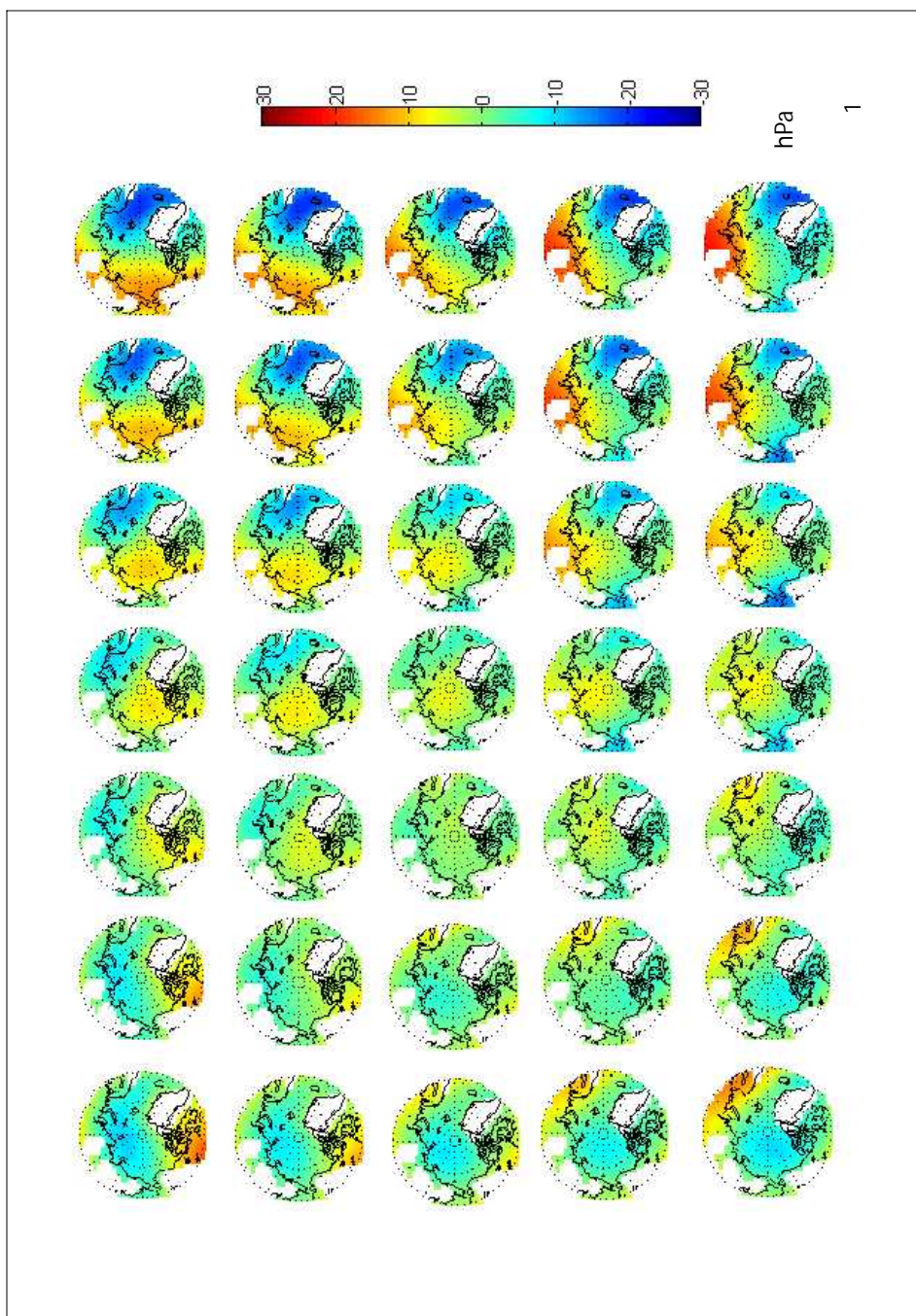
Figure 1: Master SOM of sea level pressure anomaly patterns (hPa) derived from daily SLP anomaly fields CCSM3 (1960-1999, 2010-2030, and 2070-2089), and from ERA-40 (1958-2001).
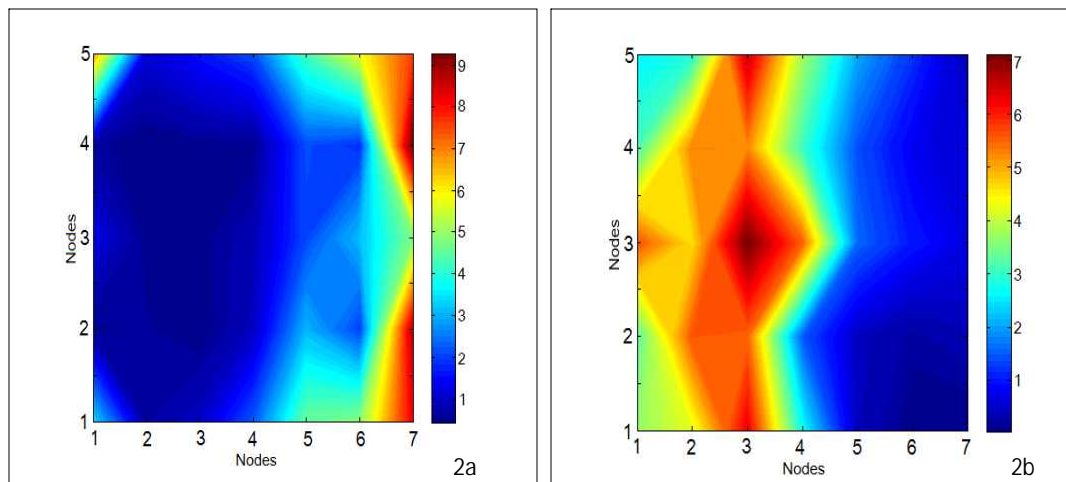
Figure 2: Frequencies of occurrences of **(a)** winter (DJF) days, and **(b)** summer (JJA) days in CCSM3. Frequencies are presented as percent of total days of the 1960-1999 period mapping to a particular cluster of the master SOM.
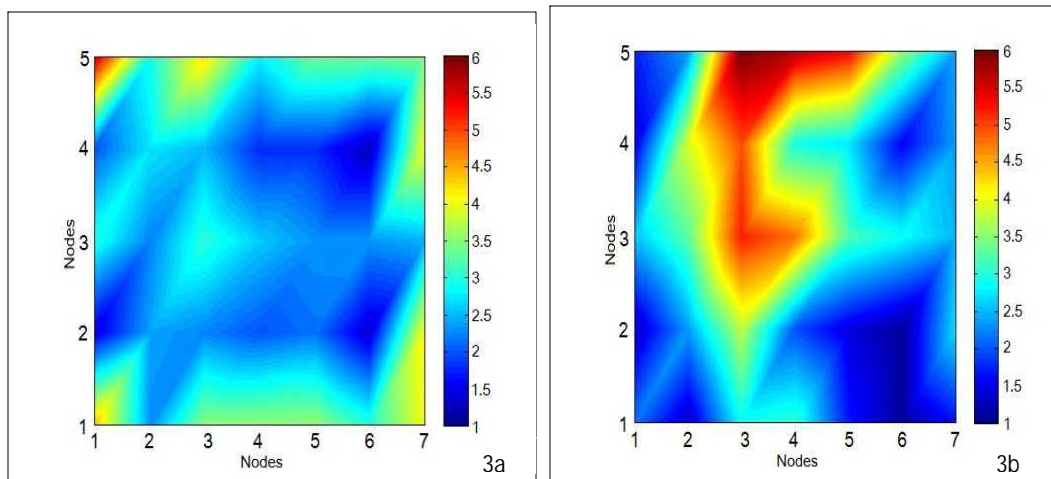

Figure 3: Frequency of occurrence of **(a)** sea-level pressure CCSM3 anomaly patterns in the period from 1960-1999, and **(b)** ERA-40 anomaly patterns from 1958-2001. Frequencies show percent of days out of a total that map to a particular SLP cluster.
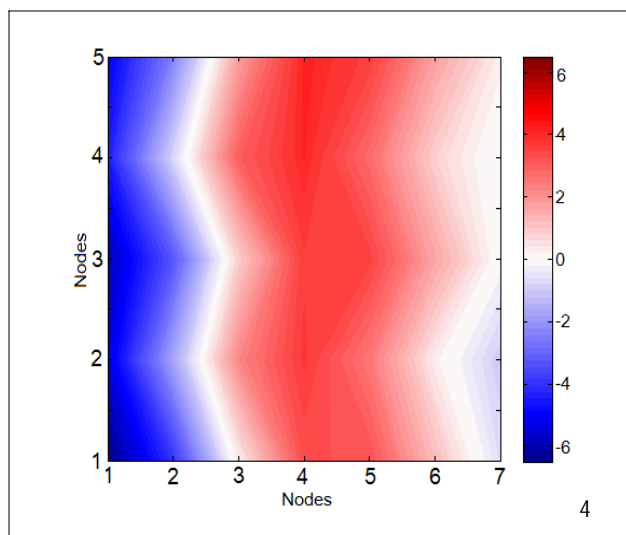
Figure 4: Mean sea-level pressure anomaly patterns (hPa) averaged for an area north of 75°N for each individual cluster in Fig. 1.
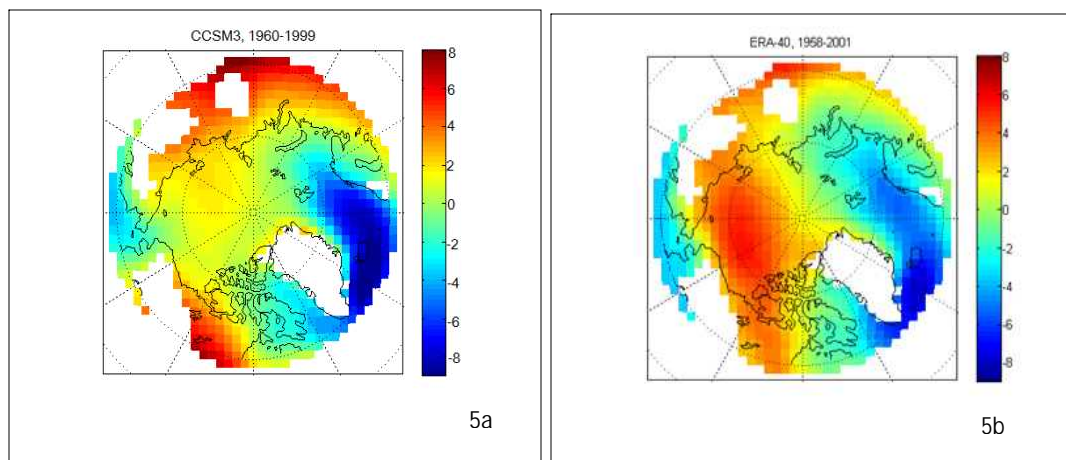
Figure 5: Mean climatology of daily sea level pressure anomalies (hPa); **(a)** CCSM3, from 1960-1999, and **(b)** ERA-40, 1958-2001.

Figure 6: Difference in frequency of occurrence of the sea-level pressure anomaly patterns between the far future (2070-2089) and the 20th century. Significantly larger (smaller) differences are indicated with a solid (dashed) line. Level of confidence is 95%.
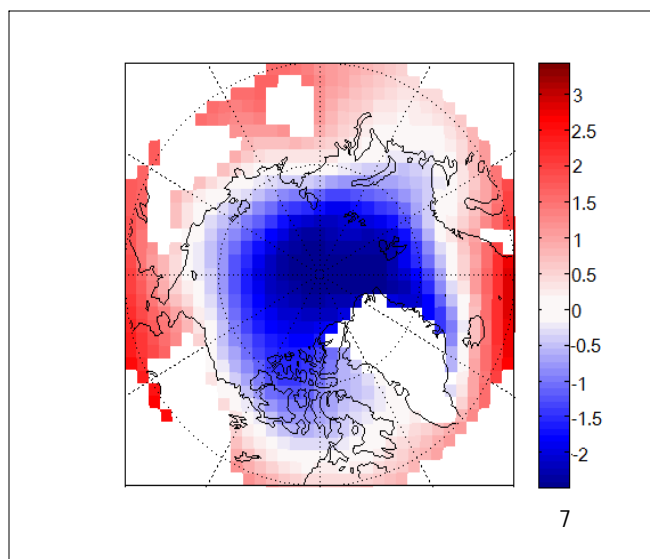
Figure 7. Difference in the mean sea-level pressure anomalies (hPa) between the far future (2070-2089) and 20th century (1960-1999) of CCSM3.

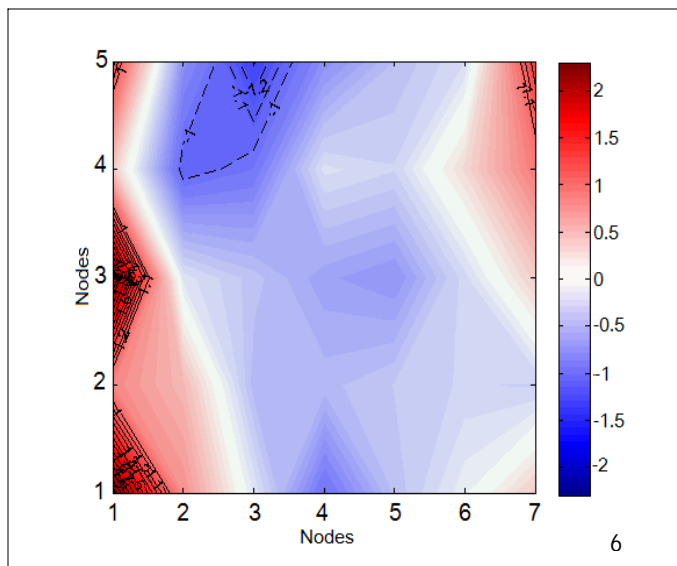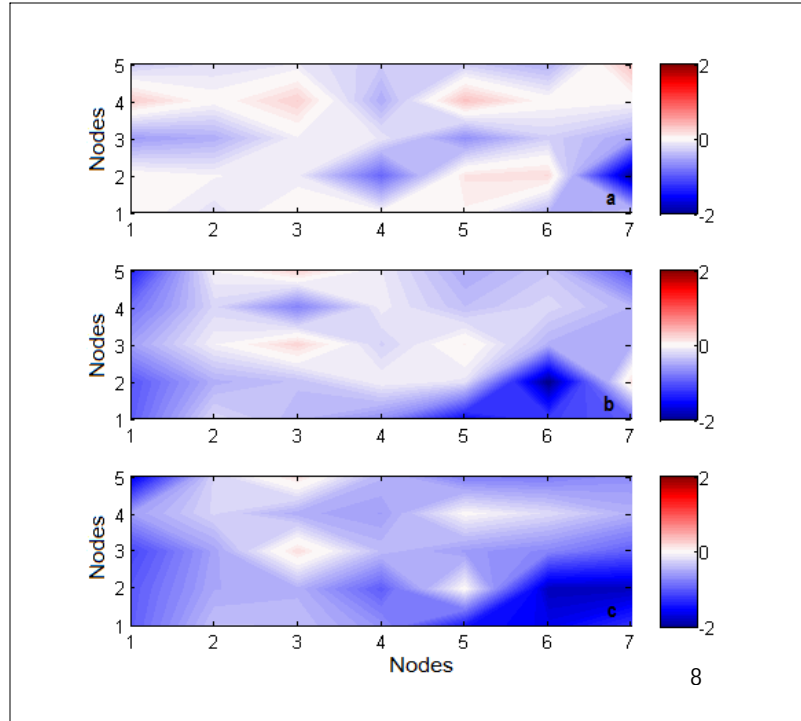**Figure 8**: Differences in the cluster-averaged SLP anomaly patterns for an area north of 75°N (hPa): **(a)** 2010-2030 minus 1960-1999, **(b)** 2070-2089 minus 2010-2030 and **(c)** 2070-2089 minus 1960-1999.
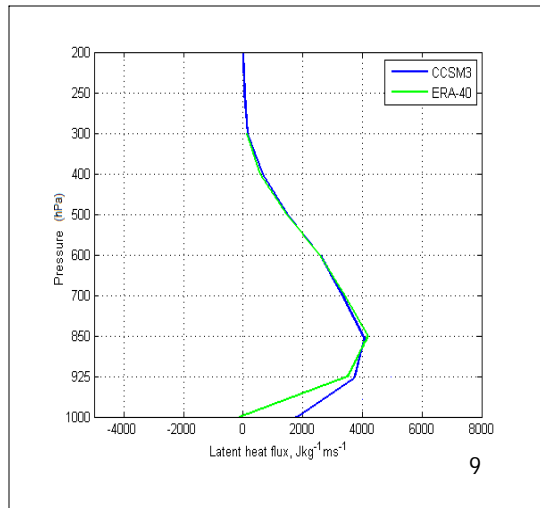
Figure 9: Vertical profiles of the 20th century mean, zonally averaged energy flux across 70°N ($Jkg^{-1}ms^{-1}$) for CCSM3 (blue line) and ERA-40 (green line).
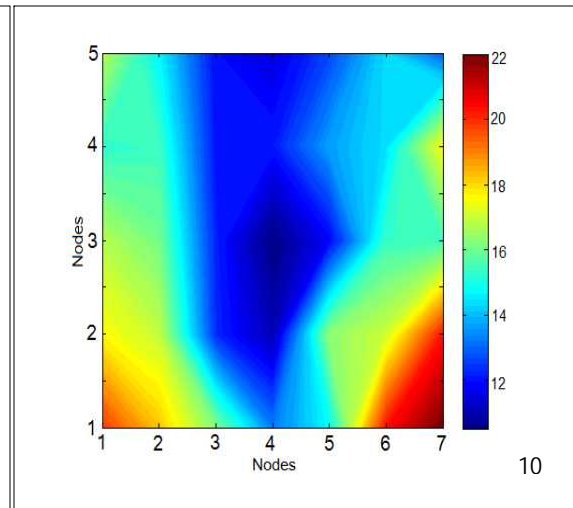
Figure 10: Cluster-averaged moisture flux across 70°N (Wm^{-2}), for CCSM3, for the period of 1960-1999.
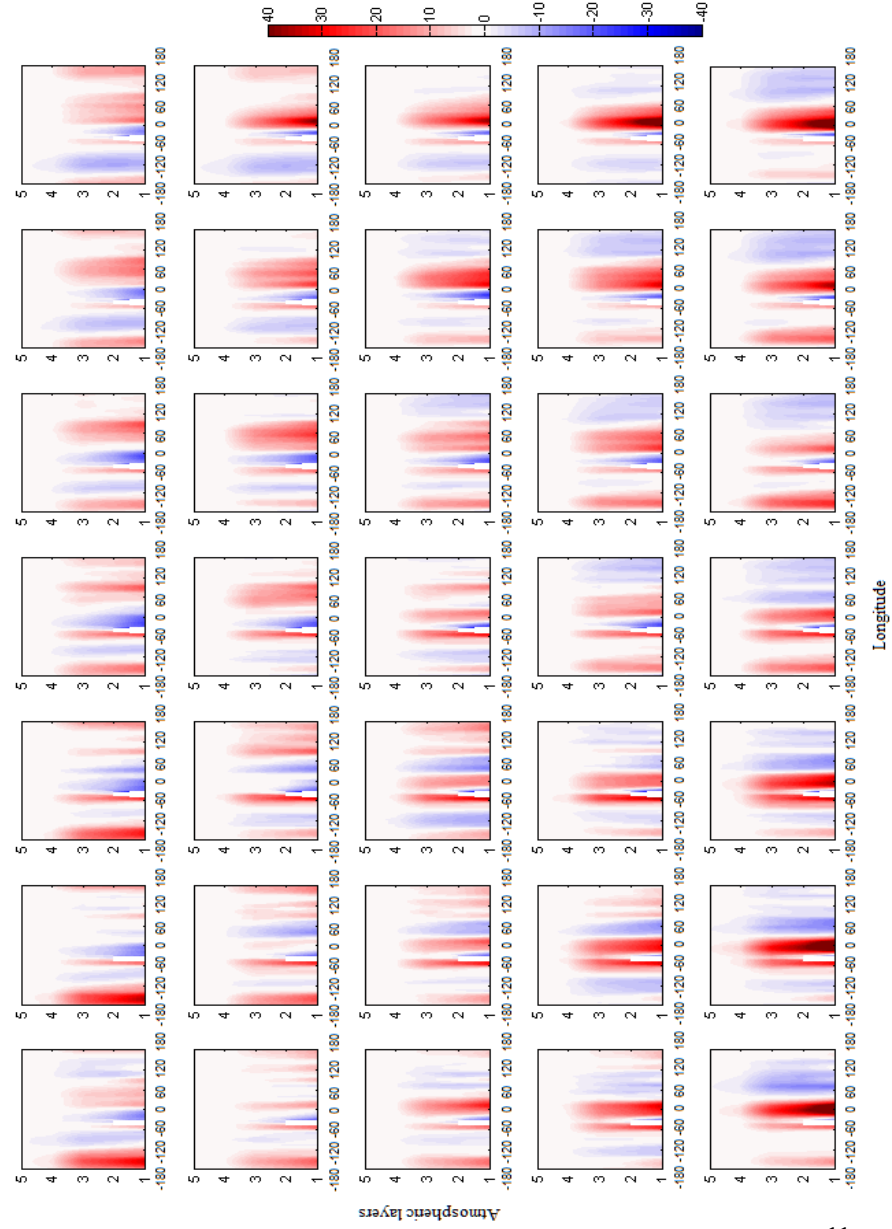
Figure 11: Longitude-height representation of five moisture flux layers across 70°N (kgm^{-1}s^{-1}) for CCSM3 mapped onto corresponding circulation patterns derived from sea-level pressure anomalies seen in figure 1.a. Red (blue) shaded areas represent northward (southward) fluxes.
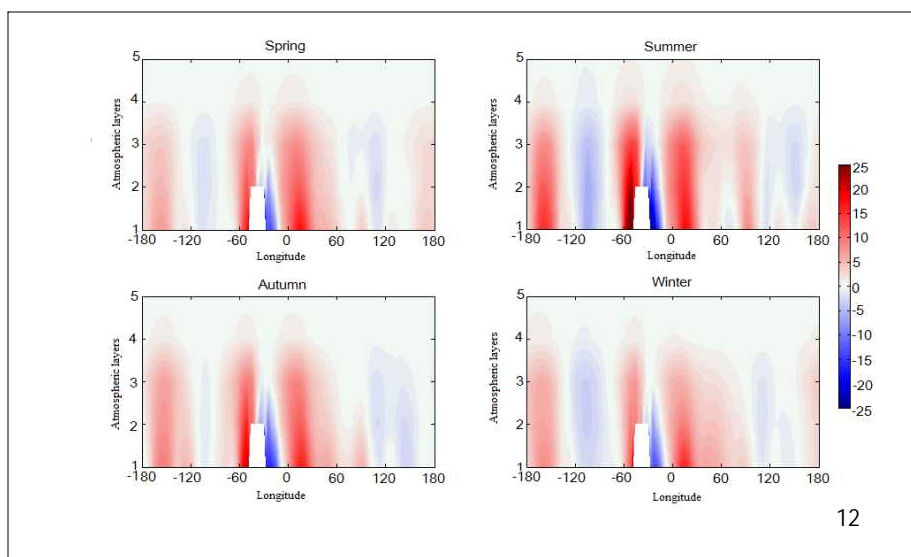
Figure 12: Longitude-height representation of mean moisture flux across 70°N (kgm^{-1}s^{-1}) for five layers averaged for four seasons, using 20th century daily fields from CCSM3.
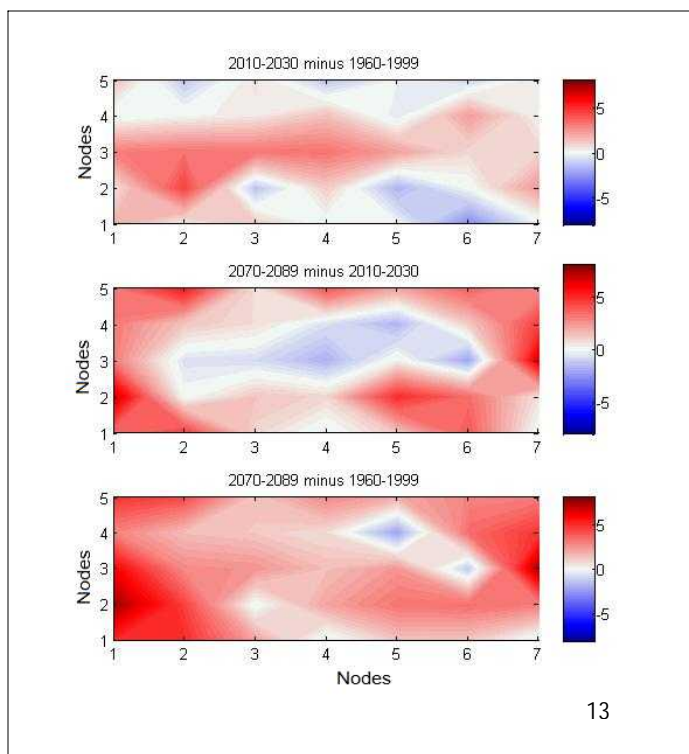
Figure 13. Differences in the cluster-averaged moisture flux (Wm^{-2}) from CCSM3 across 70°N: **(top)** 2010-2030 minus 1960-1999, **(middle)** 2070-2089 minus 2010-2030, and **(bottom)** 2070-2089 minus 1960-1999.
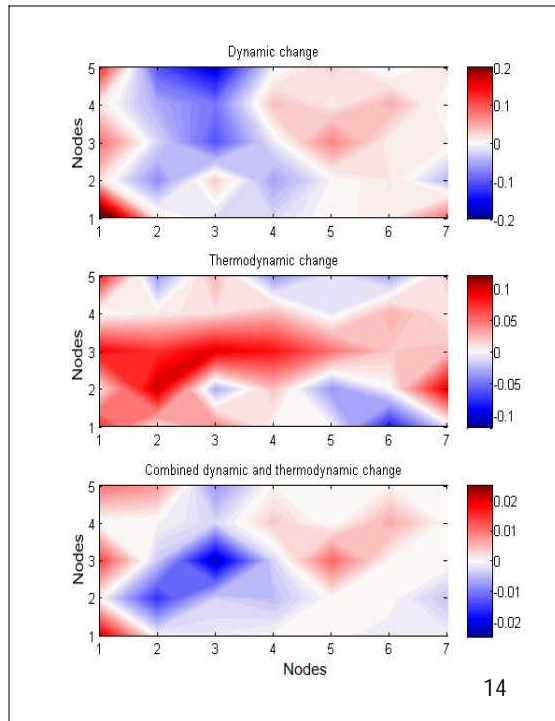
Figure 14. Contributions to the change in moisture flux from 1960-1999 to 2010-2030 (Wm^{-2}) from changes in **(top)** dynamics, **(middle)** thermodynamics and **(bottom)** combined dynamics and thermodynamics change for each cluster.
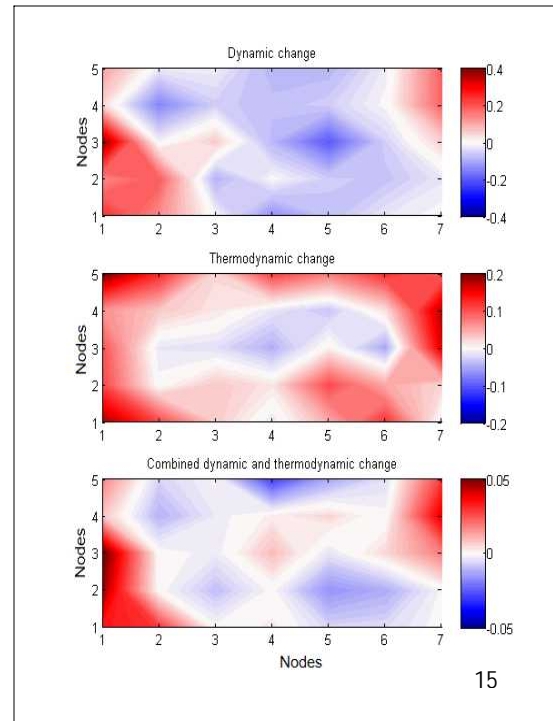
Figure 15. Same as Fig.14 but for period from 2010-2030 to 2070-2089.
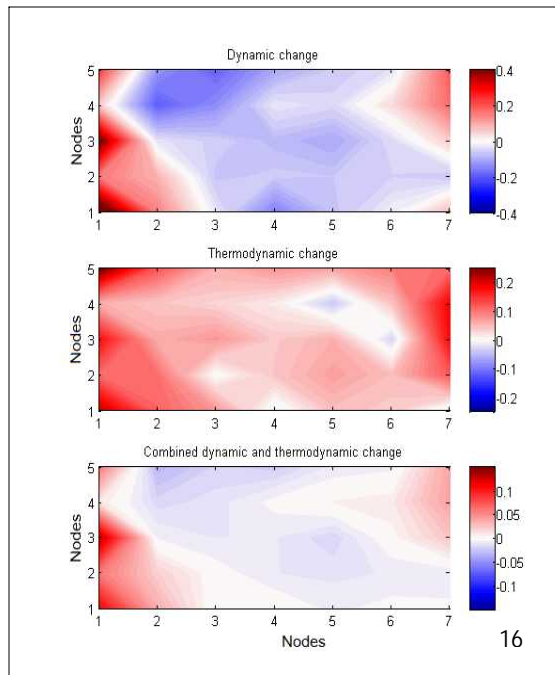
Figure 16. Same as Fig. 14 but for period from 1960-1999 to 2070-2089.

Attribution of Projected Changes in Arctic Moist Static Energy Transport

Natasa Skific[1] and Jennifer A. Francis[2]

[1]Department of Environmental Sciences, Rutgers University

[2]Institute of Marine and Coastal Sciences, Rutgers University

Corresponding author: Natasa Skific, Dept. of Environmental Sciences, 14 College Farm Rd, Rutgers University, New Brunswick, 08901, e-mail: nskific@comcast.net, tel: 732-422-0031, fax: 732-932-8644.

4. Changes in Arctic moist static energy transport

Abstract

We explore annual and seasonal changes in moist static energy transport (MSE) into the Arctic over the next 100 years derived from one simulation of the National Center for Atmospheric Research Community Climate System Model, version 3 (CCSM3). The MSE is the sum of latent heat flux (LH) and dry static energy flux (DSE), computed from multi-level fields of specific humidity, meridional wind, geopotential, and temperature spanning periods in the 20th century (1960 to 1999) and the 21st century (2070 to 2089). The 21st century simulation incorporates the Special Report on Emission Scenarios A2 scenario. Although tropospheric DSE is projected to decrease by about 3.5% by the end of 21st century, it is offset by an increase in LH of about 20% from its 20th century average. The combined changes result in a total annual increase in tropospheric MSE of about 1.6% by the late 21st century, although the largest increase during summer is offset by a decrease during winter. Sea-level pressure fields are classified using a neural-network technique called self-organizing maps to create a set of characteristic atmospheric circulation patterns over the region north of 60°N. By relating moisture transport to a particular circulation regime, future changes in MSE across 70°N are assessed and attributed to factors related to varying atmospheric dynamics and/or thermodynamics. A positive contribution to the MSE related to more frequent low pressure systems in high latitude (dynamic factor) occurs in all seasons, particularly in the summer. An increase in the LH contributes to the MSE increase owing to a strengthening of the poleward moisture gradient (thermodynamic factor). A decrease in

DSE offsets these two effects because of a projected reduction in the poleward temperature gradient. The positive contribution of the thermodynamic factor is largest in summer, while in winter it is negative. The increase in MSE projected for the end of the 21st century constitutes a positive feedback on the Arctic climate system.

4.1. Introduction

Large changes have occurred in the Arctic during recent decades. Glaciers, sea ice, and permafrost are declining (e.g., Serreze et al. 2007; Stroeve et al. 2007), patterns of rain and snowfall are shifting (Finnis et al. 2007), runoff is increasing (Peterson et al. 2002; Holland et al. 2007), and tundra vegetation is becoming shrubbier (Tape et al. 2006; Chapin et al. 2005), to name only a few. These transitions add to the growing body of evidence suggesting that the Arctic is heading toward a new state. Moreover, there are no obvious mechanisms within the Arctic that can reverse this trajectory (Ferguson et al. 2004; Overpeck et al. 2005). The motivation for this study is to explore some of the linkages between the Arctic and global climate system that may influence the sign and pace of high-latitude change.

One such mechanism is the poleward transport of atmospheric moist static energy (MSE), comprising sensible heat, latent heat, and geopotential energy. In the present climate, this component of the Arctic's energy budget supplies approximately 98% of the energy annually radiated to space north of 70°N (Nakamura and Oort, 1988; Overland et al, 1996). The contribution from surface exchanges is small, but seasonally it alternates from an input to the ocean during summer to a net loss during winter. As global-mean

warming continues, the Arctic response will be more pronounced than in lower latitudes because of the predominantly positive feedbacks involving ice and snow. The amplified Arctic warming suggests that the lower-tropospheric poleward temperature gradient will relax, poleward advection of sensible heat will decrease, and Arctic warming will weaken. Although climate model simulations support this reasoning, they also suggest that increases in the poleward transport of latent heat will compensate for the reduction in sensible heat transport (S. Vavrus, pers. comm.).

This study explores how the tropospheric moist static energy flux is projected to change in the late 21st century as the atmospheric CO_2 concentration continues to increase. We utilize a neural network technique called self-organizing maps (SOMs; Kohonen, 2001) to analyze sea-level pressure fields from one simulation by the National Center for Atmospheric Research Community Climate System Model, version 3 (NCAR CCSM3), for periods of 1960-1999 and 2070-2089. The SOM technique is selected for this analysis because it reduces large data sets into representative, fundamental patterns organized in a matrix of 2D fields – geographic maps in this case -- that are expressed in a visual and intuitive rendering. The maps are situated in the matrix relative to one another according to their similarity. For each circulation regime we derive the tropospheric latent heat flux and the flux of dry static energy across 70°N. An approach by Cassano et al. (2007) is used to evaluate the portion of change in each of these fluxes that can be attributed to changes in a parameter representing dynamics, another related primarily to thermodynamics, and a third for the interaction of the two.

Section 2 describes the data sets and a brief overview of the SOM technique. Section 3 explains the master SOM and the characteristics of the 20th century dominant

SLP clusters. Sections 4 - 6 present an analysis of future changes in fluxes of dry static energy, latent heat, and moist static energy, and an approximate attribution of those changes. Conclusions and future directions are discussed in Section 7.

4.2. Data and methodology

4.2.1 Data sets

Multi-level, six-hourly fields of specific humidity, temperature, geopotential, and meridional wind were obtained for a single run of the NCAR CCSM3 with horizontal resolution of about 1.4°. Major features of the model's hydrological cycle compare well to observations (Hack et al. 2006). The 21st century simulation incorporates the Special Report on Emission Scenario (SRES) A2 scenario (Nakicemovic and Swart 2000), which appears to be the most representative of actual emissions (Rahmstorf et al. 2007; Pielke et al. 2008). Realistic forcing is applied before 1990, after which the A2 scenario is employed. Additional details about the model and the A2 scenario are available in Skific et al. (2009a) and Collins et al. (2006a).

The original six-hourly data were interpolated from the hybrid sigma-pressure vertical coordinates to a pressure coordinate system and reduced in size by subsetting from global coverage to the region north of 60ºN, from 6-hourly time resolution to daily resolution (12 UTC only), and from 26 vertical levels to 8 levels (troposphere only). Levels above 300 hPa were not included in this analysis because model fields near and above the tropopause are less reliable (Cordero and Forster, 2006), as are validation data from reanalyses and rawinsondes. In addition, over two-thirds of the atmospheric mass and

virtually all of the water vapor in the Arctic atmosphere exists in the troposphere. The time slices used in this study span 1960-1999 from the 20th century experiment (20C3M), as well as 2010-2030 and 2070-2090 from the SRES A2 scenario. The latter two periods were chosen to be consistent with results from the Arctic Climate Assessment Report (ACIA 2004, www.acia.uaf.edu; Serreze and Francis, 2006), to represent the so-called emerging and mature greenhouse states. Sea-level pressure (SLP) fields are extracted for the same time periods. The 2010-2030 period is used only to increase the number of daily samples to train the SOM algorithm. The SLP fields are interpolated from the original 1.4º x 1.4º grid to a 200 km x 200 km Equal Area-Scalable Earth (EASE) grid (Armstrong et al, 1997; http://nsidc.org/data/ease/), covering the area north of 60ºN with 51 x 51 grid points. The EASE grid helps avoid errors that arise due to equal weighting of the original latitude-longitude grid boxes in the self-organizing map algorithm.

Daily sea-level pressure fields from the European Centre for Medium-Range Forecasts (ECMWF) Reanalysis (ERA-40; Upala et al. 2005) were also interpolated to the EASE grid. They were used to construct the SOM and to validate the model results for the 20th century. The results of this validation are presented in Skific et al. (2009a) and will be only briefly described here.

4.2.2. Self-organizing maps (SOMs)

A self-organizing map (SOM) algorithm is a neural-network technique that attempts to reduce the dimensions of a large data set by organizing it into a two-dimensional array or matrix (Kohonen 2001). For this study, the data set used for the SOM analysis consists of a time series of 2D fields of SLP over the Arctic from both

ERA-40 and CCSM3. The SOM algorithm organizes the daily fields into clusters of similar maps by identifying SLP patterns that represent the range present in the original data set. The 2D maps in the SOM matrix provide a more intuitive rendering of pattern characteristics and their relative frequency of occurrence than is achieved by other statistical tools, such as empirical orthogonal functions.

A complete description of the SOM method is presented in our companion paper, Skific et al. (2009a), and we present only a brief discussion of the mechanics here. The initial step is the creation of a first-guess set of maps consisting of an arbitrary number of SLP patterns, which are called reference vectors. Each of these reference vectors has a position or node assigned on a two-dimensional array. The size of the matrix is chosen to balance having enough nodes to capture the important features in the data while being small enough to visually interpret the patterns and display them conveniently. In this study we use a 7x5 matrix; the results are insensitive to small changes in this size (Skific et al. 2009a). The first-guess reference vectors are the two eigenvectors, derived from the covariance matrix of the SLP fields with the largest eigenvalues. The vectors are then "trained" by presenting each daily field to the SOM, and the similarity between the data sample and each of the reference vectors is then calculated, usually as a measure of Euclidean distance in space. The "best match" reference vector is identified and further refined in an iterative process through which the centroids of the clusters of daily maps matched to each node are modified to minimize the distances between the samples and the reference vectors. The resulting clusters of maps that belong to each node become organized on a 2-dimensional array in such a way that more similar patterns are placed

closer together, while those less similar are farther apart, allowing a more intuitive interpretation of patterns and their relationship to each other in the matrix.

The SOM method is applied to finding dominant patterns in the daily sea-level pressure anomaly fields from ERA-40 (1958-2001) and from CCSM3 for periods 1960-1999, 2010-2030, and 2070-2089 for the region north of 60°N. Fields from the period of 2010-2030 are included in the SOM training to increase the number of steps in the final convergence phase, which must be sufficiently long to achieve good statistical accuracy (Kohonen 2001). Daily SLP anomalies are created by subtracting the domain-averaged SLP for each daily map from the SLP at each grid point on that day. As argued by Cassano et al. (2007), these anomalies are a better representation of the SLP patterns, as eliminating the daily mean focuses the classification procedure on pressure gradients, which are a better representation of circulation features. Areas of elevation higher than 500 m are removed from the fields because pressure reduction to sea level in the areas of high elevation can lead to unrealistic patterns.

Once the SOM has been trained and the final set of reference vectors has been identified, daily fields of SLP anomalies can be mapped to the best-matching pattern to form clusters of daily maps that are most similar to each pattern. This is achieved by finding the pattern in the SOM that minimizes the Euclidean distance between itself and the daily field. Once all the SLP anomaly fields have been assigned to a node, the frequencies of occurrence can be determined, i.e., the fraction of daily fields that reside in each cluster.

Ascribing a particular daily SLP sample to a specific circulation pattern in the SOM is also useful for analyzing associated variables for the same days as those in each

cluster. By mapping the new variable onto a particular SLP-derived cluster, the matrix of maps for any other variable can be used to describe the conditions associated with a specific circulation regime. In this study, we apply this technique to investigating the characteristics and changes in the horizontal energy fluxes across 70°N. Details of this procedure are available in Skific et al. (2009a,b).

4.3 Derivation of daily fields of latent heat and dry static energy fluxes

To calculate the total latent heat flux across 70°N in units of W m^{-2}, we follow the equation given in Overland et al. (1996):

$$F_q = \iint L[\overline{vq}]\frac{dxdp}{g} \, ,$$

where the operator $[A]$ indicates a zonal mean, $\overline{A}$ is a time mean, g is gravity ($g = 9.8$ ms^{-1}) and L is the latent heat of vaporization ($L = 2.5\text{x}10^6$J kg^{-1}). After calculating the zonal mean of the time-averaged meridional moisture flux for each tropospheric level, we integrate the level-mean values over the latitude band. The expressions are then integrated vertically and divided by the area north of 70°N to obtain units of W m^{-2}.

An analogous expression is used to calculate the dry static energy flux (DSE) across 70°N (F$_{dse}$), consisting of the sum of sensible heat and geopotential energy fluxes:

$$F_{dse} = \iint c_p[\overline{vT}]\frac{dxdp}{g} + g\iint[\overline{vz}]\frac{dxdp}{g} \, ,$$

where c_p is the specific heat of air under constant pressure ($c_p = 1000$ Jkg^{-1}K^{-1}), T is temperature, and z is geopotential. We calculate daily values of DSE for available tropospheric levels. To obtain units of W m^{-2} we integrate values of vT and vz at each level over the latitude band, then integrate vertically, and finally divide this quantity by

the area north of 70°N. The moist static energy flux (MSE) across 70°N is the sum of the dry static energy flux and latent heat flux.

4.3.1 SOM of Arctic SLP Patterns

The self-organizing map of SLP anomalies north of 60°N is presented in **Fig. 1**. The matrix of maps represents the dominant circulation regimes in which the atmosphere tends to reside according to the data sets used to create it, and is hereafter called the "master SOM." Familiar features in the high-latitude pressure fields are evident, such as the Icelandic and Aleutian low pressure centers typical of winter (bottom right), Beaufort highs (upper right), and central-Arctic lows of summer (bottom left). Less distinct patterns are located near the center of the SOM. The frequency of occurrence (FO) is defined as the percent of days that map into a particular cluster out of the total number of daily fields. Values that are significantly different ($>$ 95% confidence) from an expected value for a random binomial distribution (i.e., $100\% \div 35 = 2.86\%$) are assessed. The confidence test includes an adjustment for the serial correlation and consequent reduction in degrees of freedom by dividing the number of samples by 7, as the atmosphere tends to maintain a circulation regime for approximately one week. This results in a higher threshold for determination of a significance level. For more details see Skific et al, 2009a and Cassano et al, (2007).

The frequencies of occurrence of 20th century CCSM3 SLP patterns (**Fig. 2**) show that the bordering clusters, which tend to feature pronounced gradients, occur more frequently than those positioned in the middle of the SOM. While the distribution of FOs for the

model fields does not reveal a dominance of any particular group of clusters, the real atmosphere does exhibit a preference for the regimes appearing in the middle of the SOM, which are characterized by moderate high pressure over the central Arctic. **Figure 3** presents the seasonal differences in FO between the 20th-century time slice from the CCSM3 realization and from ERA-40. The clusters in the upper-middle portion of the master SOM, characterized by moderate high pressure over the central Arctic, appear more frequently in ERA-40 during fall through spring, while the CCSM3 patterns in the bordering clusters have a higher FO. In summer, the modeled fields have a higher FO of patterns with stronger low pressure in the central Arctic (left side of the SOM). These differences are consistent with the assessment of Arctic atmospheric circulation in CCSM3 by DeWeaver and Bitz (2006). Although the differences in the distribution frequencies and SLP climatologies appear substantial, one should note that this comparison is between two single realizations of the 20th century climate, and some difference would be expected in any two representations. Moreover, studies by Cassano et al. (2007) and Chapman and Walsh (2007) found that the CCSM3 model is one of the most realistic of the group participating in the Intergovernmental Panel on Climate Change Fourth Assessment Report in simulating Arctic atmospheric circulation. Skific et al, (2009a) also found that this model simulation realistically simulates 20th century moisture flux across 70°N. One should also note that the SLP patterns themselves differ very little from one time slice to another, as explained in Skific et al. (2009a).

4.4 Attribution of annual and seasonal changes in moist static energy flux (MSE)

In this section we explore mechanisms leading to annual and seasonal changes in the CCSM3 moist static energy flux (MSE) across 70°N from the 20th century to the late 21st century. The MSE is separated into contributions from the dry static energy flux and the latent heat flux.

Dry static energy flux

The total change in the annual-mean dry static energy flux (DSE), as well as that for each season, is presented in the top panel of **Fig. 4**. As expected, the total flux decreases by the end of the 21st century in this model simulation by about 2 Wm^{-2} (3.5%). Reduced fluxes during spring, fall, and winter are offset by a small (by percent) gain during summer. The change in sensible heat transport accounts for about 70% of this reduction, as Arctic amplification alters the thermal driving of the equator-to pole temperature difference, and generates reduction in the eddy sensible heat transport.

To better understand the causes of these changes, we apply an attribution method introduced by Cassano et al, (2007) in their investigation of changing net precipitation in the Arctic. The method separates contributions owing to a change in the distribution of atmospheric circulation patterns, as described by the maps in the SOM, from changes in a variable for any one of the fixed circulation patterns in the SOM. Effects of interactions between these two factors are also accounted for. The future, domain-averaged value of a quantity is the initial value plus the temporal change, $x + \Delta x$, which consists of the sum of changes in the cluster-average values, $x_i + \Delta x_i$ for each cluster from i=1 to N (N=35 in

this study), weighted by the change in the frequency with which the atmosphere resides

in each cluster pattern, $f_i +$ f_i. With some rearrangement, the expression is:

$$\Delta x = \sum_{i=1}^{N} (x_i + \Delta x_i)(f_i + \Delta f_i) - x_i f_i \quad , \qquad (1)$$

or after expansion:

$$\Delta x = \sum_{i-1}^{N} (x_i \Delta f_i + f_i \Delta x_i + \Delta x_i \Delta f_i) \qquad (2)$$

The first term on the right of Eq. 2 represents the effects of changing frequencies

of occurrence for each pattern in the SOM, hence we refer to this term as the dynamic

factor. The second term captures changes in a variable within a SOM cluster. Because

changes in energy fluxes within a particular pattern are likely to be caused by primarily

(but not exclusively) thermodynamic effects, such as changing poleward gradients, we

refer to this term as the thermodynamic factor. The third term captures a combination of

the two, and tends to be relatively small.

The difference in FO f_i between the CCSM3 late 21st century (2070-2089) and

the 20th century (1960-1999) is shown in **Fig. 5**. The FO of the patterns on the left and

upper right side of the master SOM increase in the future. Patterns in the middle,

characterized by weak or moderate high pressure over the Arctic, decrease in FO in this

model simulation. These changes suggest that by the end of the 21st century, the Arctic

will experience generally lower pressure and likely increased storminess. The cluster-

averaged DSE, x_i, for the 20th century is shown in **Fig. 6.** The largest transports of DSE

occur for patterns with pronounced low pressure in the N. Atlantic that are found along

the right of the master SOM and for those with low pressure over the central Arctic on the left. Patterns in the middle with high pressure over the central Arctic generally do not bring much DSE into high latitudes.

The temporal change in the cluster-averaged DSE x_i is shown in **Fig. 7**. Because the sign of the second term in Eq. 2, or the thermodynamic factor, is determined by the sign of x_i, its contribution to the total change in the DSE will clearly be negative except for a few clusters along the edges of the map. The third term in Eq. 2 represents the contribution from the interaction of both changing pattern frequency and the cluster-averaged variable. This contribution tends to be relatively small.

To investigate seasonal changes and their attributions, we calculate and present the components of the three terms in Eq. 2 for each season. The FOs (f_i) for the 20th century, along with statistically significant differences from a uniform distribution, are shown in **Fig. 8,** and the corresponding cluster-averaged DSE (x_i) for the 20th century are displayed in **Fig. 9**. Summer patterns tend to occupy clusters toward the left of the master SOM more frequently, which are characterized by either a relatively diffuse pressure pattern or weak-to-moderate low pressure over the central Arctic. In winter there is a clear dominance of the clusters to the right of the SOM, corresponding to a strong Icelandic low in the Atlantic sector, a well-developed Aleutian low in the Pacific, or a high pressure over the western Arctic. Spring and autumn FOs are relatively evenly distributed throughout the SOM matrix. A common characteristic in the seasonal cluster-averaged DSE (**Fig. 9**) is weak energy transport for the clusters in the middle and strong energy transport for those along the left of the SOM. Low pressure over the central Arctic generally favors increased transport of DSE poleward across 70°N. The clusters to the right of the SOM, associated with low pressure in the Atlantic sector, generate strong

energy transport in the winter season. The energy flux is generally the weakest in fall and summer, when the poleward temperature gradient and horizontal sensible heat flux are also weakest.

The changes from the 20th to late 21st century by season are presented in **Figures 10 (** f_i**) and 11 (** x_i**).** Circulation patterns to the left of the master SOM (low pressure over the Arctic) are projected to become more frequent in all seasons, particularly during summer, in this model simulation. The patterns to the right of the SOM (low pressure in the Atlantic sector and eastern Arctic) will also occur more frequently. Patterns in the middle of the SOM (high pressure over the central Arctic) are projected to become less frequent in all seasons, particularly in the summer. The cluster-averaged dry static energy flux (**Fig. 11**) is projected to decrease for most nodes in the SOM and in all seasons, although the organization by pattern type is not distinct.

Using the attribution method described previously, we derive each of the terms in Eq. 2 to obtain the contributions to the total change in DSE by the dynamic, thermodynamic, and combined factors. The first column in **Figure 12** presents the annual and seasonal results. Dry static energy flux across 70°N decreases by about 2 W m^{-2} (3.5%), which is driven by the reduction in the thermodynamic term of approximately 2.4 W m^{-2}. The dynamic factor increases slightly owing to an increased frequency of circulation patterns that are characterized by low pressure in the central Arctic and north Atlantic sector by the end of the 21st century. These pressure patterns favor strong northward transport of sensible heat and geopotential energy. The largest changes in the dynamic term occur in fall and summer, but they are relatively small in all seasons. The reduction in the thermodynamic term arises from the general decrease in cluster-average

fluxes **(Fig. 11).** Amplification of Arctic warming during fall through spring reduces the poleward temperature gradient, resulting in reduced sensible heat advection and consequently, DSE. The reduction is driven mainly by the reduction in eddy sensible heat transports, acting to suppress initial perturbation in meridional temperature gradient (Held and Soden 2006; Hartmann 1994). Amplification is weaker in summer (Teng et al, 2006), so the reduction in the poleward temperature gradient is small, as is the change in dry static energy flux. The contribution by the combined factor to the total change, both annually and seasonally, is small.

Latent heat flux

Changes in latent heat flux (LH) across 70°N were discussed in detail in Skific et al, (2009a). The results are summarized here but from a different perspective, consistent with that for the dry static energy flux.

Daily fields of latent heat flux are associated with particular circulation patterns in the SOM as described for the DSE. The cluster-averaged values of the LH across 70°N are presented in **Fig. 13**. There are many similarities between this and the cluster-averaged DSE shown in **Fig 6**. Red areas correspond to clusters in the master SOM characterized by strong low pressure in the north Atlantic and central Arctic, both of which tend to advect large quantities of moisture poleward. The seasonal contributions to the 20th century cluster-average LH appear in **Fig. 14**. The largest poleward transports of moisture occur in the summer, primarily because of the deeper moist layer and more poleward wind vectors (Groves and Francis 2002), which together lead to stronger advection in upper levels. Once again, the patterns in the right half and far left of the SOM contribute

most. Even though the temperature gradient is weak during summer, the gradient in moisture is strong and cyclones penetrate farther northward, driven by baroclinicity that is sustained by land/ocean differential heating and augmented by the coastal orography (Serreze and Barry 2005). The LH is weakest during winter, as the moist layer is shallow and often capped by a strong surface-based inversion. Clusters in the lower right of the master SOM, corresponding to low centers in the north Atlantic and Pacific, are effective in transporting moisture during all seasons. These systems become well developed and particularly vigorous in the winter when baroclinicity is enhanced by strong north-to-south, land-sea, and ocean-atmosphere temperature gradients. Because the specific humidity is low in winter, however, the moisture transport is less than in other seasons. As in the case for the DSE, patterns in the middle of the SOM (associated with high pressure over central Arctic) are associated with low moisture transport in all seasons.

The projected annual and seasonal changes in CCSM3 latent heat flux across 70°N from the 20th to the late 21st century are presented in the middle panel of **Fig. 4**. By the end of the century, the annual LH increases by approximately 3 W m^{-2}, owing to increased atmospheric water vapor content and enhanced meridional moisture gradients. The largest increase in moisture transport occurs in summer (about 1 W m^{-2}), which accounts for about 31% of the total change. Winter, spring, and fall contribute approximately 25%, 22%, and 22%, respectively.

To better understand the causes of these changes we again apply the method for separating contributions from the dynamic, thermodynamic, and combined terms in Eq. 2 to the total change by the end of the century. The total change in cluster-averaged latent heat flux x_i is presented in **Fig. 15**. It is obvious that by the late 21st century, latent heat

flux increases in the majority of circulation patterns on the master SOM, as is also the case for the seasonal contributions displayed in **Fig 1 6**. As stated previously, these changes will determine the sign of the thermodynamic term in Eq. 2 because the annual and seasonal FOs for the 20th century f_i are always positive. The three terms in Eq. 2 are calculated for the LH using the same methodology as for the DSE.

The second column of **Fig. 12** shows total annual and seasonal changes in the latent heat flux, along with contributions from the dynamic, thermodynamic, and combined terms. The thermodynamic factor clearly plays a dominant role and is responsible for approximately 80% of the total change in latent heat flux across 70°N, annually and in each season. Thermodynamic effects are caused by an increased atmospheric moisture content and poleward moisture gradient, both of which lead to a larger transport of poleward moisture. The dynamic term accounts for about 16% of the total annual change, while 3% is due to the combined term. The positive dynamic term is related to the statistically significant increase in FO of clusters to the left of the SOM, corresponding to low pressure over the central Arctic that generally transports substantial moisture into the Arctic. In addition, the FO decreases for patterns in the middle of the SOM, which are associated with high pressure over the central Arctic and generally bring little moisture poleward.

The largest increase in poleward latent heat flux occurs in summer owing to the exponential relationship between saturation vapor pressure and temperature. In the warmer low latitudes, a given increase in temperature will lead to a relatively larger increase in saturation vapor pressure, and presumably vapor pressure, than that at higher latitudes for the same warming, which results in an increased poleward specific humidity

gradient. In summer, high-latitude poleward temperature gradients, and thus moisture gradients, are also sustained by regional land-ocean differential heating. The contribution by the dynamic term is largest in summer because statistically significant changes in FO tend to occur mainly for summer patterns (**Fig. 10**), which tend to favor a convergent circulation and larger poleward moisture fluxes.

During fall the dynamic term plays a relatively large role in the total LH change (~30%) owing to the statistically significant increase in the FO of patterns with low pressure over the central Arctic and North Atlantic **(Fig. 10),** both of which favor increased poleward moisture transport **(Fig. 14).** The thermodynamic term still dominates, however, accounting for over half of the total increase in fall moisture transport. The combined factor accounts for a small but non-negligible portion of the change (14%). Physically this may arise through an increased surface flux of moisture owing to stronger, more poleward winds or perhaps a change in circulation owing to latent heat release through condensation.

In spring and winter the total change in moisture flux from the 20th to late 21st century is governed mainly by the thermodynamic term. In winter, changes in the dynamic factor play the smallest role of any season – about 3% of the total winter increase. Although a statistically significant increase in FO of clusters in the upper right and left corners of the master SOM occurs in winter, these patterns do not have the potential to bring substantial amounts of moisture into the Arctic in the winter season **(Fig. 14).** These results clearly suggest that thermodynamic processes are responsible for the projected changes in the poleward latent heat flux in all seasons, with dynamics playing a secondary role.

Moist static energy flux

Changes in the poleward fluxes of latent heat and dry static energy, along with the mechanisms responsible for the changes, can be combined to evaluate total annual and seasonal change in the poleward moist static energy transport projected for the end of the 21st century. The percentage change in MSE is presented in the bottom panel of **Fig. 4**. In this model realization the total change in MSE across 70°N is small (about 1 W m^{-2} or 2%) and positive, driven primarily by an increase in summer that results from positive changes in both the dry static energy and latent heat fluxes. The winter change in MSE offsets the summer gain partially, and the changes during transition seasons are small owing to changes of similar magnitudes but different signs in the component fluxes. This result suggests that as greenhouse gases increase, the MSE flux from low latitudes into the Arctic will augment the already amplified warming in the Arctic, thereby constituting a positive feedback.

As for the dry static energy and latent heat fluxes, we assess the contributions to MSE changes by the three terms in Eq. 2. A summary of the results appear in the right column of **Fig. 12**. In the annual mean, the total MSE increase results from positive contributions from all three terms, with the dynamic factor contributing most. This conclusion in somewhat misleading in assessing attribution, however, because changes in the thermodynamic factor dominate in each individual season. Spring and summer changes (about 3% and 9%) are driven primarily by the thermodynamic term through an increased latent heat flux, augmented by an increase also in the dynamic term during summer. During fall and winter the smaller increases in the thermodynamic factor via LH are opposed by decreasing DSE owing mostly to suppression of large deviations of the

meridional temperature gradient by eddy heat fluxes. Consequently, the MSE during these seasons (approximately 1% and 2%, respectively) is reduced overall. .

The projected reduction in dry static energy flux compensates for about 66% of the increase in latent heat transport into the Arctic. Partial compensation for an increase in latent heat flux by the sensible heat flux is also demonstrated by Held and Soden (2006), who analyze an ensemble of fully coupled general circulation models (GCMs) forced by the SRES A1B scenario, which represents a less pessimistic estimate of future greenhouse gas emissions than the A2 scenario that forced the simulation used in our study. An earlier study by Manabe and Wetherland (1975) that explored the equilibrium responses of GCMs to warming also reveals partial compensation of a projected moisture transport increase by decreases in dry static energy.

4.5. Conclusions

The analysis presented here applies a neural-network technique called self-organizing maps (SOMs) to one simulation by NCAR's CCSM3 global climate model forced by increasing greenhouse gases. We explore projected changes in the poleward moist static energy flux in the troposphere across 70°N from the 20th to the late 21st century. Using a concept adopted by Cassano et al. (2007), this research also attempts to attribute these annual and seasonal changes to predominantly dynamic or thermodynamic mechanisms.

The transport of moist static energy is projected to increase in spring and summer, and decrease in fall and winter. The largest increase occurs in summer, and the total annual change is approximately 2% by the end of the 21st century. Based on this model realization, we conclude that *changes in the MSE, forced by realistic increases in greenhouse gas concentrations, will constitute a positive feedback onto the Arctic climate system.*

The moist static energy flux is the sum of the dry static energy and latent heat fluxes. Although the tropospheric dry static energy flux is projected to decrease by about 3.5% by the end of 21st century, it is opposed by a larger increase in the latent heat flux of about 21% from its 20th century average. These combined changes yield a total increase in the transport of tropospheric moist static energy of about 2% by the late 21st century.

The SOM technique provides a means to separate contributions to these changes from factors relating to dynamics or thermodynamics. The increase in MSE is partially due to positive contributions in all seasons from changes in the frequency of occurrence with which the atmosphere resides in particular representative circulation patterns, as identified by the SOM classification technique. Patterns that feature predominant low pressure centers in the Arctic are effective at transporting MSE poleward, and their increased frequency of occurrence accounts for much of the positive dynamic contribution. Despite the apparent importance of dynamic effects to the annual MSE change, the seasonal differences in the thermodynamic factors are more illuminating as to the mechanisms at work.

Summer exhibits the largest seasonal increase of moist static energy (9% larger than the 20th century value). The FO of high-latitude cyclones increases most in the warm

season, which accounts for about 40% of the enhanced MSE. Two opposing thermodynamic effects are responsible for the rest. A slight weakening of the poleward temperature gradient in the future, which reduces the eddy sensible heat transport, makes a small negative contribution. The dominant influence, however, is an increased flux of latent heat, resulting from a stronger poleward moisture gradient and higher water vapor content. Spring is very similar to summer in terms of contributions to the total MSE, except the dynamic factor is not a significant influence.

In fall and winter the pieces of the puzzle align very differently. In both seasons the change in MSE is negative, albeit more so in winter. While the contribution from latent heat fluxes is still positive and results almost exclusively from thermodynamic effects, it is overwhelmed by a negative contribution from the dry static energy flux. Polar amplification of warming in the future is responsible for this reduction in DSE, as advection of sensible heat is reduced.

During the summer of 2004 a group of experts on various aspects of the Arctic climate system spent a week comparing recent observations and discussing possible implications for the future. They concluded that the Arctic system appeared to be headed for a new seasonally ice-free state (Overpeck et al, 2005). They also suggested that there appeared to be no feedback mechanisms within the Arctic that were capable of diverting this trajectory, but that perhaps interactions with lower latitudes would eventually slow the pace of Arctic change. Changes in poleward energy transport were identified as one possible mechanism. It appears that this is not the case: while only one realization from one global climate model was used in this study, the results suggest that changes in

atmospheric MSE flux will exacerbate, not alleviate, the trajectory of change in the Arctic.

References:

Arctic Climate Impact Assessment (ACIA), 2004: Impacts of a Warming Arctic. Cambridge University Press , New York, New York.

Armstrong, R, M. J. Brodzik, and A. Varani, 1997: The NSIDC EASE-Grid: Addressing the need for a common, flexible, mapping and gridding scheme. *Earth System Monitor*, **7(3),** 3 pp.

Cassano, J.J, P. Uotilla, A.H. Lynch, E.N. Cassano, 2007: Predicted changes in Synoptic Forcing of Net Precipitation in Large Arctic River basins During the 21st century, *J. Geoph. Res- Biogeosciences*, **112**, G04S49, doi:10.1029/2006JG000332.

Chapin, F.S. III, Sturm, M., Serreze, M.C., McFadden, J.P., Key, J.R., Lloyd, A.H., McGuire, A.D., Rupp, T.S., Lynch, A.H., Schimel, J.P., Beringer, J., Chapman, W.L., Epstein, H.E., Euskirchen, E.S., Hinzman, L.D., Jia, G., Ping, C.L., Tape, K.D., Thompson, C.D.C., Walker, D.A. and Welker, J.M., 2005: Role of land-surface changes in Arctic summer warming. *Science,* **310**, 657-660.

Chapman, W.L. and J.E. Walsh, 2007: Simulations of Arctic temperature and pressure by global coupled models. *J. Clim*., **20**, 609-632.

Collins, W. D., C.M. Bitz, M.L Blackmon, G.B. Bonan, C.S. Bretherton, J.A. Carton, P. Chang, S.C. Doney, J.J Hack, T.B. Henderson, J.T. Kiehl, W.G. Large, D.S. McKenna, B.D. Santer, and R.D. Smith, 2006a: The Community Climate System Model Version 3 (CCSM3). *J. Climate,* **19**, 2122-2143.

Cordero, E.C. and P.M. de F. Forster, 2006: Stratospheric variability and trends in IPCC model simulations, *Atmos. Chem. Phys. Disc.,* **6**, 7657-7695.

DeWeaver, E., and C.M. Bitz, 2006: Atmospheric circulation and Arctic sea ice in CCSM3 at medium and high resolution. *J. Climate*, **19,** 2415-2436.

Ferguson, D. and members of ARCSS Committee, 2004: Arctic system synthesis encourages program integration. *Witness the Arctic*, **11***,* 8-9.

Finnis, J., M. M. Holland, M. C. Serreze, and J. J. Cassano, 2007: Response of Northern Hemisphere extratropical cyclone activity and associated precipitation to climate change, as represented by the Community Climate System Model. *Journal of Geophysical Research,* **112**, G04S42, doi:10.1029/2006JG000286.

Groves, D.G., and J.A. Francis, 2002: The moisture budget of the Arctic atmosphere from TOVS satellite data, *J. Geophy. Res*., **107**(D19), 1-21.

Hack, J.J., J.M. Caron, S.G. Yeager, K.W. Oleson, M.M. Holland, J.E. Truesdale, and P.J. Rasch, 2006: Simulation of the global hydrological cycle in the CCSM Community Atmospheric Model, Version 3 (CAM3): Mean features. *J. Climate*, **19**, 2199-2221.

Hartmann, D.L., 1994: *Global Physical Climatology*. Academic Press, 409 pp.

Held, I. M., and B. J. Soden, 2006: Robust responses of the hydrological cycle to global warming. *Journal of Climate,* **19(21),** 5686-5699.

Holland, M.M., J. Finnis, and M.C. Serreze, 2007: Simulated Arctic Ocean freshwater budgets in the twentieth and twenty-first centuries. *J. Clim.,* **19,** 6221-6242.

Intergovernmental Panel on Climate Change, 2007: Climate Change 2007: The Physical Science Basis. Contribution of Working Group I to the Fourth Assessment Report of the Intergovernmental Panel on Climate Change [Solomon, S., D. Qin, M. Manning, Z. Chen, M. Marquis, K.B. Averyt, M. Tignor and H.L. Miller (eds.)]. Cambridge University Press, Cambridge, United Kingdom and New York, NY, USA, 996 pp.

Kohonen, T., 2001:*Self-organizing maps*. 3d ed. Springer-Verlag, 501 pp.

Manabe, S., and R. T. Wetherald, 1975: The effect of doubling CO_2 concentration on the climate of the general circulation model. *J. Atmos. Sci.,* **32,** 3–15.

Nakamura, N. and A.H. Oort, 1988: Atmospheric heat budgets of the polar regions. *J. Geophys. Res.,* **93***,* 9510-9524.

Nakicemovic, N. and R. Swart, 2000: *Intergovernmental Panel on Climate Change Special report on Emission Scenarios*. Cambridge University Press, 570 pp.

Overland, J.E., P. Turet, and A.H. Oort, 1996: Regional variations of moist static energy flux in the Arctic. *J. Climate*, **9**(1), 54-65.

Overpeck, J. T., M. Sturm, J. A. Francis, D. K. Perovich, M. C. Serreze, R. Benner, E. C. Carmack, F. S. Chapin III, S. C. Gerlach, L. C. Hamilton, L. D. Hinzman, M. Holland, H. P. Huntington, J. R. Key, A. H. Lloyd, G. M. MacDonald, J. McFadden, D. Noone, T. D. Prowse, P. Schlosser, and C. Vörösmarty, 2005: Arctic System on Trajectory to New, Seasonally Ice-Free State. *EOS*, **86**, 309-316.

Peterson, B.J., R.M. Holmes, J.W. McClelland, C.V. Vorosmarty, R.B. Lammers, A.I. Shiklomanov, I.A. Shiklomanov, and S. Rahmstorf, 2002: Increasing river discharge to the Arctic Ocean. *Science*, **13**, 2171-2173.

Pielke, R., T. Wigley, and C. Green, 2008: Dangerous assumptions. *Nature,* **452**, 531-532.

Rahmstorf, S., A. Cazenave, J.A. Church, J.A. Hansen, R.F. Keeling, D.E. Parker, and R.J. Somerville, 2007: Recent climate observations compared to projections. *Science*, **316**, 709.

Serreze, M.C., and R.G. Barry, 2005: *The Arctic Climate System*. Cambridge University Press, 146 pp.

_____, and J.A. Francis, 2006: The Arctic on the fast track of change. *Weather,* **61**, 3.

_____, M. M. Holland, and J. Stroeve, 2007: Perspectives on the Arctic's shrinking sea-ice cover. *Science,* **315(5818),** 1533-1536. doi:10.1126/science.1139426.

Skific, N., J.A. Francis, and J. J. Cassano, 2009a: Attribution of projected changes in atmospheric moisture transport in the Arctic: A self –organizing map perspective. *J. Clim.,* accepted.

Skific, N., J.A. Francis, and J. J. Cassano, 2009b: Attribution of seasonal and regional changes in Arctic moisture convergence. *J. Climate*, submitted.

Stroeve, J., M. M. Holland, W. Meier, T. Scambos, and M. Serreze, 2007: Arctic sea ice decline: Faster than forecast. *Geoph. Res. Letters,* **34**, L09501. doi:10.1029/2007GL029703.

Tape, K., M. Sturm, C. Racine, 2006: The evidence for shrub expansion in northern Alaska and the pan-Arctic. *Global Change Biology*, **12,** 686-702.

Teng, H., W.M. Washington, G.A. Meehl, L.A. Buja and G.W. Strand, 2006: 21st Century Arctic Climate Change in the CCSM3 IPCC Scenario Simulations. Climate Dynamics, doi: 10.1007/s00382-005-0099-z.

Uppala, S.M., P.W. Kallberg, A. J. Simmons, U. Andrae, V.D. Bechtold, M, Fiorino, J.K. Gibson, J. Haseler, A. Hernandez, G. A. Kelly, X. Li, K. Onogi,S. Saarinen, N. Sokka, R. P. Allan, E. Andersson, K. Arpe, M. A. Balmaseda, A. C. M. Beljaars, L. Van De Berg, J. Bidlot, N. Bormann, S. Caires, F. Chevallier, A. Dethof, M. Dragosavac, M. Fisher, M. Fuentes, S. Hagermann, E. Holm, B.J. Hoskins, L. Isaksen, P.A.E.M. Janssen, A.P. McNally, J.F. Mahfouf, J.J. Morcreete, N.A. Rayner, R.W. Saunders, P. Simon, A. Sterl, K. E. Trenberth, A. Untch, D. Vasiljevic, P. Viterbo, and J.Wollen, 2005: The ERA-40 reanalysis. *Quart. J. Royal. Met. Soc*., **131**, 2961-3012.
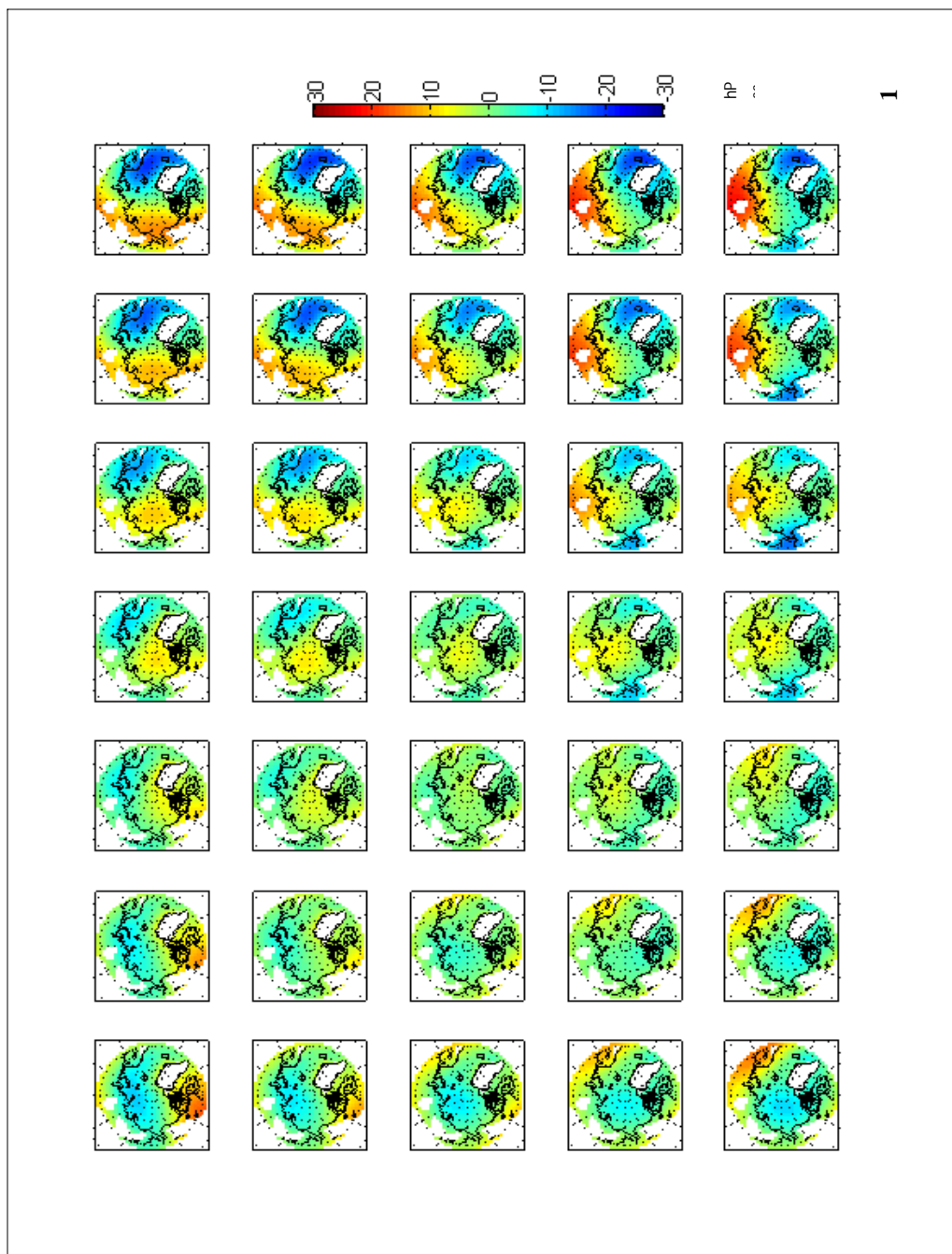
Figure 1: Master SOM of sea level pressure anomalies derived from daily SLP anomaly fields CCSM3 (1960-1999, 2010-2030, and 2070-2089), and from ERA-40 (1958-2001), units of hPa.
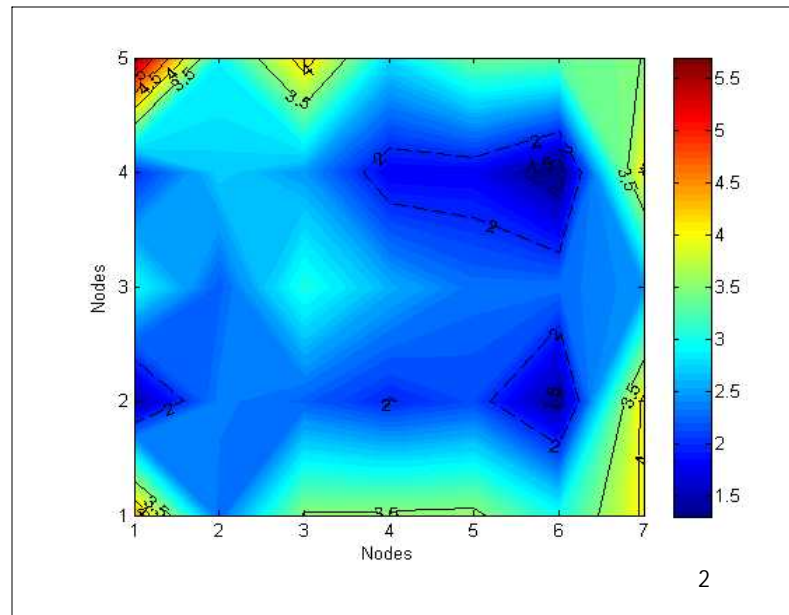
Figure 2: Frequency of occurrence of modeled daily sea-level pressure anomaly maps during 1960-1999. Frequencies show percent of days out of a total that map to a particular SLP node. Black solid (dashed) lines indicate significantly higher (lower) frequencies at the 95% confidence level.
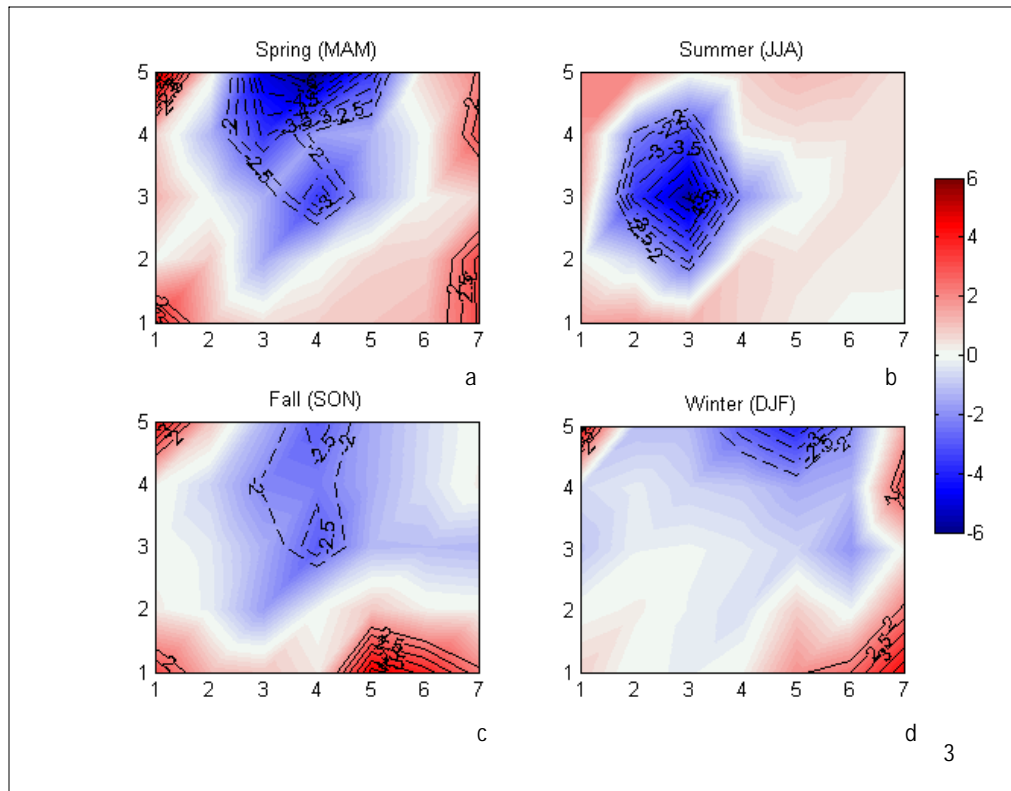
Figure 3: Differences in the frequencies of occurrence between CCSM3 20th century experiment and ERA-40 for: **a** spring (MAM); **b** summer (JJA); **c** fall (SON); **d** winter (DJF). Areas where model is significantly larger (smaller) are marked with solid (dashed) line. Level of confidence is 95%.
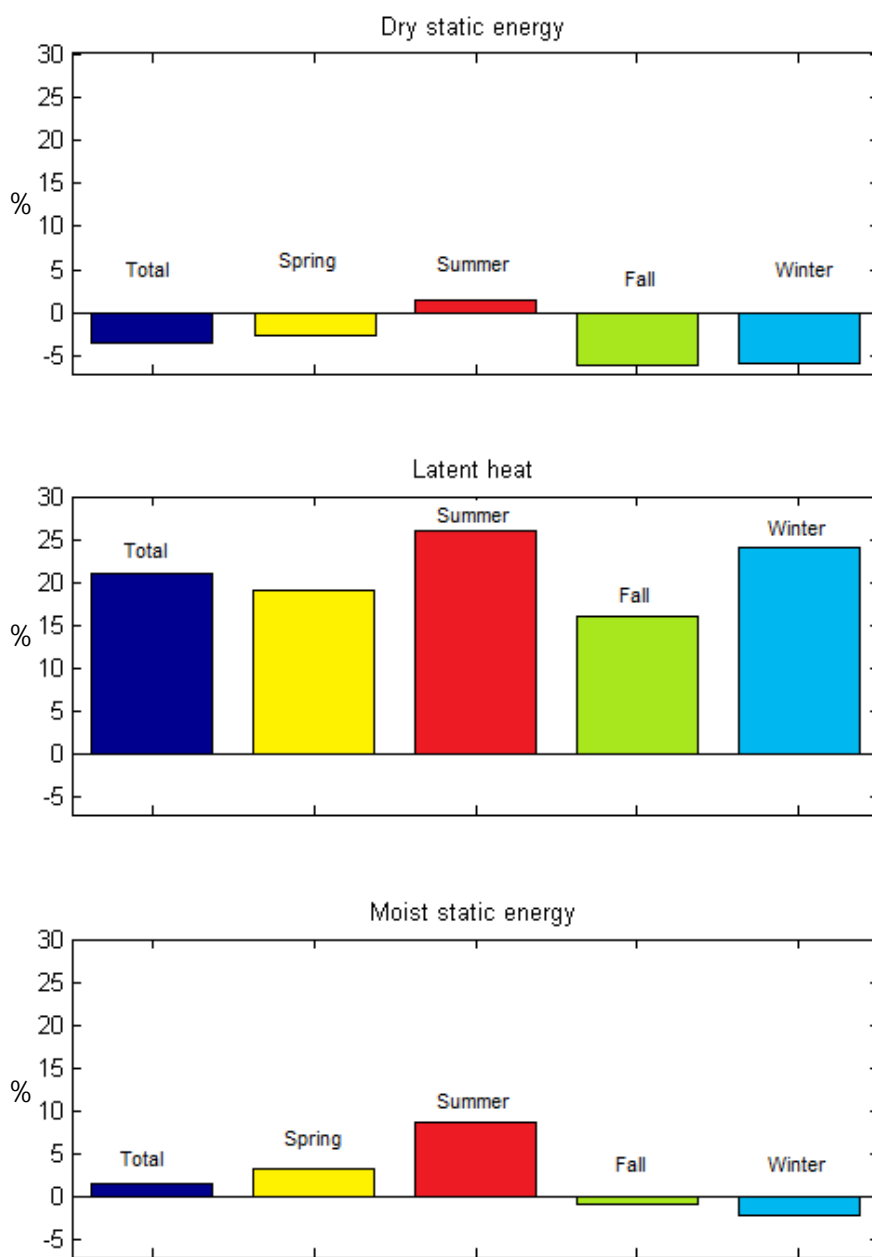
Figure 4: **Top panel**: total change in dry static energy; **Middle panel**: latent heat flux; **Bottom panel**: moist static energy flux across 70°N expressed as a % change for the CCSM3 late 21st century (2070-2089) relative to the 20th century (1960-1999) (dark blue bar), and the change occurring in each season (spring, MAM, yellow; summer, JJA, red; autumn, SON, green; winter, DJF, blue).

Figure 5: Difference in frequency of occurrence of the sea-level pressure anomalies between the late 21st century (2070-2089) and the 20th century (1960-1999). Black solid (dashed) lines indicate areas where differences are significantly higher (lower) at the 95% confidence level.
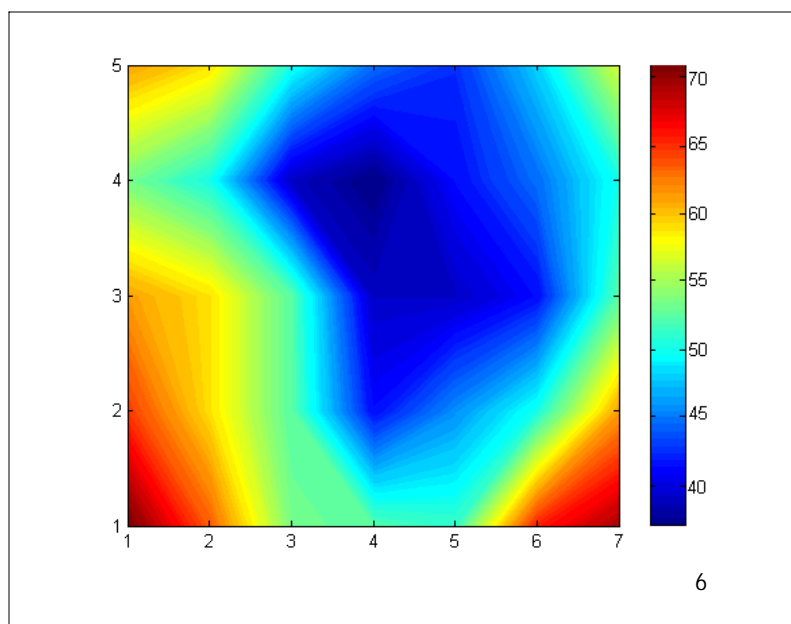
Figure 6: Contours of cluster-averaged tropospheric dry static energy flux across 70°N (Wm^{-2}) for the 20th century (1960-1999) from CCSM3.

Figure 7: Differences in the cluster-averaged tropospheric dry static energy flux across 70°N (Wm^{-2}) between the late 21st century (2070-2089) and the 20th century (1960-1999) from CCSM3.

Figure 8: Frequency of occurrence of the sea-level pressure anomalies for the 20th century (1960-1999), for **upper left**: spring (MAM); **upper right**: summer (JJA); **lower left**: fall (SON); **lower right**: winter (DJF). Black solid (dashed) lines indicate areas where differences in frequencies of occurrence are significantly higher (lower) at the 95% confidence level.

Figure 9: Contours of cluster-averaged tropospheric dry static energy flux across 70°N (Wm^{-2}) for the 20th century (1960-1999) from CCSM3, for **upper left:** spring (MAM); **upper right**: summer (JJA); **lower left**: fall (SON); **lower right**: winter (DJF).
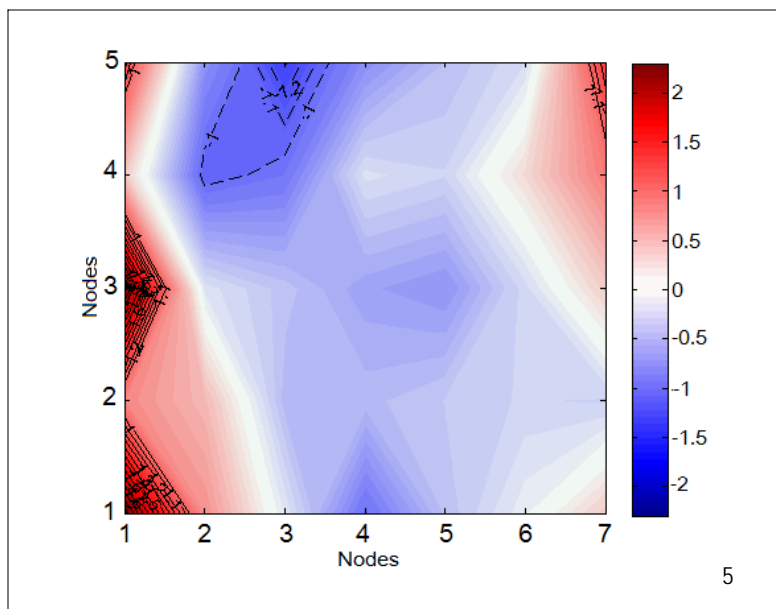

Figure 10: Difference in frequency of occurrence of the sea-level pressure anomalies between the late 21st century (2070-2089) and the 20th century (1960-1999), for **upper left**: spring (MAM); **upper right**: summer (JJA); **lower left**: fall (SON); **lower right**: winter (DJF). Black solid (dashed) lines indicate areas where differences in frequencies of occurrence are significantly higher (lower) at the 95% confidence level.
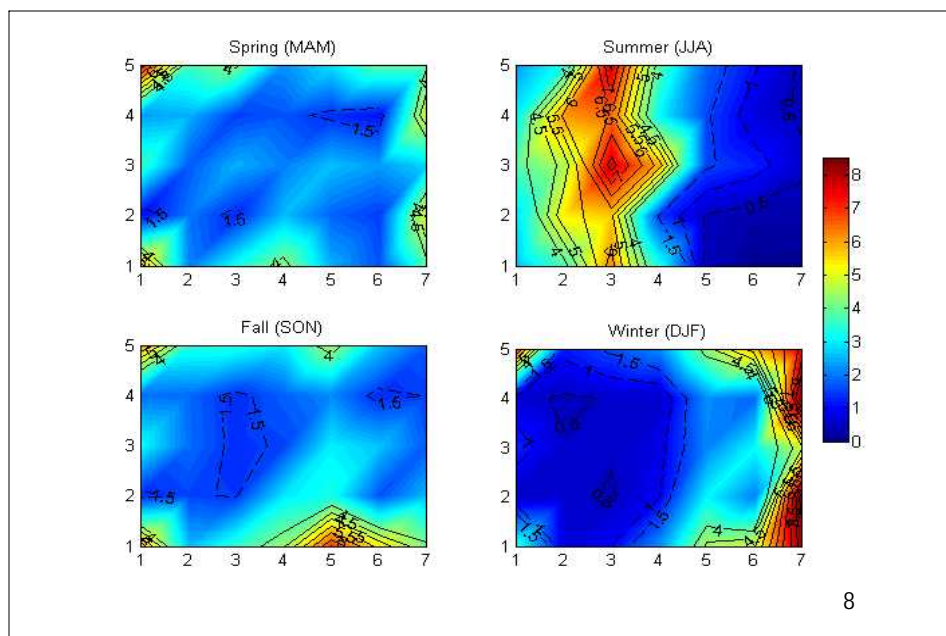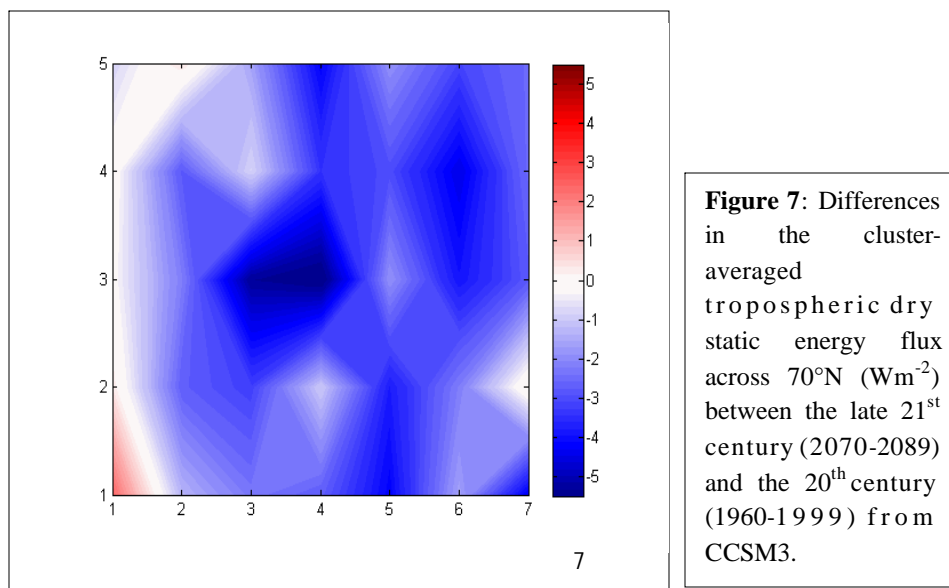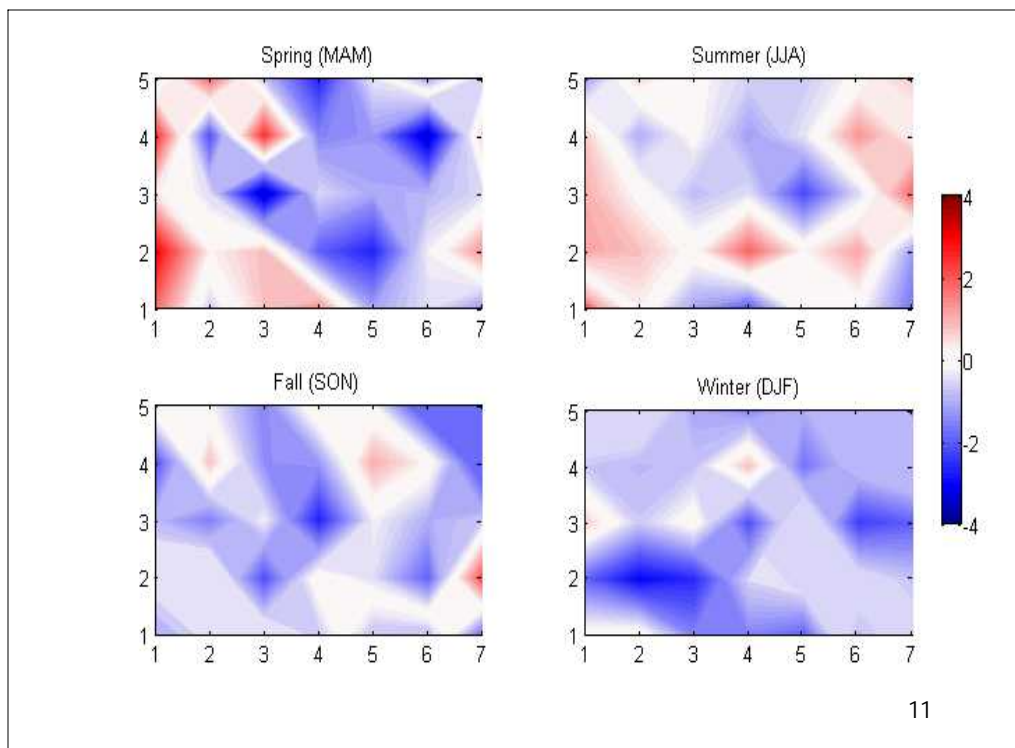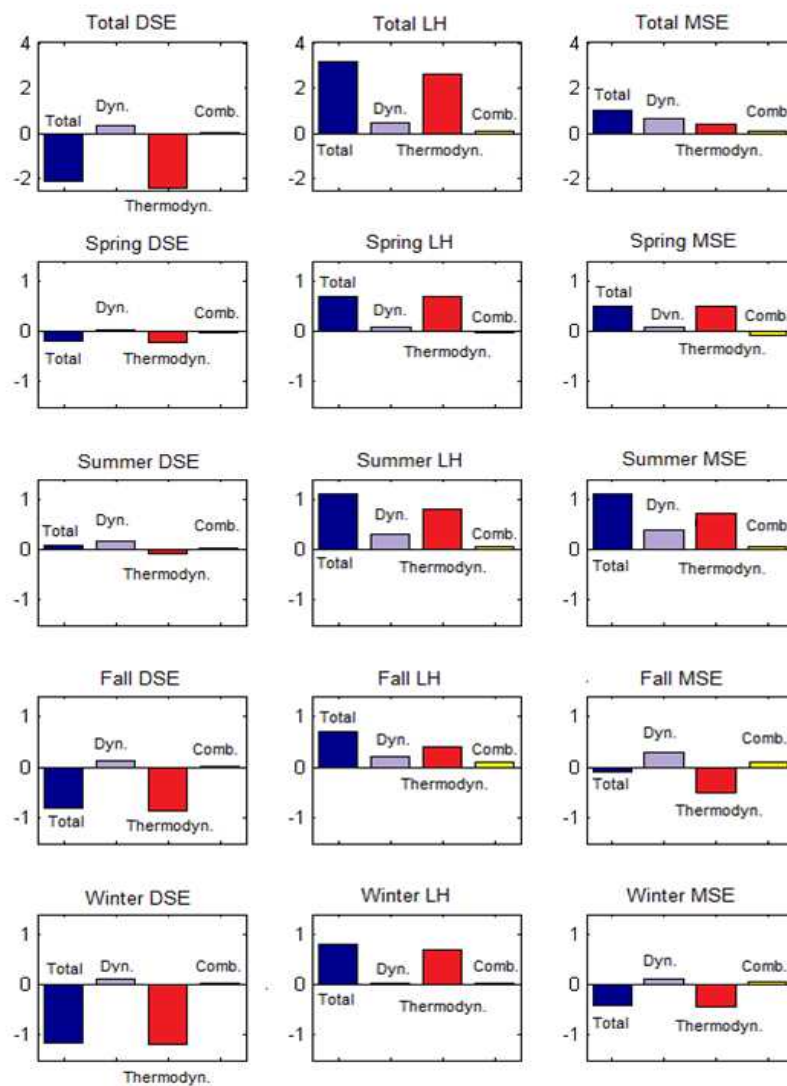
11

Figure 11: Difference in the cluster-averaged tropospheric dry static energy flux across 70°N (Wm^{-2}) between the late 21st century (2070-2089) and the 20th century (1960-1999), for **upper left**: spring (MAM); **upper right**: summer (JJA); **lower left**: fall (SON); **lower right**: winter (DJF). Values are shown as the portions of a total change.

Figure 12: Annual and seasonal changes in tropospheric dry static energy flux, DSE (first column), latent heat flux, LH (second column) and moist static energy flux, MSE (last column) across 70°N in the CCSM3 from the 20th century (1960-1999) to the late 21st century (2070-2089) (blue bar). Contributions to the total change are also displayed: dynamic (gray bar), thermodynamic (red bar), and combined term (yellow bar). Units are Wm[-2].

13

Figure 13: Contours of cluster-averaged tropospheric latent heat flux across 70°N (Wm^{-2}) for the 20th century (1960-1999) from CCSM3.
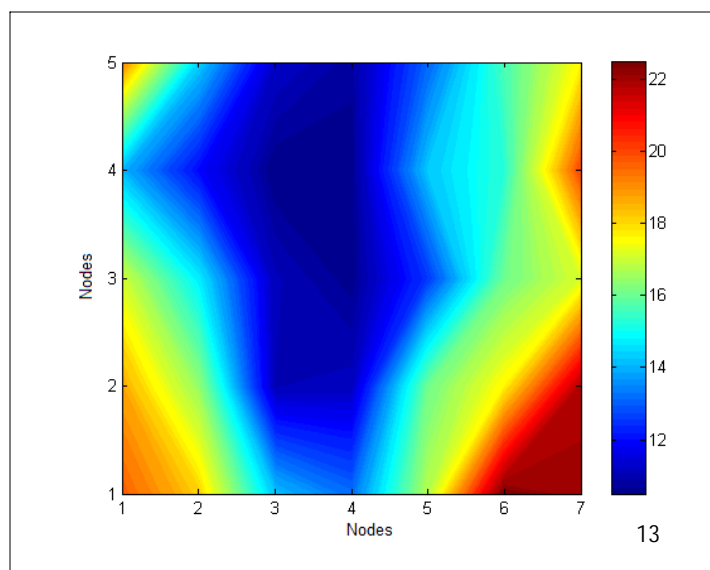

14
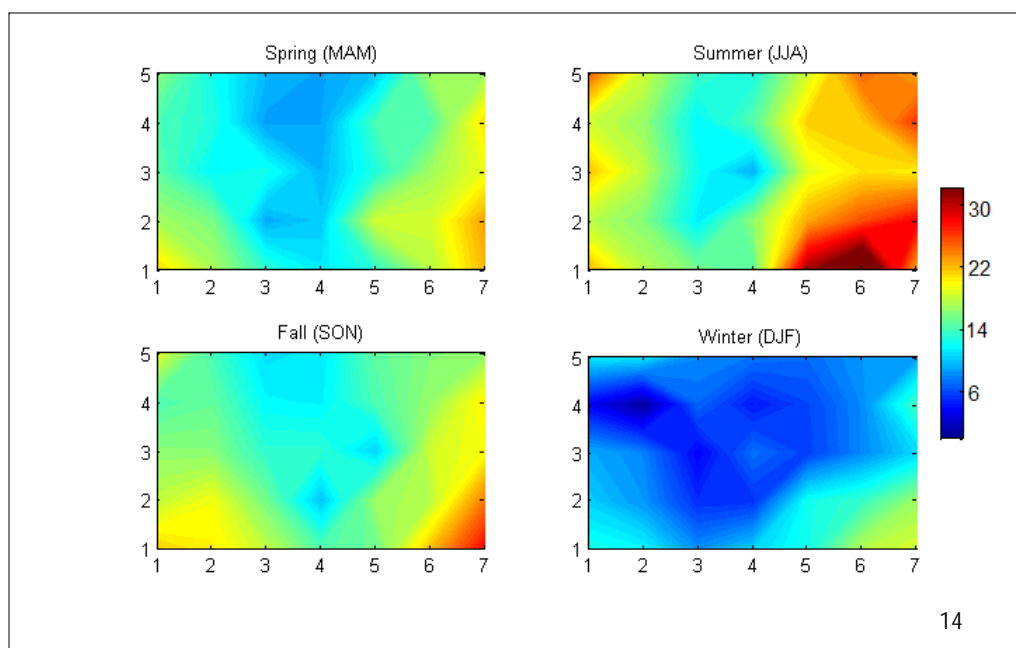
Figure 14: Contours of cluster-averaged tropospheric latent heat flux across 70°N (Wm^{-2}) for the 20th century (1960-1999) from CCSM3, for **upper left**: spring (MAM); **upper right**: summer (JJA); **lower left**: fall (SON); **lower right**: winter (DJF).
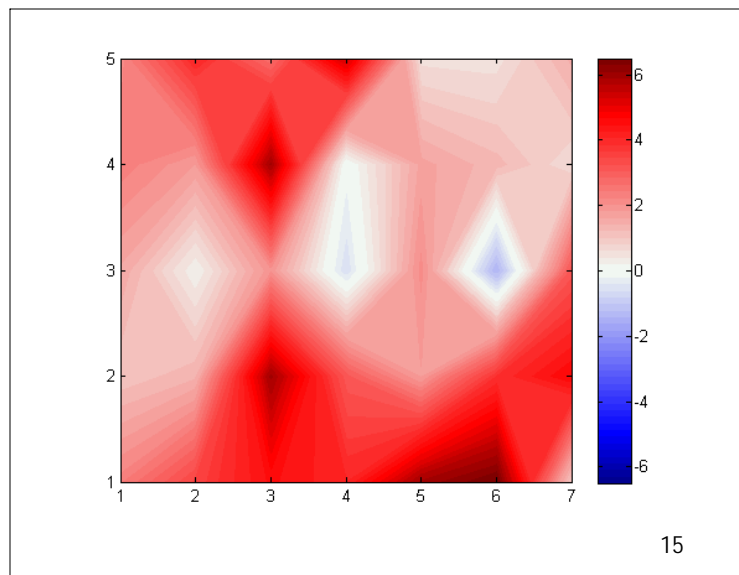
Figure 15: Differences in the cluster-averaged tropospheric latent heat flux across 70°N (Wm^{-2}) between the late 21st century (2070-2089) and the 20th century (1960-1999) from CCSM3.
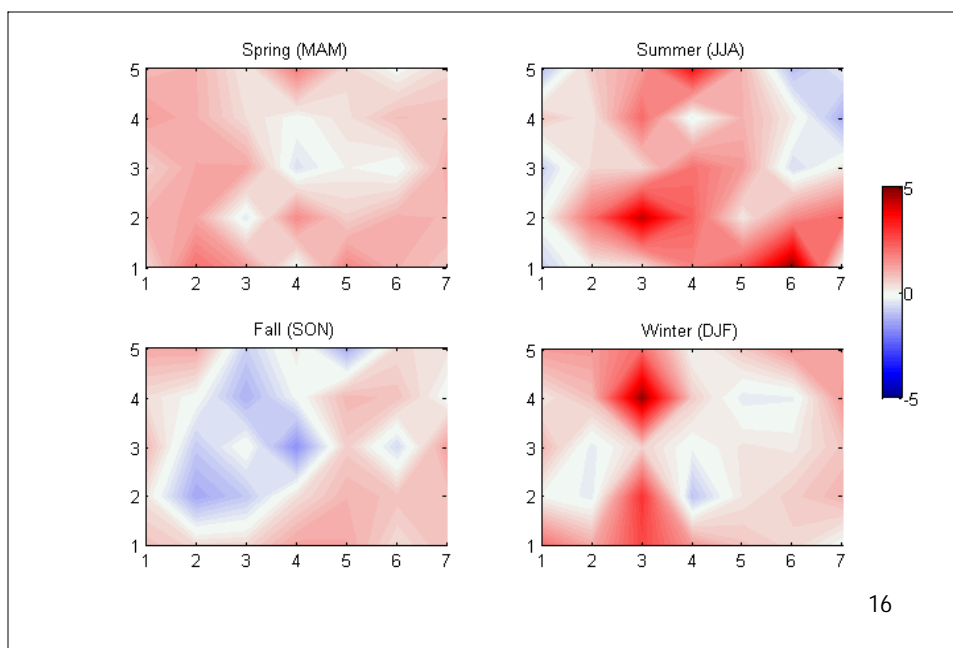
Figure 16: Difference in the cluster-averaged tropospheric lstent heat flux across 70°N (Wm^{-2}) between the late 21st century (2070-2089) and the 20th century (1960-1999), for **upper left**: spring (MAM); **upper right**: summer (JJA); **lower left**: fall (SON); **lower right**: winter (DJF). Values are shown as the portions of a total change.

Attribution of Seasonal and Regional Changes in
Arctic Moisture Convergence

Natasa Skific[1], Jennifer A. Francis[2], and John J. Cassano[3]

[1] Department of Environmental Sciences, Rutgers University, New Brunswick, New Jersey

[2] Institute of Marine and Coastal Sciences, Rutgers University, New Brunswick, New Jersey

[3] Department of Atmospheric and Oceanic Sciences, University of Colorado, Colorado

Corresponding author : Dr. Jennifer Francis, IMCS, 71 Dudley Rd., New Brunswick, NJ, 08901 Tel : 732-708-1217, Fax : 732-872-1586, e-mail : francis@imcs.rutgers.edu

5. Attribution of Seasonal and Regional Changes in Arctic Moisture Convergence

Abstract

We investigate spatial and temporal changes in high-latitude moisture convergence simulated by the National Center for Atmospheric Research Community Climate System Model, version 3 (CCSM3). Moisture convergence is calculated using the aerological method with model fields of specific humidity and winds spanning the periods from 1960 to 1999 and from 2070 to 2089 (the 21st century incorporates the Special Report on Emissions Scenarios A2 scenario). The model's realism in reproducing the 20th century moisture convergence is evaluated by comparison with values derived from the European Centre for Medium Range Weather Forecasts reanalysis (ERA-40). In the area north of 75°N we find that summer moisture convergence is similar to observations, but the model is generally larger in winter, spring and autumn. The model also underestimates (overestimates) the mean annual moisture convergence in the eastern (western) Arctic. Late 21st century annual, seasonal, and regional changes are determined by applying a self-organizing map technique to the model's sea-level pressure fields to identify dominant atmospheric circulation regimes and their corresponding moisture convergence fields. Changes in moisture convergence from the 20th to the 21st century result primarily from thermodynamic effects (~70%), albeit shifts in the frequency of dominant circulation patterns exert a larger influence on future changes in the eastern Arctic. Increased moisture convergence in the central Arctic (North Atlantic) stems mainly from thermodynamic changes in summer (winter). Changes in the strength and location of poleward moisture gradients are most likely responsible for projected variations in

moisture transport, which are in turn a consequence of increasing anthropogenic greenhouse gas emissions.

5.1. Introduction

One of the keys to diagnosing the Arctic's complex climate system and predicting its future trajectory is to understand the processes that drive its hydrologic cycle. Observations and some modeling experiments indicate that the Arctic's freshwater cycle is not only sensitive to global climate change, but also that the high-latitude regional changes in hydrology will affect the global climate (e.g., Manabe et al.,1991; Manabe and Stouffer 1994; 1995; 1997; Min et al., 2008). These studies suggest that the enhanced warming in the Arctic, owing to processes such as the ice-albedo feedback, may decrease the salinity of high-latitude oceans, both through increased runoff and ice melt, and enhance high-latitude precipitation. The oceanic thermohaline circulation may then weaken, which would, in turn, affect global temperatures. Lawrence and Slater (2005) find that increased temperature and water availability in the Arctic soil will result in a northward expansion of shrub and boreal forests. Such an expansion would lead to further lowering of surface albedo over snow-covered shrubs and forests compared with snow-covered tundra (Betts 2000; Chapin et al., 2005), which would further accelerate snow and ice melt. The links between arctic hydrology and human-induced environmental change have been demonstrated in a number of studies, which have often focused on one particular element of hydrology (ACIA 2004).

Net precipitation is a particularly valuable measure for assessing Arctic change because it combines both precipitation and evaporation. Its determination in high latitudes,

however, is often hampered by the low density of observing stations, harsh Arctic conditions that frequently lead to station failure, errors in gauge catchment of solid precipitation (Yang 1999; Yang and Ohata 2001; Cherry et al., 2007), and varying measurement techniques (Mekis and Hogg 1999). The so-called aerological approach used in this study circumvents these problems, as the net precipitation is computed from wind and precipitable water profiles as the change in the advection of vertically integrated water vapor.

Changes in the net precipitation in high-latitudes were investigated by Cassano et al. (2007), who used forecast values of precipitation and evaporation from an ensemble output from 15 GCMs. They found that over 75% of the projected increase in net precipitation is due to changes in thermodynamic processes. Emori and Brown (2005) explored future extreme precipitation and found that changing dynamics plays a secondary role in high latitudes, while the increase in thermodynamics is consistent in magnitude. Finnis et al. (2007) analyzed precipitation in a five-member ensemble of CCSM3 in the 21st century, and concluded that global changes in thermodynamics would lead to large precipitation increases over high latitudes. These studies focused on the Arctic region as a whole using the "middle of the road" Special Report on Emission Scenarios (SRES) A1B scenario for greenhouse gas emissions (Nakicemovic and Swart 2000). However, according to latest studies (Pielke et al., 2008; Rahmstorf et al., 2007) this projection underestimates actual emission rates. In this study we instead use the A2 scenario, or one of the "worst case scenarios", which appears to be most similar to the observed trends. In addition, we investigate and compare changing net precipitation in the

four seasons and in various regions of the Arctic, and apply the self-organizing map method to identify predominant mechanisms for the changes.

Climate models provide the best available tool to help understand processes of past variability and predict future change. The National Center for Atmospheric Research Community Climate System Model, version 3 (NCAR CCSM3) is a state-of-the-art GCM that realistically simulates the Arctic atmospheric circulation and hydrologic cycle (Cassano et al. 2006, 2007; Chapman and Walsh 2007). A brief summary of the model's properties and recent improvements is provided in Section 2. In this study we use one realization of the CCSM3. While this introduces uncertainty related to the realism of the projection, we emphasize that the primary goal of this work is to explore the fundamental mechanisms leading to projected increases in moisture convergence, both regionally and seasonally, under the assumption that the basic physics of the model are correct in responding to the forcing dictated by the A2 SRES scenario.

This study focuses on characterizing the future spatial and temporal changes of the Arctic moisture convergence by the late 21st century, and understanding the processes that drive these changes. We use daily time series of specific humidity and wind profiles from the CCSM3 for two time intervals: from 1960 to 1999 ("20th century") and from 2070 to 2089 ("21st century"). Daily fields of moisture convergence, an estimate of net precipitation, are derived from these products using the aerological approach. The realism of the 20th century model's simulation of moisture convergence is evaluated by comparing the annual and seasonal mean fields with those calculated from the European Centre for Medium-Range Weather Forecasts (ECMWF) reanalysis (ERA-40). These results appear in Section 3. Section 4 describes the application of the self-organizing map

(SOM) method (Kohonen 2001) to CCSM3 and ERA-40 sea-level pressure (SLP) fields to create a matrix of SLP patterns, and also describes how these circulation patterns are related to a particular net precipitation pattern. The SOM technique is selected for this analysis because it breaks down very large data sets into representative, fundamental clusters organized in a matrix of 2D fields – geographic maps in this case -- that are expressed in a visual and intuitive rendering. The maps are situated in the matrix relative to one another according to their similarity. In Section 5 we apply an approach devised by Cassano et al. (2007) to quantify the portion of change in moisture convergence that can be attributed to changes in a parameter representing dynamics, another related to thermodynamics, and a combination of the two. We contrast annual and seasonal changes in the central Arctic and North Atlantic from the 20th to the 21st century, and also analyze annual changes in several peripheral seas. The conclusions and summary are provided in Section 6.

5.2. Data sources and methods

5.2.1. Data sets

The model output used in this study is six-hourly, multilevel fields of specific humidity, as well as zonal and meridional winds from a single run of the NCAR CCSM version 3.0. Fields were obtained from the Program for Climate Model Diagnostics and Intercomparison (PCMDI) at the Lawrence Livermore National Laboratory. The atmospheric module of this version of CCSM3 includes new treatment of cloud and precipitation processes, as well as improvements in radiative parameterizations. It

incorporates 26 vertical levels, a top at 2.2 hPa, 13 layers above 200 hPa, and a horizontal resolution of about 1.4º. Overall the atmospheric component realistically represents the major features of the global hydrologic cycle (Hack et al. 2006). The 20th century experiment (20C3M) includes the direct effect of sulfates (Smith and Wigley 2001; Smith et al., 2005), and also incorporates ozone (Kiehl et al., 1999) and solar (Lean et al., 2002) forcing. The model includes observed concentrations of CO_2, CH_4, N_2O and CFCs, and effects of volcanic eruptions are parameterized (Ammann et al., 2003).

The 21st century simulation for the A2 scenario assumes a continuously increasing population (15 billion by the year 2100) and slow implementation of new technologies. The scenario is employed from 1990 to the end of the 21st century, at which time the carbon dioxide concentrations reach 850 ppm. Sulfate emissions peak around 2030 at 110 TgS and decrease to 60 TgS by 2100. The original 6-hourly PCMDI data were interpolated from the hybrid sigma-pressure vertical coordinates to a pressure coordinate system and reduced in size by subsetting from global coverage to the region north of 60ºN, from 6-hourly to daily resolution (12 UTC only), and from 26 vertical levels to 10 (troposphere only). Horizontal moisture transport was calculated for five tropospheric layers (1000-850, 850-700, 700-500, 500-400, and 400-300 hPa). Moisture transport is generally largest in the troposphere where the concentration of water vapor is largest. It peaks below 600 hPa in high latitudes, associated with transient eddies defining the North Atlantic and Pacific storm tracks. Above the polar tropopause water vapor concentration is sparse and moisture fluxes are small (Serreze and Barry 2005). The time slices used in this study span periods of 1960-1999 for the 20th century experiment and 2070-2089 from the SRES A2 scenario. The latter period is chosen to be consistent with results from the

Arctic Climate Assessment Report (ACIA 2004, www.acia.uaf.edu) to represent the mature greenhouse state (Serreze and Francis 2006). Sea-level pressure fields are also extracted for the same time periods and interpolated from the original 1.4º x 1.4º grid to a 200 km x 200 km Equal Area-Scalable Grid (EASE; Armstrong et al. 1997), covering the area north of 60ºN. Interpolation to an equal-area grid averts errors that might arise due to equal weighting of the original latitude-longitude grid points in the self-organizing map algorithm described in the next section.

Daily SLP output from the ERA-40 reanalysis (Upala et al., 2005) was used to validate the model's performance for the 20th century. These fields were interpolated to the same grid as CCSM3. The ERA-40 incorporates a full range of sea ice concentrations, thermal effects of frozen soil hydrology, and realistic albedos for snow-covered surfaces. The output achieves an approximate annual balance between the moisture flux convergence derived from assimilated and forecast values of P-E (Bromwich et al. 2002). Daily multi-level fields of zonal and meridional winds and specific humidity were also retrieved from ERA-40, and the aerological method was applied to derive the reanalysis horizontal moisture convergence. The absolute accuracy of wind and moisture profiles is not known owing to a dearth of independent rawinsonde data, but the assimilation of a variety of conventional and satellite information is expected to produce fields of state variables that are realistic. Cullather et al. (2000) and Serreze et al. (2005) report, however, that aerological estimates of net precipitation from ERA-40 in the Arctic appear to have shortcomings compared to available and also imperfect observations, but there is no better alternative identifiable at this time. Aerological estimates from reanalysis are believed to be superior to those derived from rawinsondes only because the primary

moisture conduits into the Arctic from lower latitudes are not captured by the sounding network, while additional data assimilated by reanalysis are more successful in representing these moisture transports (Cullather et al., 2000; Serreze et al., 2006).

5.2.2. Self-organizing maps (SOMs)

A self-organizing map (SOM) algorithm is a neural-network technique that attempts to reduce the dimensions of a large data set by organizing it into a two-dimensional array or a matrix (Kohonen 2001). For this study, the data set used for the SOM analysis consists of a time series of 2D fields of SLP over the Arctic from both ERA-40 and CCSM3. The SOM algorithm organizes the daily fields into clusters of similar maps by identifying SLP patterns that represent the range present in the original data set. The 2D maps in the SOM matrix provide a more intuitive rendering of pattern characteristics and their relative frequency of occurrence than is achieved by other statistical tools, such as empirical orthogonal functions.

A complete description of the SOM method is presented in our companion paper, Skific et al. (2009), and we present only a brief discussion of the mechanics here. The initial step is the creation of a first-guess set of maps consisting of an arbitrary number of SLP patterns, which are called reference vectors. The projection of the reference vector on a 2-dimensional array is usually referred to as a node. In this study we chose the number of nodes to be 35, spanning a two-dimensional array of 7x5. Initial testing of slightly smaller and larger SOM matrices indicate that this matrix is a suitable size to capture and separate the important differences in pressure patterns and that the results of

the analysis are not sensitive to the number of nodes chosen. The major difference between the SOM and the traditional clustering algorithms is the fact that reference vectors of all neighboring nodes are adjusted toward the best matching vector of the input data sample, not only that of the closest node (Hewitson and Crane 2002). Because of this updating scheme, the resulting clusters of maps that belong to each node become organized on a 2-dimensional array in such a way that more similar clusters are placed closer together, while those less similar are farther apart, allowing a more intuitive interpretation of patterns and their relationship to each other in the matrix.

We apply a linear map initiation, as described in Kohonen (2001), which begins by first determining the two eigenvectors, derived from the covariance matrix of the SLP fields, with the largest eigenvalues, then letting these eigenvectors span the two-dimensional linear subspace. Linear initialization helps achieve faster convergence, but the SOM results are not sensitive to the selected initialization method. In the process of training, each data sample (i.e., one daily map of SLP) is presented to the SOM matrix in the order it occurs in the original data set. The similarity between the data sample and each of the reference vectors is then calculated, usually as a measure of Euclidean distance in space. The "best match" node is identified and the reference vectors further refined through an iterative process through which the centroids of the clusters of daily maps matched to each node are modified to minimize the distances between the samples and the reference vectors.

Although the measure of similarity between the data and the reference vector is linear, it is this iterative training procedure that allows the SOM to account for the non-linear data distributions (Hewitson and Crane 2002). The non-linear approximation of the

data space is therefore a great advantage of the method compared to some other approaches, such as empirical orthogonal functions (EOFs) (Reusch et al., 2005). For further detail, please see Skific et al. (2009) and Cassano et al. (2007).

5.3. Comparison of ERA-40 and CCSM3 moisture convergence fields

The moisture convergence results from the net transport of precipitable water into or out of a layer and is equivalent to net precipitation when assessed over a period of several months. It is computed using the "aerological" approach (Serreze and Barry 2005) as

$$\nabla \cdot (Q_k \overrightarrow{V_k}),$$

where Q_k is the precipitable water in a layer defined as

$$Q_k = \frac{1}{g} \int_{p_1}^{p_2} q \cdot dp$$

and V_k is the wind velocity in layer k (Groves and Francis 2002). Cloud liquid water storage and moisture transport across the tropopause are neglected, as they are usually small factors in the column moisture budget in polar conditions (Groves and Francis 2002). Total moisture convergence in the tropospheric column is derived by summing the convergence in all layers.

The long-term, annual-mean moisture convergence for ERA-40 and CCSM3 during the 20th century is presented in **Fig. 1**. Overall the model result is similar to that derived from ERA-40, although some regional differences are evident. The annual net

precipitation off the east coast of Greenland and around Iceland, as well as over the southern coast of Alaska, is more pronounced in ERA-40 than in the CCSM3, partially due to the lower spatial resolution of model orography and output. The long-term mean values of moisture convergence from the model and observations for the 20th century in the various regions shown in **Figure 2** are given in **Table 1**. Values from the model that are significantly higher or lower than those from ERA-40 at a 95% confidence level are highlighted in bold.

The model's moisture convergence in the Atlantic sector is lower than the ERA-40 value by about 32%, while over the central Arctic the model is about 17% higher. In general the results in **Table 1** indicate that the model underestimates moisture convergence in the eastern Arctic (Atlantic sector, Barents and Kara Seas) relative to the analysis, but significantly overestimates it in the western Arctic (Laptev, East Siberian, Chukchi and Beaufort Seas). In the Laptev and East Siberian Seas, the model's moisture convergence is about 18% and 38.7% higher, and differences become more pronounced in the Chukchi and Beaufort Seas, where the model's values are double those in ERA-40. These results agree with conclusions by Finnis et al. (2008a, 2008b), who found that modeled Mackenzie River Basin cyclones are too intense, too persistent, and/or occur too frequently.

Seasonal-mean moisture convergence fields for the 20th century from ERA-40 and CCSM3 are compared in **Fig. 3**. The negative values in the Barents Sea and south of Svalbard that appear in both the CCSM3 and ERA-40 during non-summer seasons are associated with large evaporation rates owing to a strong temperature contrast between open water and the cold, dry air above. Maximum (minimum) moisture convergence in

most areas occurs during summer (winter), while the region east of Greenland and along southern Alaska have a cold-season maximum and warm season minimum. The summer maximum over the central Arctic is related to cyclones penetrating deeper into the Arctic Ocean (Serreze and Barry 2005). Negative values of moisture convergence over Eurasia in summer result from evaporation exceeding precipitation. Drying of the land surface during summer leads to greater warming than over sea ice where temperatures are confined to the melting point. These contrasts increase baroclinicity in the summer Arctic, which is usually also enhanced by steep coastal orography (Serreze and Barry 2005). These conditions favor cyclogenesis over northeastern Eurasia and Alaska/Yukon. These disturbances often migrate into the Arctic, resulting in increased precipitation over central Arctic region during summer. Another pathway of cyclones into the Arctic in the summer is from systems generated along the weakened North Atlantic storm track (Reed and Kunkel 1960). Areas near Iceland and east of Greenland experience maximum moisture convergence in the autumn and winter, which reflects the influence of the well defined storm track and relatively heavy precipitation.

Table 2 summarizes the 20th century seasonal and regional differences in moisture convergence between ERA-40 and CCSM3. Model values of summer moisture convergence over the central Arctic are similar to those from ERA-40. In the autumn, winter, and spring seasons, the model's moisture convergence over the central Arctic exceeds that from ERA-40 by 15%, 32%, and 59%, respectively. In the north Atlantic, moisture convergence from the model is the most similar to ERA-40's values in the spring, when CCSM3 values are lower by 18%. Differences are more pronounced in the autumn, winter and summer when modeled moisture convergence falls significantly

behind the reanalysis by 39%, 39%, and 29%, respectively. In the Barents Sea differences between the model and the reanalysis are most pronounced and statistically significant at the 95% confidence level in the winter (spring), when moisture convergence in the model is lower (higher) than the reanalysis by 0.77 (0.68) cm/month, while they are the most similar in the summer. In the Kara Sea the model is lower by about 23% in summer and autumn, while in spring the model exceeds the reanalysis value by 14.3%. Differences are the smallest in the winter. In the Laptev, East Siberian, Chukchi and Beaufort Sea, the model is most similar to that of the reanalysis in the summer months. In the western Arctic, the model generally overestimates moisture convergence in all seasons, with largest differences (about 1.5 cm/month) in the autumn and winter in the Chukchi and Beaufort Seas. These results agree with findings by Finnis et al.(2008a; 2008b), who found that the CCSM3 oversimulates cyclogenesis in the Mackenzie Basin during autumn, winter and spring, leading to overestimation of precipitation in that area. In addition, Alexander et al. (2006) suggests that the resolution of topography plays a crucial role in simulating lee-cyclogenesis in the model. This could explain large differences between the model and the reanalysis in the lee of the Rocky Mountains. We also note that differences may arise owing to the comparison of two single realizations of the system, one modeled and one from the real world, and that long-term cycles of natural variability may be out of phase in the two realizations.

5.4.   Links between moisture convergence and circulation patterns: a self-organizing map (SOM) approach

The SOM method described in Section 2 is applied to the daily sea-level pressure anomalies from a combination of both ERA-40 and CCSM3 output for all time periods. Daily SLP anomalies are created by subtracting the domain-averaged SLP for each daily map from the SLP at each grid point on that day. As argued by Cassano et al. (2007), these anomalies are a better representation of the SLP patterns, as eliminating the daily mean focuses the procedure for pattern classification on pressure *gradients*, which are a better representation of circulation features. Areas of elevation higher than 500 m are removed from the fields because pressure reduction to sea level in the areas of high elevation can lead to unrealistic patterns.

Figure 4 shows the self-organizing map of SLP anomalies north of 60°N, hereafter called the "master SOM." The same master SOM is presented in Skific et al. (2009). The matrix of maps represents the dominant circulation regimes in which the atmosphere tends to reside according to the data sets used to create it. Patterns with a strong Icelandic low and moderate-to-strong Aleutian low, accompanied by high pressure over the northern Eurasian continent, are found in the bottom right. Maps in the upper right are characterized by pronounced low pressure in the Atlantic sector extending into Barents Sea, while the western central Arctic, continental regions, and the Pacific sector are dominated by high pressure. These patterns correspond to a moderate or strong Beaufort high in winter. In the bottom left corner of the map are conditions with a pronounced low pressure area in the central Arctic and high pressure over northwestern

Eurasia. Towards the upper left corner the low is centered in the Kara and Laptev Sea area, while high pressure is located over the northeast American continent. The patterns in the middle of the SOM are dominated by high pressure over the central Arctic.

The frequency of occurrence (FO) for 20th century SLP anomaly patterns in CCSM3 (1960-1999) are presented in **Figure 5, top** panel. Frequencies of occurrence are defined as the percent of days that map into a particular cluster out of the total number of daily fields. Black solid (dashed) contours show values of FO that are significantly higher (lower) than an expected value for a random binomial distribution (i.e., 2.86%), with a confidence level of at least 95% (for more details see Cassano et al. 2007). Because this statistical test does not account for the effects of serial correlation in the daily SLP fields, and thus likely overestimates the degrees of freedom, we determine an approximation for the effective degrees of freedom by dividing the number of samples of the two data sets by 7. This value is determined from the serial correlation of the SLP time series, which indicates that the atmosphere tends to reside in a circulation regime for about one week. This procedure decreases the degrees of freedom, thus establishing a higher threshold for determination of a significance level.

The features evident in the top panel of **Fig. 5** show that the bordering clusters occur more frequently, while those positioned in the middle of the matrix, representing transitional circulation patterns between the most dominant regimes, are less common. Skific et al. (2009) compared 20th century FOs of the CCSM3 single run to those from ERA-40 and found that the modeled fields occupy clusters with high pressure in the central Arctic less frequently, while clusters with pronounced low pressure in the Atlantic

region (on the right of the SOM) are occupied more frequently than in ERA-40. This results in the model's mean sea-level pressure of the 20th century being lower in the central Arctic and in the Atlantic sector compared to the reanalysis, while pressure in northern Eurasia and northeastern American continent is higher.

The FO of winter (DJF) and summer (JJA) patterns in the 20th century CCSM3 is shown in **Fig. 5, middle** and **bottom** panel. The most common winter patterns are on the right side of the master SOM; circulation patterns on the left side are more characteristic of summer conditions.

The master SOM can be used to identify which days belong to each cluster in the matrix. Maps of other variables corresponding to the days in each cluster can then be analyzed as well, allowing patterns of other quantities to be assessed for a fixed circulation regime. **Figure 6** shows the result of mapping moisture convergence onto the SLP clusters from **Figure 4**. Once all the 20th century daily fields have been assigned to a particular SLP cluster, we subtract the domain-average, 20th-century-mean moisture convergence from each cluster-average map to derive anomalies. Red shading corresponds to positive values, i.e., precipitation exceeds evaporation, which usually occurs east of low-pressure systems and west of high-pressure systems. Blue shading corresponds to moisture divergence, i.e., where evaporation exceeds precipitation. Patterns in the lower right corner of **Figure 6** correspond to winter patterns with a pronounced Icelandic low and a moderate-to-strong Aleutian low. This situation brings more precipitation in the Atlantic and Pacific sectors, as well as to northwestern Europe and Canada. In the upper right corner of the matrix, moisture convergence corresponds to a circulation pattern characterized by low pressure in the Atlantic sector that extends

northeastward, and well-defined high pressure over the central Arctic. Positive values of moisture convergence also exist across the Eurasian continent. Toward the left in the top row of **Fig. 6**, an area of negative moisture convergence in the Atlantic sector is related to low pressure in the Kara and Barents Sea, which favors evaporation in the Atlantic sector by bringing colder and drier Arctic air onto the warmer Atlantic waters. In the lower left corner, circulation patterns are characterized by high pressure over northwestern Eurasia and low pressure over the central Arctic. This configuration will favor positive moisture convergence in the north Atlantic and negative values over northwestern Eurasia.

5.5. Future changes in moisture transport for various regions of the Arctic

5.5.1. Demonstration of SOM technique for pan-Arctic domain

In this section we use the SOM approach to identify changes in the model's simulation of moisture convergence in the late 21st century relative to the 20th century and determine the causes of these changes. Even thought the CCSM3 simulation for the 20th century differs from the ERA-40 in some areas, the projected future changes in the model output forced by the reasonable conditions described by the A2 scenario are instructive for understanding the mechanisms driving the changes.

There are two ways that a temporal change can be quantified. One is any difference in the frequency with which each of the SOM clusters is occupied by the individual daily fields. Physically this can be interpreted as a change in the atmosphere's preference for a particular fixed weather pattern, as captured by the SOM matrix. The other way is through a change in the variable averaged over all the daily maps that belong

to a particular cluster. For example, the mean water vapor content for a cluster of similar pressure patterns may increase in the future, resulting in the cluster-mean value for water vapor increasing even though the pressure patterns themselves do not change significantly.

This rationale is the basis of a procedure developed by Cassano et al. (2007) that separates the contributions from changing atmospheric dynamics, as represented by changes in the FOs; thermodynamics, as estimated by the change in the cluster-mean variable of interest, or a combination of the two. A brief summary of the procedure is provided here; details are available in Cassano et al. (2007) and Skific et al. (2009).

The factors contributing to the total temporal change in a variable x across a region can be expressed mathematically as

$$x_{future} = \sum_{i=1}^{N}(f_i\, x_i + \Delta f_i x_i + f_i \Delta x_i + \Delta f_i \Delta x_i) \tag{1}$$

where x_i is the cluster-averaged variable in the initial time period, f_i is the frequency of occurrence (FO) of cluster i during the initial period, and N is the total number of clusters (N = 35 in this study. The first term represents the mean value of a variable in a cluster weighted by its FO during the initial time period, the other three terms define contributions to the change between the initial and the later period. The second term, $f_i x_i$, relates the changes in a variable of interest to changes occurring due to a shift in the FO of a particular circulation regime or cluster. This term therefore identifies the portion of a change caused primarily by varying dynamics, i.e., more or less frequent occurrence of a particular circulation regime. The third term, $f_i\ x_i$, describes the contribution due to changes in the cluster-averaged variable of interest that occurs for a fixed circulation regime, and is referred to as the thermodynamic factor. The final term, $f_i\ x_i$, is the

combined dynamic/thermodynamic factor, which describes the contribution by changes in FO acting on changes in cluster-averaged variable of interest. The differentiation between these factors may be indistinct in some cases -- the attribution presented in this work is meant to be an indication of the character and magnitude of the causes of change projected by the model, not a quantitative prediction of contributions. Assuming the basic model physics are correct in their response to the A2 SRES forcing, we submit that the explanations for projected change by the end of the 21st century are a valuable tool for understanding system behavior in the mature greenhouse world.

This section summarizes results from Skific et al. (2009) as background for the analysis of regional and seasonal projections. Change in the FO of sea-level pressure anomalies (i.e., f_i) between the late 21st century (2070-2089) and the 20th century (1960-1999) is shown in **Figure 7**. Black solid (dashed) lines identify areas where differences in FO are significantly higher (lower) with a confidence level greater than 95%. Numbers shown on black solid (dashed) lines indicate values of the difference in FO along that contour. A more pronounced, statistically significant increase in patterns with low pressure over the central Arctic (clusters on the left of the master SOM in **Fig. 4**) is evident, as well as in clusters with strong high pressure across the western Arctic region and strong low pressure in the Atlantic sector and eastern Arctic (upper right side of the SOM). The clusters in the middle, mostly representing weak or moderate high pressure in the central Arctic, have decreased. These changes in the FO of SLP patterns represented by each cluster in the SOM suggest that in the greenhouse-gas-forced future, the pressure in the central Arctic will generally decrease, and the SOM reveals which SLP patterns are responsible for the change. Skific et al. (2009) analyze future changes of CCSM3 sea-

level pressure anomalies using the SRES A2 scenario, and find that this model realization exhibits an Arctic-mean pressure decrease of about 1.8 hPa in the late 21st century relative to the 20th century.

The cluster-averaged moisture convergence (x_i in Eq. 1) for the pan-Arctic region (area north of 60°N) for the 20th century is shown in **Figure 8**. Circulation patterns in the lower right (those corresponding to well-pronounced Icelandic and Aleutian low), and lower left corner (low pressure across the central Arctic) favor higher moisture convergence, or net precipitation, in the pan-Arctic region. The clusters in the middle of the SOM (those showing high pressure across the central Arctic) favor less moisture convergence in the region.

Figure 9 shows x_i, the change in the cluster-averaged moisture convergence between the late 21st century (2070-2089) and the 20th century (1960-1999). This change is positive for each circulation pattern of the SOM, which means that the thermodynamic factor, defined by multiplying x_i (**Fig. 9**) by f_i (**Fig. 5**), will be positive. Physically, a thermodynamic change may result from any change in the horizontal moisture gradients. The change due to thermodynamics is positive for all clusters, and its total contribution summed over all clusters, is 67 mm yr^{-1}.

The separate dynamic, thermodynamic, and combined factors are presented in **Figure 10** for each individual cluster using the same scale to illustrate their relative importance. The dynamic term, derived by multiplying x_i (**Fig. 8**) by f_i (**Fig. 7**), is positive for the circulation patterns to the left and to the right of the SOM, and negative for the clusters in the middle of the SOM. Its total value summed over all clusters is 2.76 mm yr^{-1}. Physically, the dynamic factor arises from a change in the FO of a particular

cluster. The contribution from the combined factor (**Fig. 10**, bottom) is relatively very small. The total increase in moisture convergence for the pan-Arctic region (north of 60°N), derived by summing the contributions by all three terms, is about 70 mm yr^{-1}, with the factor described as thermodynamics accounting for 95% of the total increase. In the next section, we apply this principle to derive and compare changes in moisture convergence for particular regions of the Arctic.

5.5.2. Attribution of regional changes

Here we focus on eight regions: the central Arctic, North Atlantic, Barents, Kara, Laptev, East Siberian, Chukchi and Beaufort Seas (see **Fig. 2**). In the CCSM3 20th century simulation, the moisture convergence in each Arctic region is averaged for each daily map within a cluster and is presented in **Figure 11**. These contours represent x$_i$ in equation (1) and indicate which clusters in the master SOM are responsible for maxima and minima in moisture convergence occurring in each region.

The moisture convergence in the central Arctic and north Atlantic is largest for clusters in the lower right section of the master SOM (i.e., a strong Icelandic low) and in the lower left (i.e., low pressure in the central Arctic and high-pressure in the northwestern Eurasia), as shown in the first row of plots in **Figure 11**. These clusters favor more precipitation over evaporation, while those in the center and the top of the master SOM (i.e., weak and moderate high pressure over Arctic) have lower net precipitation. The Kara and Barents Seas have a higher moisture convergence for clusters on the right side of the SOM. These circulation patterns are characterized by low pressure in the Atlantic sector extending northward and eastward into the coastal seas of

the eastern Arctic, while high pressure is generally located over northern Eurasia and across the western Arctic. Clusters in the upper- and middle-left sides of the SOM favor higher precipitation in the Laptev, East Siberian, Chukchi and Beaufort Seas. These patterns feature low pressure over these seas, along with high pressure in northeast Canada. The Beaufort and Chukchi Seas also have higher moisture convergence values when there is a strong Aleutian low (lower middle and right of the SOM). Low pressure in the Atlantic (clusters on the right) generally has little influence on the moisture convergence in the western Arctic regions.

The third term of equation (1), i.e., $x_i f_i$, describes the change in moisture convergence resulting from changing physical characteristics in a particular cluster but with a fixed frequency of occurrence of that pattern. Physically, this term represents primarily the thermodynamic portion of the total change. Contributing factors may include changes in moisture content of the atmosphere or other processes that may affect the moisture gradient in an area. Regional changes in the cluster-averaged moisture convergence between the late 21st century and the 20th century are shown in **Figure 12**. Because the sign of the change in thermodynamics is determined by the sign of cluster-averaged moisture convergence from the earlier to later time intervals, it is obvious from **Figure 12** that this term contributes significantly to the total overall increase in most regions. Nevertheless, some clusters of the matrix show a large decrease in moisture flux convergence (unlike for the pan-Arctic region in **Fig. 9**). These reductions in moisture flux convergence account for the negative thermodynamic changes in the Barents and Kara Seas.

The fourth term in equation (1) describes the portion of total change arising from combined dynamic and thermodynamic effects. This change could, in a physical sense, describe a change of thermodynamics (such as changes in atmospheric moisture content) that result from a particular circulation regime occurring more or less frequently. For example, more frequent occurrence of low pressure circulation patterns could lead to changes in atmospheric thermodynamic properties, either through intensified surface mixing and consequent increase in evaporation, or an increase in the FO of precipitation events. The term definition, as given in equation (1), relates f_i, the changes in the FO (**Fig. 7**), to x_i, the changes in cluster-averaged moisture convergence (**Fig. 12**). The two are multiplied and summed over all the clusters.

Figure 13 presents the total changes in moisture convergence in the late 21st century relative to the 20th century, as well as the individual contributions by the dynamic, thermodynamic, and combined terms in various regions of the Arctic. In the central Arctic north of 75°N, about 85% of the increase in moisture convergence is due to changes in the thermodynamic factor. The second largest contribution is the combined term, accounting for about 9% of the total change, while the dynamic factor accounts for only about 5%. For the A2 scenario, the model projects that the total moisture convergence will increase by about 39 mm yr^{-1} (15.7%) in the central Arctic by the late 21st century relative to the 1960-1999 period. Of all the regions studied, the N. Atlantic will experience the largest increase in moisture convergence of about 55 mm yr^{-1} (17.7%). However, large spatial variations are evident in the annual mean values in the Atlantic sector (**Fig. 14**): while the area south of Svalbard and east of Greenland experiences a decrease in moisture convergence, it increases by over 200 mm mo^{-1} west

of Scandinavia. Approximately 24% of the total change in this region is due to dynamic effects, while 87% is due to thermodynamics. The combined term has a small, negative contribution of about -11%. In the eastern Arctic the dynamic term appears to have a stronger influence than in the western Arctic. The Kara and Barents Seas experience decreased moisture convergence, particularly in the Kara Sea (-15 mm yr^{-1}). Thermodynamics and the combined term contribute to a reduced moisture convergence in these regions. A negative sign in the thermodynamic term indicates that evaporation becomes larger relative to precipitation, most likely due to substantial regional atmospheric warming, which would lead to decreased poleward gradients in temperature and humidity and reduced moisture advection into a region. This could also be related to extensive losses of sea ice in these two regions, which exposes large areas of open water and leads to increased evaporation. The positive dynamic term, however, results from an increase in the FO of the clusters in the upper right corner of the master SOM, which would likely increase the precipitation events in these regions. The combined term may result from effects of changing storm frequencies on surface turbulent fluxes or perhaps changes in surface moisture fluxes on storm development.

A common feature in the Laptev, East Siberian, Chukchi, and Beaufort Seas is the strong influence of thermodynamic effects, which favor an increase in moisture convergence of > 40 mm yr^{-1}. Interestingly, dynamic changes in these seas contribute negatively to moisture convergence in the future, according to this model run. To explain these features, we compare cluster-averaged moisture convergence of the 20th century for seas of the western Arctic (**Fig. 11**) with changes in the FO from the 20th to 21st centuries (**Fig. 7**). Clusters with high moisture convergence in these regions appear in the upper-

middle and upper left side of the SOMs, and the FO of these clusters decreases significantly in the late 21st century. The Chukchi and Beaufort Seas also show higher moisture convergence for the clusters in the lower right of the SOM, which are related to a pronounced Aleutian low. The FO of this feature also decreases in the late 21st century (**Fig. 7**), contributing to the negative dynamic factor in the Chukchi and Beaufort Seas.

5.5.3. Seasonal changes

Changes in FO of the sea-level pressure anomalies from the 20th to the 21st centuries and for each season are presented in **Figure 15**. These changes represent f_i in Eq. (1), and when multiplied by the cluster-average moisture convergence x_i, represent the contribution of changing dynamics to total future change. The FO of circulation patterns on the left side of the master SOM, featuring dominant low pressure over the central Arctic, are projected to increase in all seasons, particularly in summer and fall. Patterns in the upper right corner, characterized by low pressure anomalies in the N. Atlantic extending northeastward into the Arctic along with high pressure over the western Arctic, occur more frequently in the spring and winter. Clusters positioned in the middle of the SOM with weak or moderate high pressure over Arctic become less common in the late 21st century. Significant decreases in these clusters are most pronounced in the summer, but the general decrease occurs in all seasons. These changes have important implications for the moisture convergence.

Changes in moisture convergence in the CCSM3 from the 20th to late 21st centuries for each season are shown in **Figure 16**. Histograms on the left (right) are for the central Arctic (North Atlantic). Portions of the total seasonal change that are due to dynamic, thermodynamic, and combined terms in Eq. (1) are also shown.

In the central Arctic the largest changes in total moisture convergence occur in summer (57%). This is consistent with Skific et al. (2009), who found that the largest projected increases in northward moisture flux by the late 21st century will occur in summer, corresponding to highest increases in moisture content in the warmest season. The increase in spring moisture convergence accounts for about 24% of the total change. Autumn and winter changes are the smallest, contributing about 13% and 6%. In all seasons, the thermodynamic contribution plays a major role in governing moisture convergence changes and is most pronounced in the spring and summer, accounting for about 87% of the total change. In spring and summer, dynamics is the second largest term, contributing about 13% and 8% to a total change, while the combined factor only contributes about 4.2% and -0.3%. In fall the contribution of thermodynamics to the total change is smaller but still dominant at about 47%, followed by the combined factor (31%) and the dynamic factor (22%). In winter the largest change in moisture convergence occurs through combined dynamic-thermodynamic influences, accounting for about 53% of the total change. The thermodynamic factor is the second largest, contributing 34% to the total change, while the dynamic factor accounts for about 13%. An increased frequency and/or more northward penetration of storms in the future could account for the combined term being largest.

In the North Atlantic (**Fig. 16**, right), the largest changes in the late 21st century moisture convergence are projected to occur in winter, accounting for about 44 % of the total change. Autumn, spring, and summer contribute about 25%, 22%, and 9%, respectively. The North Atlantic sector receives most precipitation in winter when the gradients are strong and the winter storm track associated with Icelandic low is

pronounced. The individual contributions from various factors to the total winter increase in moisture convergence indicate that the winter increase is driven primarily by changes in thermodynamics, which account for about 89% of the total change, along with smaller contributions by dynamics (5%) and the combined term (6%). These results suggest that the pronounced increase in winter moisture convergence is not due to an increase in the FO of the Icelandic low pattern, but rather due to changes in the moisture content of the atmosphere, which leads to changes in the moisture convergence forced by a particular circulation pattern in winter. Thermodynamics play the primary role in governing changes in moisture convergence in the North Atlantic in the spring and autumn (115% and 83%) as well, although dynamic changes are also important in autumn (38%).

Differences in the FO between the 20th and 21st century may shed some light as to why the changes in these two regions occur. In fall there is a significant increase in frequency of occurrence of clusters along the left side of the master SOM (**Fig. 15**, lower left), along with a noticeable but statistically insignificant increase of clusters to the right. Both the clusters in the lower left (with dominant low pressure anomalies in the central Arctic, **Fig. 4**), and those in the lower right (clusters with a dominant Icelandic low in the Atlantic sector) favor increased moisture convergence in the North Atlantic (**Fig. 11**, upper right). During both fall and spring, the contribution of the combined term to the total change in moisture convergence in the North Atlantic is negative. This arises because the combined term is derived by multiplying the difference in the cluster-averaged FO (**Fig. 15**) by the difference in the cluster-averaged moisture convergence (**Fig. 17**), i.e., f_i x_i. The negative f_i values in the upper left, middle, and lower middle clusters of **Fig. 15** have a strong influence on the N. Atlantic combined factor during

spring. The sign of the combined factor in spring is mostly determined by the spring difference in FO (**Fig.15**, upper left), as the change in the cluster-averaged moisture convergence for that season is mostly positive (**Fig. 17**, upper left). The negative contribution by the combined factor during fall arises mainly from the preponderance of decreasing FO in all clusters except along the far right and left of the SOM. These central clusters represent transitional surface pressure patterns, which tend to occur in late summer and fall. In summer the total increase in moisture convergence in the N. Atlantic is the smallest. This tendency is governed by changes in the FO of precipitation events owing to a weakened storm track, which in summer shifts more northward into the Arctic basin. **Figure 15** (upper right) reveals that there is a strong, statistically significant increase in the FO of clusters in the bottom left of the SOM, which have low-pressure anomalies over the central Arctic (**Fig. 4**) characteristic of summer conditions (**Fig. 5**). These are also the clusters that favor increased moisture convergence in the N. Atlantic (**Fig. 11**, upper right).

The dynamic contribution explains about 85% of the total summer moisture increase in the N. Atlantic in the late 21st century. Only 15% of the total change in the summer in this region is due to thermodynamic changes, and the combined term is neglectable. In contrast to the central Arctic, thermodynamics plays a secondary role in governing changes in moisture convergence in the N. Atlantic summer. It is likely that by the end of the 21st century the portion of precipitation in N. Atlantic derived from evaporation would increase. More frequent occurrence of storms could also increase the evaporation by intensifying the surface mixing, which could also explain the negative sign of the combined term. It is also likely that some of the surface-evaporated moisture

in N. Atlantic summer is advected northward, into the central Arctic where it would contribute to regional net precipitation increase. This eventuality is likely cause by highest increases in Arctic moisture transport in the summer season in this model run (Skific et al. 2009). In addition, N. Atlantic is the main pathway of moisture into the Arctic (Serreze and Barry 2005).

5.6. Summary and conclusions

Better understanding of future global climate change will require not only improved model simulations, but also a more system-oriented, interdisciplinary approach (Serreze and Barry 2005). This study demonstrates that if today's trends in greenhouse-gas emissions continue the Arctic will likely experience large changes in the hydrologic cycle. By the late 21st century of the SRES A2 scenario, a simulation by the CCSM3 projects that annual-mean moisture convergence into the Arctic, or equivalently net precipitation, will increase by about 20%, with over 85% of that increase being attributed to changes in thermodynamic factors such as increased precipitable water and a strengthening of the poleward moisture gradient. This conclusion is consistent with previous studies by Cassano et al. (2007), Emori and Brown (2005), and Finnis et al. (2007). This study expands on previous research by investigating the roles of thermodynamic and dynamic influences on moisture convergence regionally within the Arctic and during the four seasons.

Dynamic influences on net precipitation, owing to changing frequency of particular circulation patterns, are more pronounced in the Atlantic sector than in the

Pacific sector of the Arctic. Changes in the model's moisture content of the Arctic atmosphere result from enhanced transport across the 70°N latitude circle, which appear to be linked with anthropogenic greenhouse gas increases (Skific et al., 2009).

Net precipitation in the central Arctic will increase by about 40 mm yr^{-1} (16%), with the largest change occurring in summer, and to a lesser extent in spring. Thermodynamic factors are the primary driver in both seasons. As the Arctic continues to warm, it is likely that this region will experience a more frequent occurrence of rain rather than snow, particularly during summer, which will exacerbate the loss of sea ice, permafrost, and low-elevation land ice. Consequently, not only will the added water vapor in the atmosphere enhance the greenhouse effect in the Arctic (Francis and Hunter 2007), an increase in liquid precipitation will also act as yet another positive feedback to the system to augment Arctic and global warming.

Net precipitation in the North Atlantic region, in contrast to the central Arctic, will increase more in non-summer months, with largest increases in winter of about 55 mm yr^{-1} (18%). Thermodynamic effects are again the primary contribution, but changing dynamics play a larger role than in the central Arctic. For example, the CCSM3 projects an increased frequency in patterns characterized by a strong cyclonic feature near Iceland, which tends to enhance precipitation in the N. Atlantic region. While the net precipitation change in summer is small, results suggests that both precipitation and evaporation increase, and that some of that additional moisture will likely be advected northward, contributing to the thermodynamic increase in net precipitation in the central Arctic.

Because the Arctic is characterized by a variety of climate interactions and feedbacks resulting from a sensitive balance between the atmosphere, ocean, cryosphere and biosphere, future increases in net precipitation could affect this balance in profound ways. Also, because changes in the Arctic will likely affect the global climate, predicting future changes in Arctic hydrology is essential for understanding both the magnitude and quality of change in the entire system.

References

Alexander, M., J. Yin, G. Branstator, A. Capotondi, C. Cassou, R.Cullather, Y. Kwon, J. Norris, J. Scott, I. Wainer, 2006: Extratropical Atmosphere-Ocean variability in CCSM3. *Journal of Climate*, **19**, 2496-2525.

Ammann, C. M., G. A. Meehl, W. M. Washington, and C. S. Zender, 2003: A monthly and latitudinally varying volcanic forcing dataset in simulations of 20th century climate. *Geophys. Res. Lett.,* **30**, 1657, doi:10.1029/2003GL016875.

Arctic Climate Impact Assessment (ACIA), 2004: Impacts of a Warming Arctic. Cambridge University Press , New York, New York.

Armstrong, R., M.J. Brodzik, and A. Varani, 1997: The NSIDC EASE-Grid: Addressing the need for a common, flexible, mapping and gridding scheme. *Earth System Monitor*, **7**, 3 pp.

Betts, R. A., 2000: Offset of the potential sink from boreal forestation by decreases in surface albedo. *Nature.,* **408**, 187–190.

Bromwich, D.H., S.H. Wang, and A.J. Monaghan, 2002: ERA-40 representation of the Arctic atmospheric moisture budget. *Proceedings of the ECMWF Workshop on Re-analysis*, Reading, U.K, ERA-40 Project Report Series, #3, 287-298.

Cassano, J.J., P. Uotila, & A Lynch, 2006. Changes in synoptic weather patterns in the polar regions in the 20th and 21st centuries. Part 1: Arctic. *International Journal of Climatology*, **26**, 1027-1049.

_____, P. Uotilla, A.H. Lynch, and E.N. Cassano, 2007: Predicted changes in synoptic forcing of net precipitation in large Arctic river basins during the 21st century. *J. Geoph. Res.*, **112**, G04S49, doi:10.1029/2006JG000332.

Chapin, F. S. III, M. Sturm, M. C. Serreze, J. P. McFadden, J. R. Key, A. H. Lloyd, A. D. McGuire, T. S. Rupp, A. H. Lynch, J. P. Schimel, J. Beringer, W. L. Chapman, H. E. Epstein, E. S. Euskirchen, L. D. Hinzman, G. Jia, C.L. Ping, K. D. Tape, C. D. C. Thompson, D. A. Walker, and J. M. Welker, 2005: Role of land-surface changes in Arctic summer warming. *Science.*, **310**, 657-660.

Chapman, W.L., and J. E. Walsh, 2007: Simulations of Arctic surface temperature and sea-level pressure by global coupled models. *J.Climate*, **20**, 609-632.

Cherry, J.E., L.B. Tremblay, M. Stieglitz, G. Gong, and S. Déry, 2007: Development of the pan- Arctic snowfall reconstruction: new land-based solid precipitation estimates for 1940-1999. *Journal of Hydrometeorology.*, **8**, 1243-1263.

Cullather, R.I., D.H. Bromwich, and M.C. Serreze, 2000: The atmospheric hydrologic cycle over the Arctic basin from reanalyses, Part I: Comparisons with observations and previous studies, *J. Climate*, **13**, 923-937.

Emori, S. and S.J. Brown, 2005: Dynamic and thermodynamic changes in mean and extreme precipitation under changed climate. *Geophy. Res. Lett,* **32**, L17706.

Finnis, J., J. Cassano, M. Holland, M. Serreze, and P. Uotilla, 2008a: Synoptically Forced Hydroclimatology of Major Arctic Watersheds in General Circulation Models, Part 1: the Mackenzie River Basin. *Int. J. Climatology*, in press.

————, J., J. Cassano, M. Holland, M. Serreze, and P. Uotilla, 2008b: Synoptically Forced Hydroclimatology of Major Arctic Watersheds in General Circulation Models, Part 2: Eurasian Drainage. *Int. J. Climatology,* in press.

————, M. Holland, M.C. Serreze, and J.J. Cassano, 2007: Response of Northern Hemisphere extratropical cyclone activity and associated precipitation to climate change, as represented by CCSM3. $J. Geoph. Res.$, **112**, G04S42, doi:10.1029/2006JG000286.

Francis, J.A. and E. Hunter, 2007: Changes in the fabric of the Arctic's greenhouse blanket. *Environ. Res. Lett.,* **2**, doi:10.1088/1748-9326/2/4/045011.

Groves, D., and J.A. Francis, 2002: Moisture budget of the Arctic atmosphere from TOVS satellite data. *J. Geoph. Res.,* **107**, 11-21.

Hack, J.J., J.M. Caron, S.G. Yeager, K.W. Oleson, M.M. Holland, J.E. Truesdale, and P.J. Rasch, 2006: Simulation of the global hydrological cycle in the CCSM Community Atmospheric Model, Version 3 (CAM3): Mean features. *J. Climate*, **19**, 2199-2221.

Hewitson, B.C., and R.G. Crane, 2002: Self-organizing maps: applications to synoptic climatology. *Clim. Res*., **22**, 13-26.

Kohonen, T., 2001:*Self-organizing maps*. 3d ed. Springer-Verlag, 501 pp.

Kiehl, J., T. Schneider, R. Portmann, and S. Solomon, 1999: Climate forcing due to tropospheric and stratospheric ozone. *J. Geophys. Res.*, **104**, 31239-31254.

Lawrence, D.M. and A.G. Slater, 2005: A projection of severe near-surface permafrost degradation during the 21st century. *Geoph. Res. Lett.*, **32**, L24401, doi:10.1029/2005GL025080.

Lean, J., Y.-M. Wang, and N. R. Sheeley Jr., 2002: The effect of increasing solar activity on the sun's total and open magnetic flux during multiple cycles: Implications for solar forcing of climate. *Geophys. Res. Lett.,* **29**, 2224, doi:10.1029/2002GL015880.

Manabe, S., and R. J. Stouffer, 1997: Coupled ocean-atmosphere model response to freshwater input: Comparison to Younger Dryas event. *Paleoceanography.,* **12(5),** 321-336.

_____, and _____, 1995: Simulation of abrupt climate change induced by freshwater input to the North Atlantic Ocean. *Nature.,* **378**, 165-167.

_____, and _____, 1994: Multiple-century response of a coupled ocean-atmosphere model to an increase of atmospheric carbon dioxide. *Journal of Climate.,* **7(1)**, 5-23.

_____, R. J. Stouffer, M. J. Spelman, and K. Bryan, 1991: Transient responses of a coupled ocean-atmosphere model to gradual changes of atmospheric CO_2. Part I: Annual mean response. *Journal of Climate.,* **4(8)**, 785-818.

Mekis, É. and W. D. Hogg, 1999: Rehabilitation and Analysis of Canadian Daily Precipitation Time Series. *Atmosphere-Ocean.,* **37(1),** 53-85.

Min, S. K., X. Zhang, and F. Zwiers, 2008: Human-induced Arctic moistening. *Science.,* **320**, 518-520.

Nakicemovic, N. and R. Swart, 2000: Intergovernmental Panel on Climate Change Special Report on Emission Scenarios. Cambridge University Press, 570 pp.

Pielke, R., T. Wigley, and C. Green, 2008: Dangerous assumptions. *Nature,* **452**, 531-532.

Rahmstorf, S., A. Cazenave, J.A. Church, J.A. Hansen, R.F. Keeling, D.E. Parker, and R.J. Somerville, 2007: Recent climate observations compared to projections. *Science.,* **316**, 709.

Reed, R.J., and B.A. Kunkel, 1960: The Arctic circulation in the summer. *J.Meteorology*, **17**, 489-506.

Reusch, D.B., R. Alley and B.C. Hewitson, 2005: Relative performance of self-organizing maps and principal component analysis in pattern. Extraction from synthetic climatologic. *Polar Geography*, **29,** 188-212.

Serreze, M., and J.A. Francis, 2006: The Arctic on the fast track of change. *Weather., 61*, 3.

_____, A. P. Barrett, A. G. Slater, R. A. Woodgate, K. Aagaard, R. B. Lammers, M. Steele, R. Moritz, M. Meredith, and C. M. Lee, 2006: The large-scale freshwater cycle of the Arctic. *Journal of Geophysical Research,* **111(C11),** doi:10.1029/2005JC003424.

_____, A.P. Barrett, and F. Lo, 2005: Northern high-latitude precipitation as depicted by atmospheric reanalyses and satellite retrievals. *Mon. Wea. Rev*., **133**, 3407- 3430.

_____, and R.G. Barry, 2005: *The Arctic Climate System.* Cambridge University Press. 385 pp.

Skific, N., J.A. Francis, and J.J. Cassano, 2009: Projected changes in atmospheric moisture transport in the Arctic and its links to general circulation: a self-organizing map perspective. *J. of Climate.,* accepted.

Smith, S.J., H. and T.M.L Wigley, 2001: Global and regional anthropogenic sulfur dioxide emissions. *Global and Planetary Change*., **29**, 99-119.

Smith, S.J., H. Pitcher, and T.M.L. Wigley, 2005: Future sulfur dioxide emissions. *Climatic Change*., **73(3),** 267–318.

Uppala, S.M. and coauthors, 2005: The ERA-40 reanalysis. *Quart. J. Royal. Met. Soc*., **131**, 2961-3012.

Yang, D., 1999: An improved precipitation climatology for the arctic ocean. *Geophys. Res. Lett*., **26**, 1625–1628.

Yang, D., and T. Ohata, 2001: A bias corrected Siberian regional precipitation climatology. *J. Hydrometeorol*., **2**, 122–139.

Table 1.

REGION	ERA-40 (cm/mo)	CCSM3 (cm/mo)
CENTRAL ARCTIC	1.76	2.06
NORTH ATLANTIC	3.81	**2.59**
BARENTS SEA	1.34	1.30
KARA SEA	2.41	2.17
LAPTEV SEA	1.56	1.84
EAST SIBERIAN SEA	1.42	**1.97**
CHUKCHI SEA	1.15	**2.42**
BEAUFORT SEA	1.28	**2.41**

Table 1: Annual mean moisture convergence (cm mo^{-1}) averaged for various regions in the Arctic during the 20th century from ERA-40 and CCSM3. Model values that are significantly larger or smaller than those from ERA-40 at the 95% confidence level are bold.

Table 2.

REGION	SPRING (MAM)		SUMMER (JJA)		AUTUMN (SON)		WINTER (DJF)	
	ERA-40	CCSM	ERA-40	CCSM	ERA-40	CCSM	ERA-40	CCSM
CENTRAL ARCTIC	1.20	1.91	2.63	2.61	1.84	2.11	1.20	1.59
NORTH ATLANTIC	2.88	2.36	3.99	**2.83**	4.77	**2.90**	3.64	**2.23**
BARENTS SEA	1.10	**1.78**	2.00	2.04	1.54	1.43	0.70	**-0.07**
KARA SEA	2.16	2.47	3.07	**2.35**	2.50	1.95	1.96	1.98
LAPTEV SEA	1.26	1.76	2.54	2.45	1.52	1.79	0.91	1.35
EAST SIBERIAN SEA	0.95	**1.86**	2.09	2.41	1.56	1.89	1.06	**1.70**
CHUKCHI SEA	0.86	**2.06**	1.84	**2.93**	0.65	**2.05**	1.25	**2.59**
BEAUFORT SEA	0.85	**2.06**	2.18	**3.04**	1.07	**2.62**	0.83	**2.51**

Table 2: Seasonal mean moisture convergence (cm mo^{-1}) averaged for various regions in the Arctic from ERA-40 and CCSM3 during the late 20th century. Model values significantly larger or smaller than that of ERA-40 at the 95% confidence level are indicated with bold type.
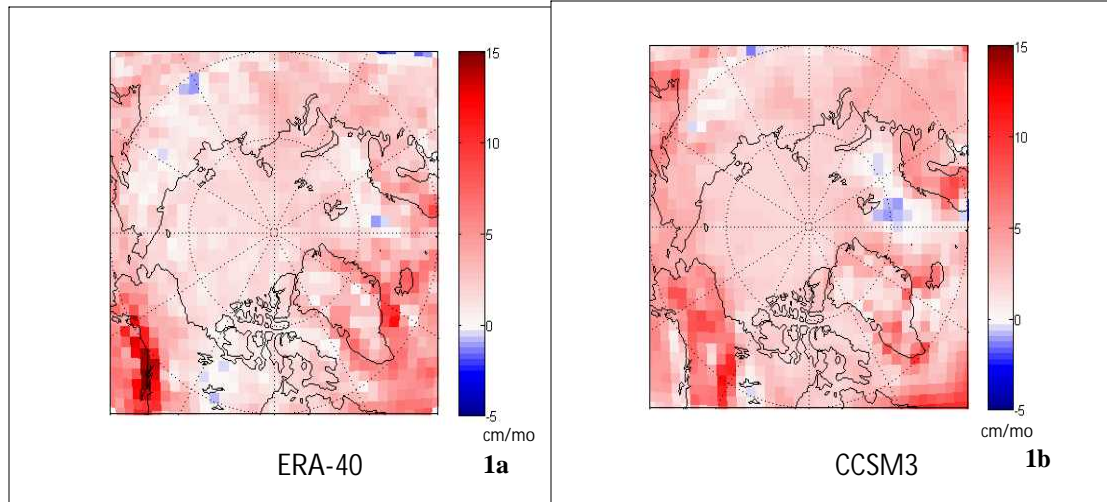
Figure 1: Long-term annual mean moisture convergence (cm mo^{-1}) for the 20th century from (**a**) ERA-40 and (**b**) CCSM3.
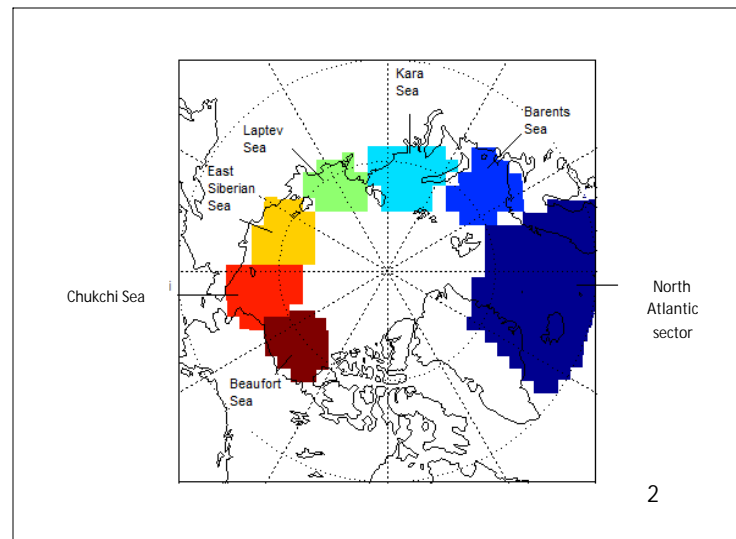
Figure 2: Arctic regions analyzed in this study. The central Arctic is defined as the area north of 75°N.
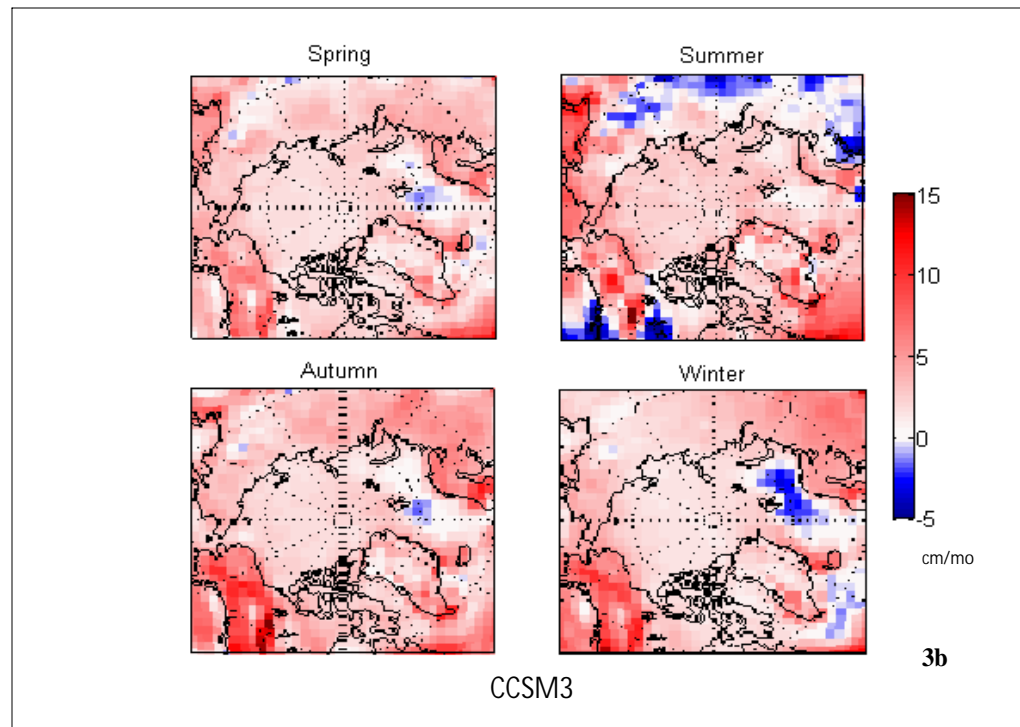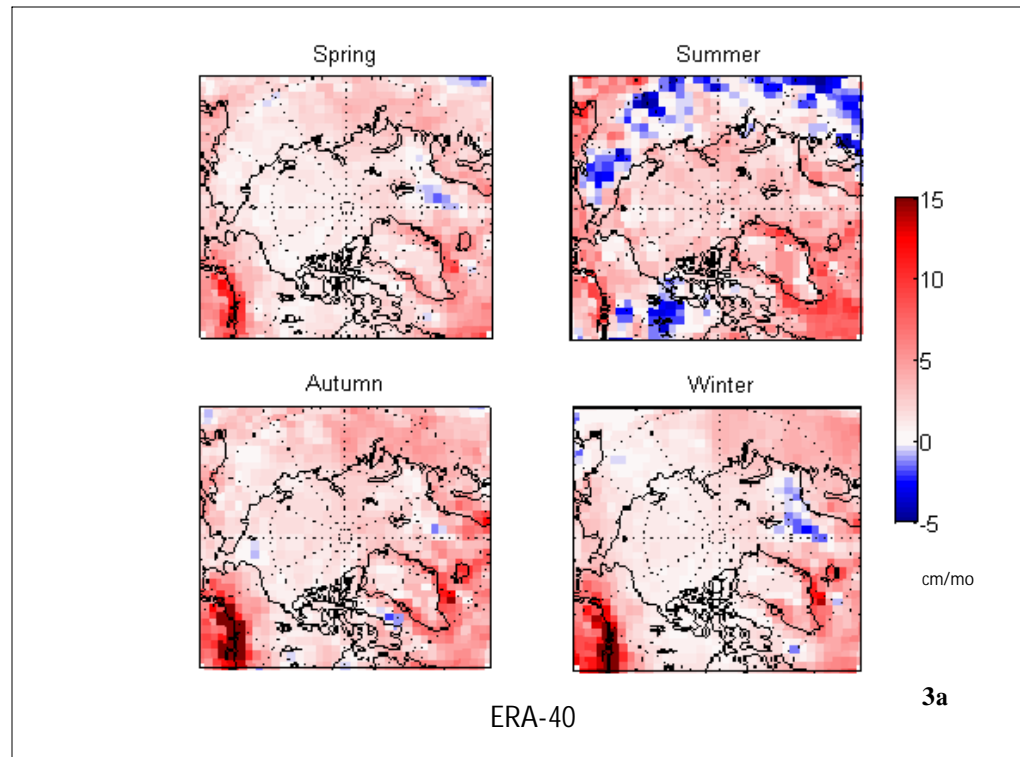
Figure 3: Seasonal mean moisture convergence (cm mo⁻¹) for the 20th century during spring (MAM), summer (JJA), autumn (SON) and winter (DJF); (a) ERA-40 and (b) CCSM3.
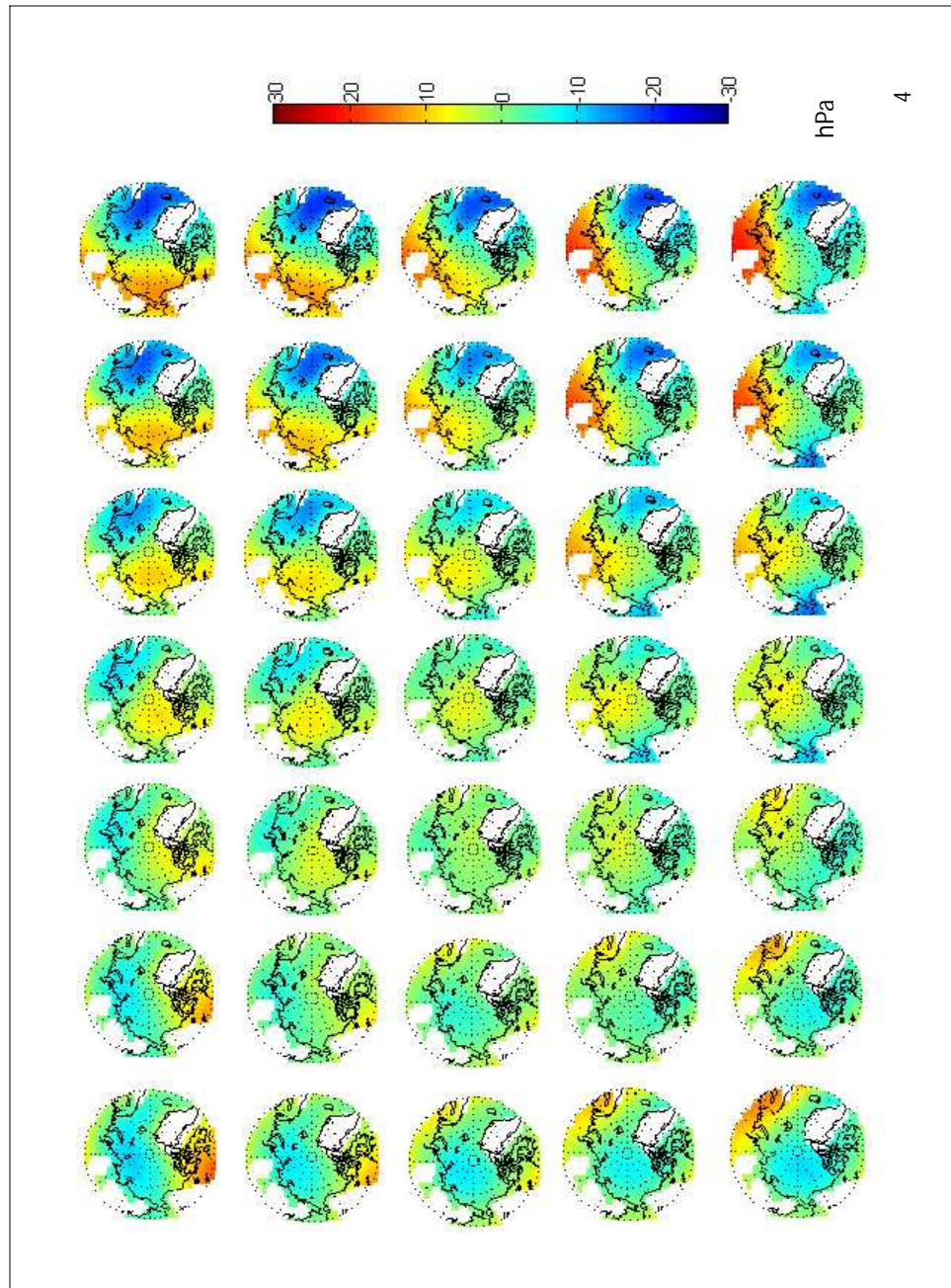
Figure 4: Master SOM of sea level pressure patterns (hPa) derived from daily SLP anomaly fields from CCSM3 (1960-1999, 2010-2030, and 2070-2089), and from ERA-40 (1958-2001).
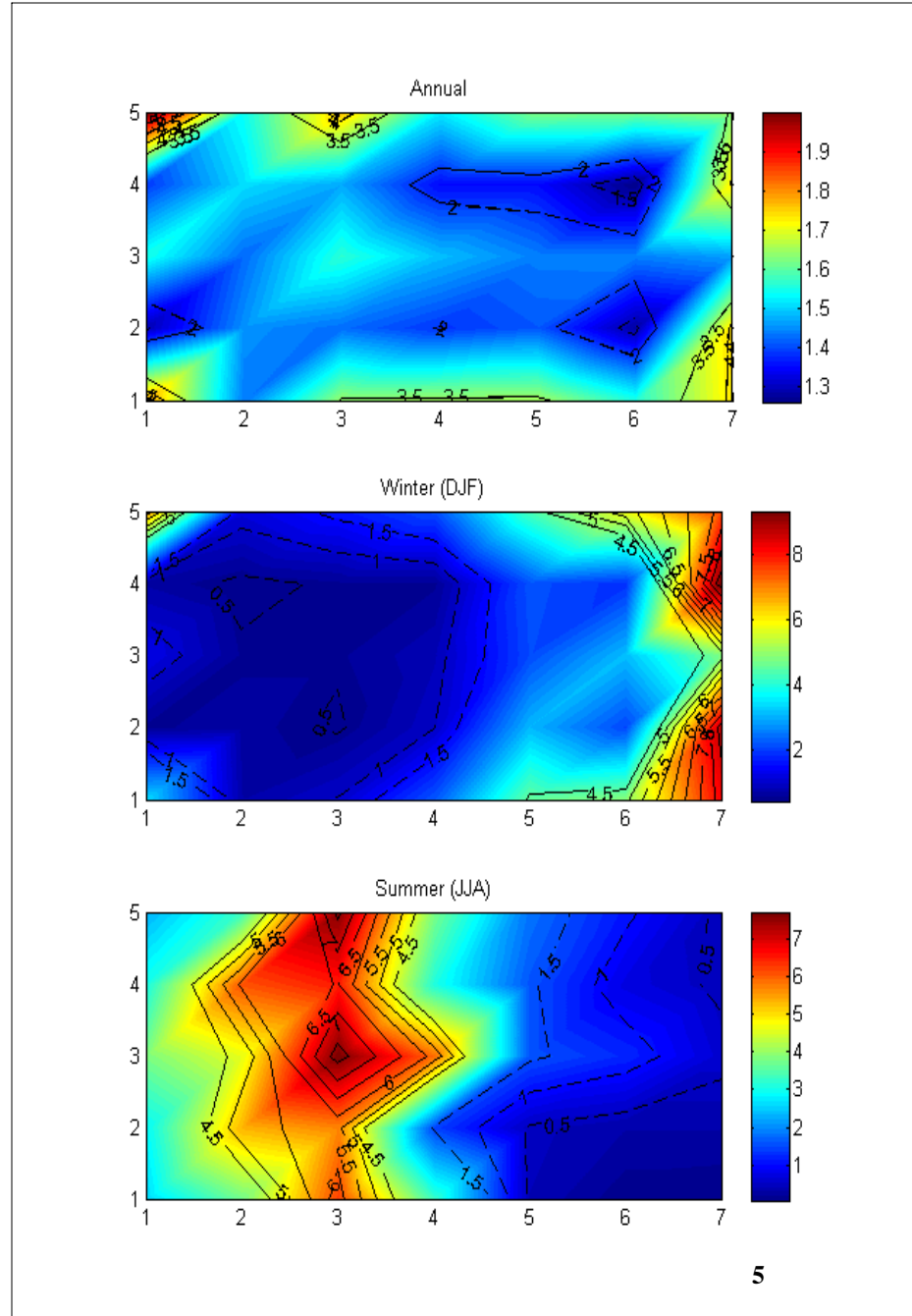
Figure 5: Frequency of occurrence of CCSM3 daily sea-level pressure anomaly maps during the 20th century **(top)**, winter **(DJF, middle),** and summer **(JJA, bottom).** Frequencies represent the percent of days out of the total number of daily fields that map to a particular SOM node. Black solid (dashed) lines indicate frequencies that are significantly higher (lower) than the expected value for the random binomial distribution with a confidence level of at least 95%.

Figure 6: Moisture convergence anomaly fields (cm mo^{-1}) from the CCSM3 20th century corresponding to SLP clusters in Figure 4.
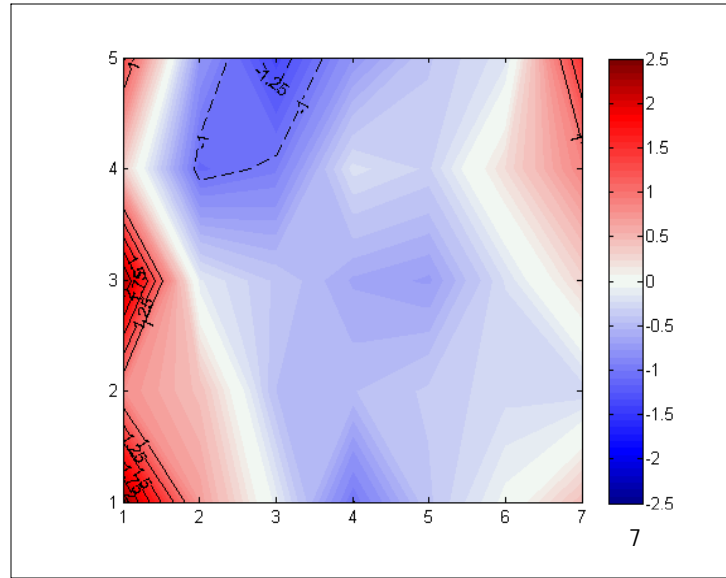
Figure 7: Difference in frequency of occurrence of the CCSM3 sea-level pressure anomalies between the late 21st century (2070-2089) and the 20th century (1960-1999). Black solid (dashed) lines indicate differences that are significantly higher (lower) with a confidence level above 95%.
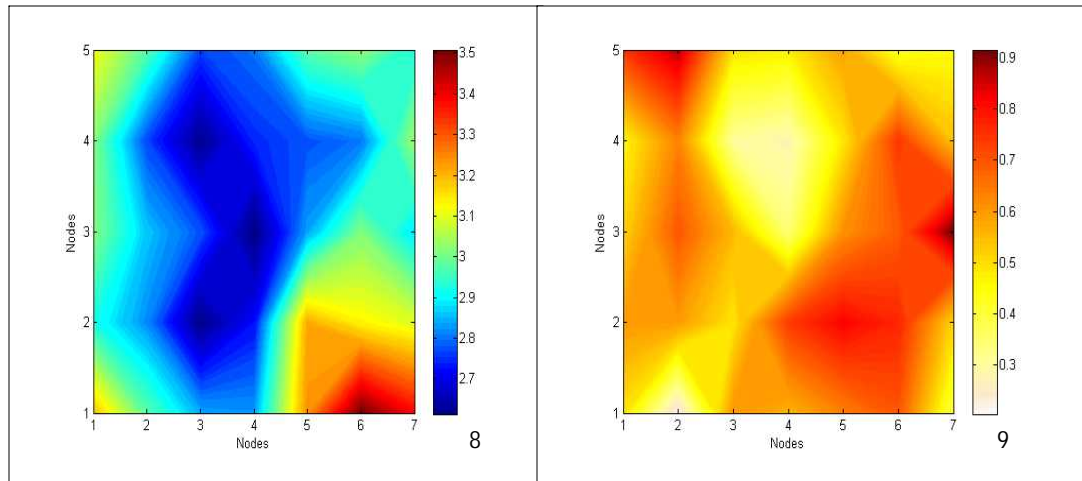
Figure 8: Contours of cluster-averaged moisture convergence (cm mo^{-1}) for the 20th century from CCSM3, averaged for the pan-Arctic region (north of 60°N).

Figure 9: Differences in the cluster-averaged moisture convergence (cm mo^{-1}) between the late 21st century (2070-2089) and the 20th century (1960-1999) from CCSM3, pan-Arctic region (north of 60°N).
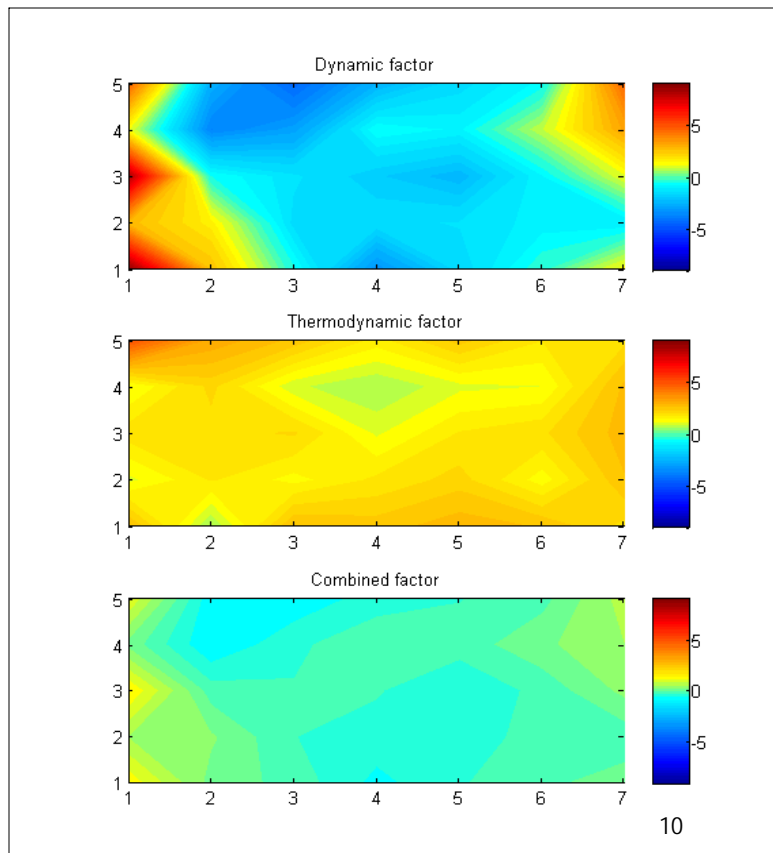
Figure 10: Dynamic (**top**), thermodynamic (**middle**) and combined dynamic and thermodynamic (**bottom**) contributions to the difference in moisture convergence [mm yr^{-1}] in each cluster, between 2070-2089 and 1960-1999, for CCSM3, pan-Arctic region (north of 60°N).
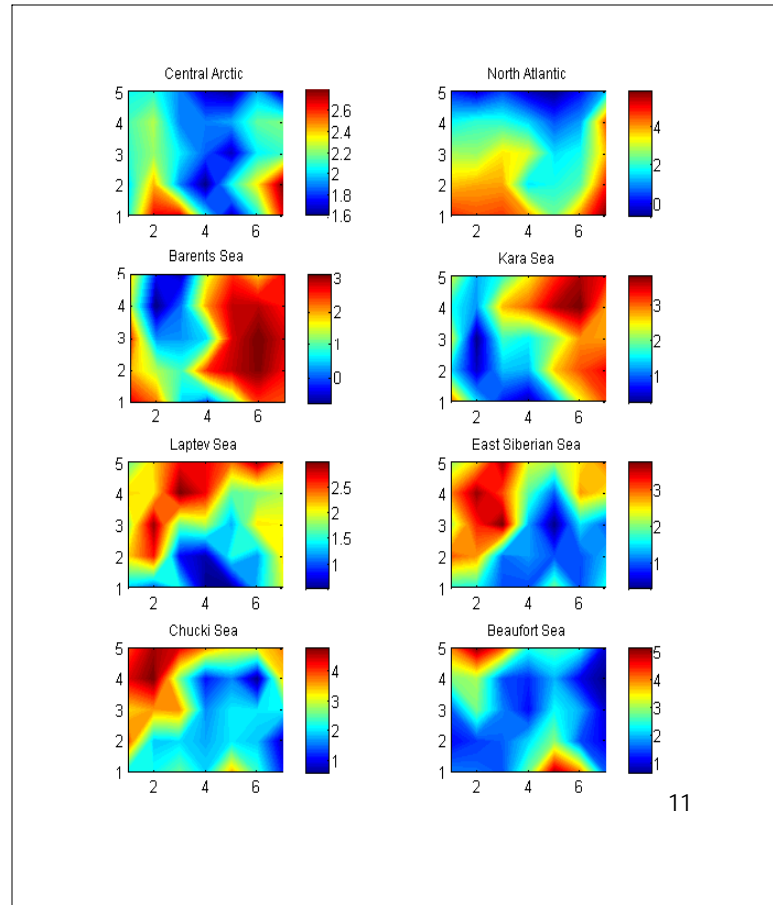
Figure 11: Contours of cluster-averaged moisture convergence (cm mo^{-1}) for the 20th century (1960-1999) from CCSM3 in the various regions of the Arctic shown in Fig. 3.
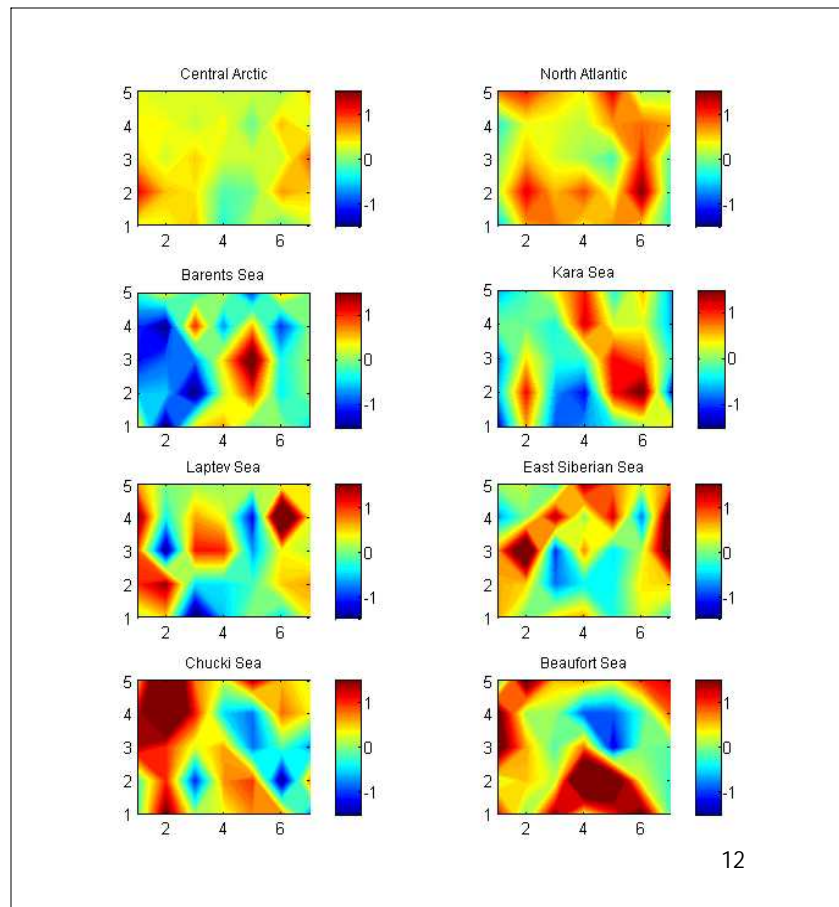
Figure 12: Differences in the regional cluster-averaged moisture convergence (cm mo⁻¹) from the 20th century (1960-1999) to the late 21st century (2070-2089) in CCSM3.
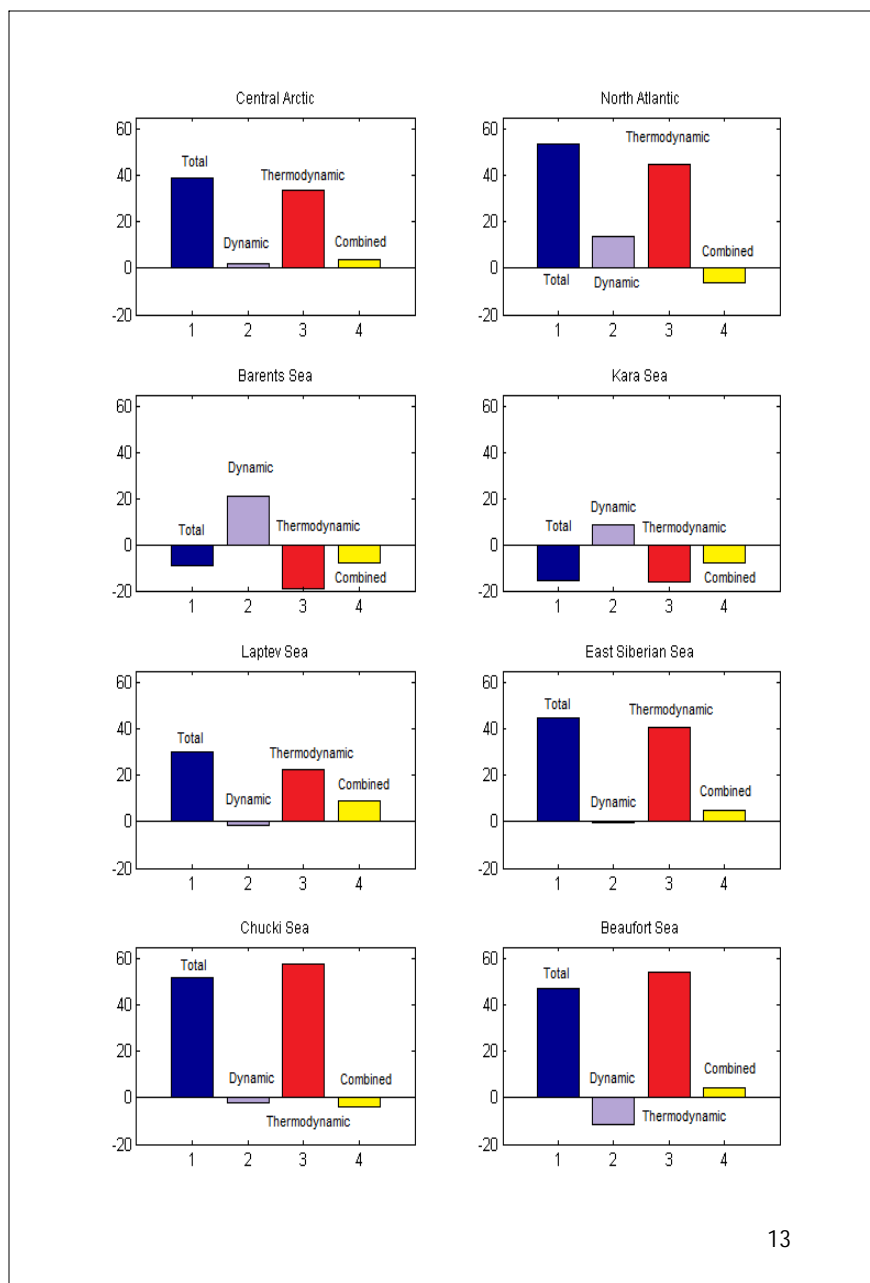
Figure 13: Total change (blue) in regional moisture convergence (mm yr^{-1}) in the CCSM3 from the 20th century (1960-1999) to the late 21st century (2070-2089). Contributions to the total change are also displayed: dynamic (gray), thermodynamic (red), and combined term (yellow).
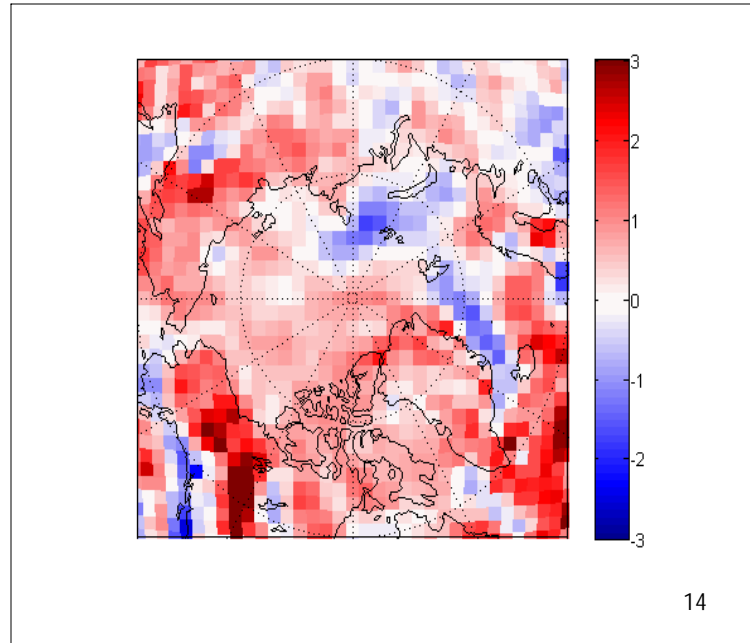
Figure 14: Difference in annual-mean moisture convergence (cm mo^{-1}) from the 20th century (1960-1999) to the late 21st century (2070-2089) in CCSM3.

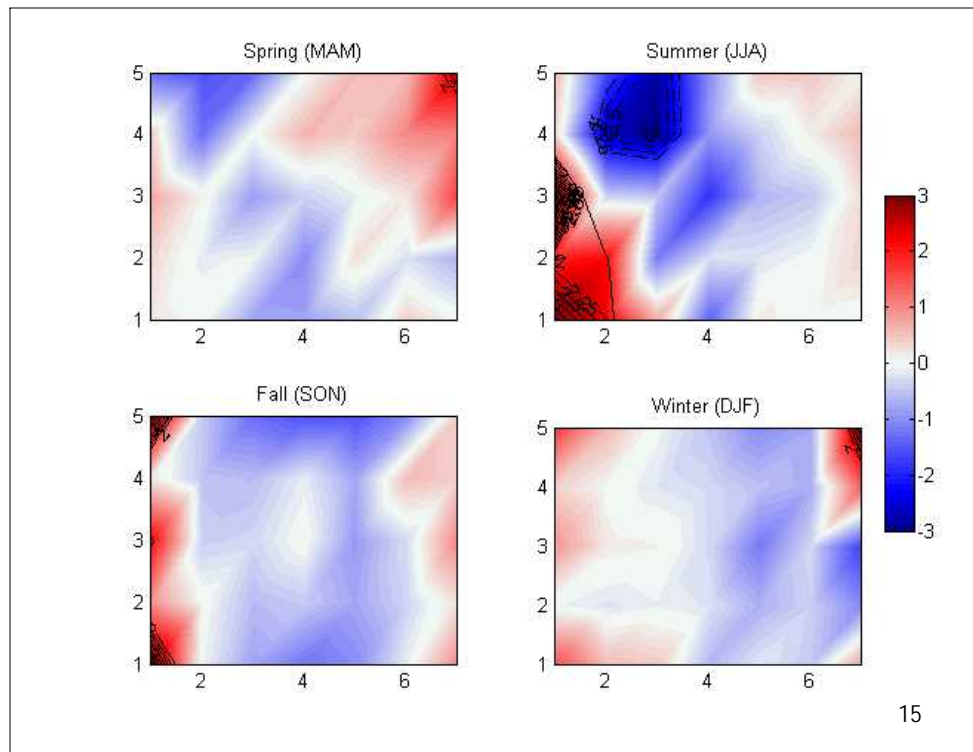**Figure 15**: Seasonal differences in frequency of occurrence of sea-level pressure anomalies from the 20th century (1960-1999),to the late 21st century (2070-2089) in CCSM3: spring (MAM, upper left), summer (JJA, upper right), fall (SON, lower left) and winter (DJF, lower right). Black solid (dashed) lines indicate differences in frequencies of occurrence that are significantly higher (lower) at the 95% confidence level.
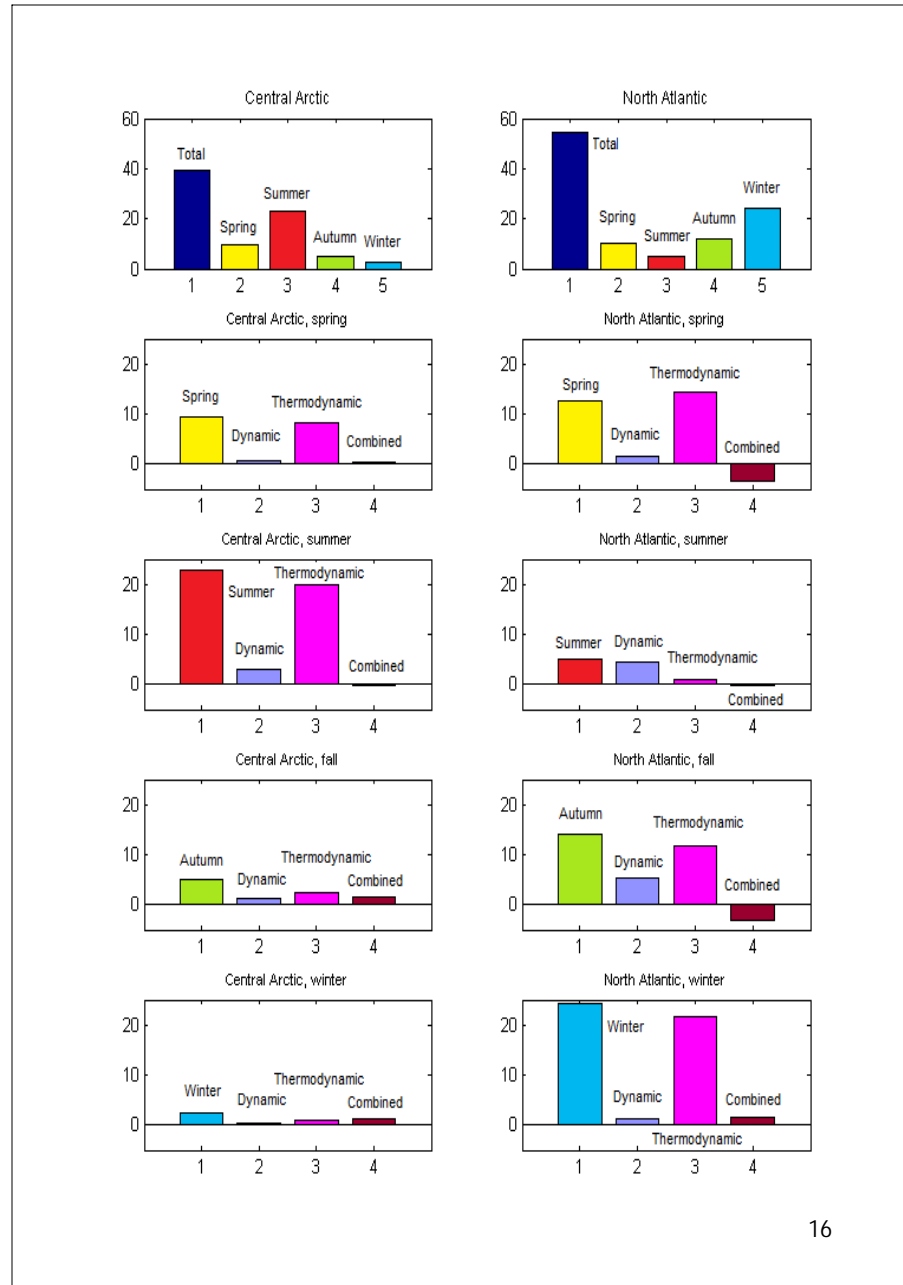
Figure 16: Total change in moisture convergence (mm yr^{-1}) from the 20th century (1960-1999),to the late 21st century (2070-2089) in CCSM3 (dark blue bar), and the portions of the change occurring in each season (MAM, yellow; JJA, red; SON, green; DJF, blue) for the central Arctic (left) and north Atlantic (right). For each season, contributions to the total change by dynamics (gray), thermodynamic (magenta), and combined term (dark red) are also shown.
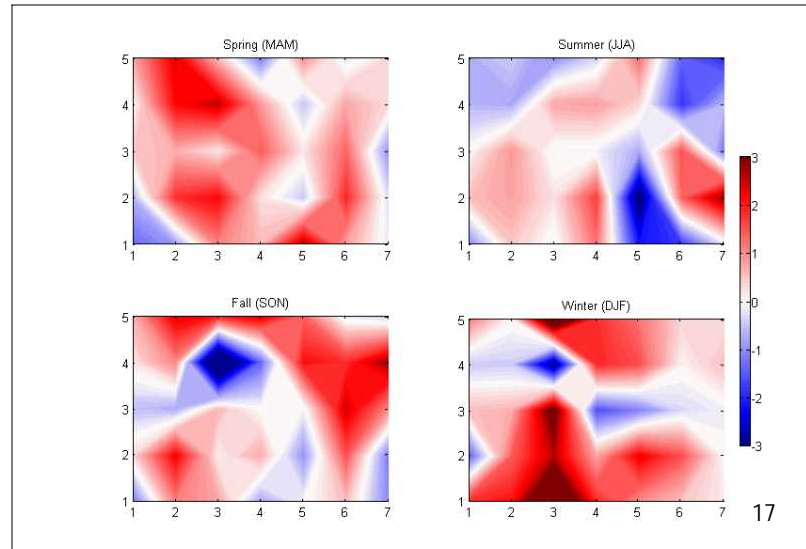
Figure 17: Seasonal differences in the North Atlantic cluster-averaged moisture convergence (cm mo^{-1}) from the 20th century (1960-1999), to the late 21st century (2070-2089) in CCSM3.

Conclusions

The focus of this study is to explore changes in physical processes that represent potential drivers of Arctic climate change. If one thinks of the Arctic as a container with the top at the top the atmosphere, bottom at the surface, and side defined by an imaginary wall at 70^oN, observations reveal that approximately 98% of the energy supplied to the container comes from the transport across the wall from lower latitudes. This energy, in addition to the small fraction from the surface on annual average, is lost to space in the form of infrared radiation (Nakamura and Oort, 1988). Observations and model simulations show that the Arctic responds sensitively to perturbations in the global climate system. Recent decades of warming on the global scale (approximately 1 degree Celsius since 1900) have been substantially larger in the Arctic (about 4^oC). As the Arctic warms more than the mid-latitudes of the northern hemisphere, an intuitive expectation would be that poleward transport of heat would decrease. Concurrent with changes in temperature, however, are changes in the atmospheric water vapor content and the transport of that moisture. Until now, it has been unclear whether the transport of latent energy, in the form of water vapor, would be large enough to offset the reduction in heat transport. This unanswered question forms the hypothesis for the research presented in this dissertation: *Future changes in the poleward transport of latent energy will be larger than the reduction in sensible heat transport, thus changes in total energy transport into the Arctic will augment the amplified warming at high northern latitudes.*

Regional and seasonal changes in Arctic poleward moist static energy and net precipitation, as well as the mechanisms responsible for the changes, are presented

through a conceptually appealing neural-network technique called self organizing maps, introduced in Cassano et al. (2007). Given the rapid changes in the Arctic climate system during recent decades, combined with uncertainties associated with many climate feedbacks related to the reduction of snow cover and permanent ice forms, this technique offers a valuable contribution toward understanding the relative attribution to changing atmospheric circulation patterns, as well as the associated energy transport and net precipitation. The major difference between the SOM and the traditional clustering algorithms is the fact that not only the best matching centroid, but also all its neighbors are adjusted toward the input data sample. Because of this updating scheme, the resulting clusters become organized on a 2-dimensional array in such a way that more similar clusters are placed closer together, while those less similar are farther apart, allowing a more intuitive interpretation of patterns and their relationship to each other in the matrix. State-of-the-art global climate-system models, such as the CCSM3 model used in this study, are a valuable tool for assessing future changes in high latitudes.

According to this model run, moist static energy transport into high latitudes is projected to increase by about 1.6% from its 20th century value over the next 100 years. This is driven mainly by an increase in latent heat flux of about 20%, which responds to an increased poleward moisture gradient. Dry static energy decreases by about 3.5% by the end of the 21st century, in connection to a decreased poleward temperature gradient. The response of individual components of energy to poleward gradients is revealed by domination of changes in thermodynamic factors, which reflect changes in eddy transports of energy. These eddies, or travelling disturbances, form as the system attempts to establish thermodynamic equilibrium in a perturbed climate. The largest

increases (decreases) in poleward energy transport are projected to occur in the summer (winter), as these two seasons exhibit opposite behavior in terms of projected changes in the fluxes of DSE and LH. The summer increase in moist static energy arises from a large increase in the poleward moisture gradient during warm months combined with a weaker Arctic amplification, which also leads to weaker DSE because ocean surface temperatures are fixed near the melting point. During winter the LH increases as the poleward moisture gradient increases in response to strong Arctic amplification, along with a smaller decline in the DSE. An increase in energy transport due to dynamics, related to more frequent occurrence of high latitude cyclones, is positive in all seasons, but plays a secondary role.

Moisture convergence in most high-latitude regions is projected to increase between 15-20%. The Kara and Barents Seas are the only regions in which evaporation would likely exceed precipitation by the end of the 21st century owing to large losses of the summer ice cover in these areas. Increased moisture convergence is mainly governed by thermodynamics, which explains over 70% of the total change in the Arctic. Changes in dynamics contribute to increased moisture convergence in the eastern Arctic and a decrease in the western Arctic. The thermodynamic response of moisture convergence involves increased moisture content of the atmosphere. Precipitating weather systems feed on the moisture that already exists in the atmosphere, mostly through convergence of moisture in the lower and middle troposphere in the vicinity of these disturbances. Therefore, it is expected that the seasons in which these systems are most vigorous, or most effective in precipitating, are seasons in which the increase in moisture convergence

is expected to be most pronounced. This likely explains the resulting largest increases in moisture convergence in the central Arctic (North Atlantic) to occur in summer (winter).

Several important aspects of the hydrologic response to warming in the Arctic region are a direct consequence of the increase in lower-tropospheric water vapor. One such response, as revealed from the analysis of the CCSM3 presented in this study, is an increase in poleward energy transport, governed by an increase in poleward latent heat transport. Reduction of dry static energy compensates for about 70% of the increase in latent heat transport in the troposphere. This is consistent with Held and Soden (2006), who analyze various model ensembles using the A1B or "middle of the road" scenario and find that reductions in the sensible heat transport in high latitudes is driven mostly by a reduction in eddy transport.

One can speculate how the poleward energy transport may change once all the summer (permanent) ice is lost. For example, a much larger increase in poleward energy transport may occur in response to a weaker Arctic amplification, analogous to the differences we see between the present-day summer and winter seasons. Graversen et al. (2009) show, however, that Arctic amplification continues even when the ice-albedo feedback is held constant in a model simulation. In their study, the polar amplification is only 15% stronger when the ice-albedo feedback is included. They explain that polar amplification occurs not only because of the direct changes in albedo as the ice cover declines, but also because of indirect effects of warming in the lower levels of the troposphere, such as increased water vapor content, and cloud changes.

Another response to an increase in atmospheric moisture content in the Arctic is an increase in net precipitation. This study finds that by the late 21st century net

precipitation is expected to increase by about 16%, which will likely affect high-latitude vegetation, watershed ecosystems, and marine productivity near river mouths in the Arctic Ocean. The increase in net precipitation would also likely affect the Arctic energy balance through its effect on surface albedo. The sign of that change will largely depend on the season and the type of precipitation. However, some recent studies (Lambert et al. 2008; Wentz et al. 2007) reveal uncertainties related to precipitation changes projected by global climate models. These studies show that modeled precipitation increases (1-3% per degree of global temperature change) depart significantly from the observed rates (7% per K). This disparity is likely associated with aerosol and cloud changes that are not captured realistically in the models, pointing to a need for improved understanding and parameterizations for these processes. Moreover, if state-of-the-art models are generally underestimating changes in precipitation as the globe continues to warm, actual precipitation changes may be 2 or 3 times larger than expected (Lambert et al. 2008). This would have serious consequences not only for the Arctic region, but for the entire global climate system, as fluctuations in freshwater availability directly affects agriculture, water resources, and consequently the global economy. In addition, substantial changes in net precipitation would also call for new adaptation strategies and faster implementation of new technology to ensure people are well prepared and their property protected in case of extreme events.

A far greater source of concern regarding climate model projections stems from the fact that SRES emission scenarios may have severely underestimated future greenhouse gas emissions (Pielke et al. 2008). These authors describe China's carbon-dioxide emissions alone to be rising at a rate between 11 to13% per year for the period

2000-2010, which is far higher than that assumed by the "worst-case" SRES scenario for Asian emissions (2.6 to 4.8% per year). From that perspective, future climate changes projected by the present climate models may be only a "mild" version of what lies ahead.

References:

Arctic Climate Impact Assessment, ACIA, 2004: Impacts of a Warming Arctic: Arctic Climate Impact Assessment. Cambridge University Press.

Alexeev, V.A., P.L. Langen, and J.R. Bates, 2005: Polar amplification of surface warming on an aquaplanet in "ghost forcing" experiments without sea ice feedbacks. *Clim. Dynamics*, **24,**655-666.

Bengtsson, L., V.A. Semenov, and O.M. Johannessen, 2004: The early twentieth-century warming in the Arctic – a possible mechanism. *J. Clim.,* **17,** 4045–4057.

Cassano, J.J, P. Uotilla, A.H. Lynch, E.N. Cassano, 2007: Predicted changes in Synoptic Forcing of Net Precipitation in Large Arctic River basins During the 21st century, *J. Geoph. Res- Biogeosciences*, **112**, G04S49, doi:10.1029/2006JG000332.

Chapin, F. S. III, M. Sturm, M. C. Serreze, J. P. McFadden, J. R. Key, A. H. Lloyd, A. D. McGuire, T. S. Rupp, A. H. Lynch, J. P. Schimel, J. Beringer, W. L. Chapman, H. E. Epstein, E. S. Euskirchen, L. D. Hinzman, G. Jia, C.L. Ping, K. D. Tape, C. D. C. Thompson, D. A. Walker, and J. M. Welker, 2005: Role of land-surface changes in Arctic summer warming. *Science.*, **310**, 657-660.

Church, J. A., and N. J. White, 2006): A 20th century acceleration in global sea-level rise, *Geophys. Res. Lett.*, **33,** L01602, doi:10.1029/2005GL024826.

Clark, P.U., S.J. Marshall, G.K. Clarke et al., 2001: Freshwater forcing of abrupt climate change during the last glaciations. Science, **293**, 283-287.

Clark, P.U., N.G. Pisias, T.F. Stocker, and A.J. Weaver, 2002: The role of the thermohaline circulation in abrupt climate change. *Nature,* **415**, 863-869.

Curry, J. A., J.E. Schramm, E.E. and Ebert, 1995: On the ice albedo climate feedback mechanism. *J. Clim.,* **8**, 240-247.

Garrett, T. J. and C. Zhao, 2006: Increased Arctic cloud longwave emissivity associated with pollution from mid-latitudes. *Nature*, **440**, 787-789.

Graversen, R.G., and M. Wang, 2009: Polar amplification in a coupled climate model with a locked albedo. *Clim. Dynamics*, accepted.

Graversen, R.G., T. Mauritsen, M. Tjernström, E. Källen and G. Svennson, 2008: Vertical structure of recent Arctic warming. *Nature*, **451**, 53-56.

Grenfell, T. C., and D.K. Perovich, 2004: Seasonal and spatial evolution of albedo in a snow-ice-land- ocean environment. *J. Geophys. Res.*, **109** (C01001), doi: 10.1029/2003JC001866

Hartmann, D.L., 1994: *Global Physical Climatology*. Academic Press, 409 pp.

Held, I. M., and B. J. Soden, 2006: Robust responses of the hydrological cycle to global warming. *Journal of Climate,* **19(21),** 5686-5699.

Hoerling, M.P., J.W. Hurrell, T. Xu, T.G. Bates, and A. Phyllips, 2004: Twentieth century North Atlantic climate change. Part II: Understanding the effect of Indian Ocean warming. *Clim. Dynamics*, **23**, 391-405.

Hurrell, J.W., Y. Kushnir, G. Ottersen, and M. Visbeck, 2003: An overview of the North Atlantic Oscillation. *The North Atlantic Oscillation: Climatic Significance and Environmental Impact,* J.W. Hurrell, Y. Kushnir, G. Ottesen and M. Visbeck, Eds., *Geophysical Monograph Series*, 1-36.

Intergovernmental Panel on Climate Change, 2007: Climate Change 2007: The Physical Science Basis. Contribution of Working Group I to the Fourth Assessment Report of the Intergovernmental Panel on Climate Change [Solomon, S., D. Qin, M. Manning, Z. Chen, M. Marquis, K.B. Averyt, M. Tignor and H.L. Miller (eds.)]. Cambridge University Press, Cambridge, United Kingdom and New York, NY, USA, 996 pp.

Johanessen, O. M., L. Bengtsson, M.W. Miles, S.I. Kuzmina, V.A. Semenov, G.V. Aledseev, A.P. Nagumyi, V.F. Zakharov, L.P. Bobylev, L.H. Pettersson , K. Hasselmann, and H.P. Cattle, 2004: Arctic climate change: observed and modelled temperature and sea-ice variability. *Tellus,* **56A**, 328–341.

Lambert, F. H., A.R. Stine, N.Y. Krakauer, and J.C.H. Chiang, 2008: How much will precipitation increase with global warming?, *EOS, Transactions, American Geophysical Union*, **89**, 193-194.

Lawrence, D.M. and A.G. Slater, 2005: A projection of severe near-surface permafrost degradation during the 21st century. *Geoph. Res. Lett.*, **32**, L24401, doi:10.1029/2005GL025080.

Manabe, S., R. J. Stouffer, M. J. Spelman, and K. Bryan, 1991: Transient responses of a coupled ocean-atmosphere model to gradual changes of atmospheric CO_2. Part I: Annual mean response. *Journal of Climate.,* **4(8)**, 785-818.

_____, and R. J. Stouffer, 1994: Multiple-century response of a coupled ocean-atmosphere model to an increase of atmospheric carbon dioxide. *Journal of Climate.,* **7(1)**, 5-23.

Meehl, G., and co-authors, 2007: Global Climate Projections. in Solomon, S.; D. Qin; M. Manning; Z. Chen; M. Marquis; K.B. Averyt; M. Tignor and H.L. Miller. Climate Change 2007: The Physical Science Basis. Contribution of Working Group I to the Fourth Assessment Report of the Intergovernmental Panel on Climate Change. Cambridge, United Kingdom and New York, NY; USA: Cambridge University Press.

Min, S. K., X. Zhang, and F. Zwiers, 2008: Human-induced Arctic moistening. *Science.*, **320**, 518-520.

Nakamura, N. and A.H. Oort, 1988: Atmospheric heat budgets of the polar regions. *J. Geophys. Res.,* **93**, 9510-9524.

Overland, J.E., P. Turet, and A.H. Oort, 1996: Regional variations of moist static energy flux in the Arctic. *J. Climate*, **9**(1), 54-65.

Pielke, R., T. Wigley, and C. Green, 2008: Dangerous assumptions. *Nature,* **452**, 531-532.

Rahmstorf, S., A. Cazenave, J.A. Church, J.A. Hansen, R.F. Keeling, D.E. Parker, and R.J. Somerville, 2007: Recent climate observations compared to projections. *Science.*, **316**, 709.

Randall, W. *et al.*, 2007: Climate Models and their Evaluation. in Solomon, S.; D. Qin; M. Manning; Z. Chen; M. Marquis; K.B. Averyt; M. Tignor and H.L. Miller. Climate Change 2007: The Physical Science Basis. Contribution of Working Group I to the Fourth Assessment Report of the Intergovernmental Panel on Climate Change. Cambridge, United Kingdom and New York, NY; USA: Cambridge University Press.

Schweiger, A. J., 2004: Changes in seasonal cloud cover over the Arctic seas from satellite and surface observations. *Geophy. Res. Lett,* **31**, L 1 2 207, doi:10.1029/2004GL020067.

Serreze, M.C., and R.G. Barry, 2005: *The Arctic Climate System.* Cambridge University Press, 146 pp.

_____, and J.A. Francis, 2006: The Arctic on the fast track of change. *Weather.,* **61**, 3.

Skific, N., J.A. Francis, and J.J. Cassano, 2008: Attribution of seasonal and regional changes in Arctic moisture convergence. *J. of Climate.,* submitted.

Stouffer, R. J., and S. Manabe, 2003: Equilibrium response of thermohaline circulation to large changes in atmospheric CO_2 concentration. *Climate Dynamics*, **20(7/8)**, 759-773.

Sturm, M., C. Racine, and K. Tape, 2001: Climatic change: Increasing shrub abundance in the Arctic. *Nature,* **411**, 546-547.

Trenberth, K.E., and J.M. Caron, 2001: Estimates of meridional atmosphere and ocean heat transports. *J.Climate*, **15**, 3433-3443.

Wentz, F.J., L. Ricciardulli, K. Hilburn, and C. Mears, 2007: How much more rain will global warming bring?. *Science*, **317(5835),** 233-235.

Acknowledgement of Previous Publications

Curriculum Vitae

Natasa Skific

Education

September 1993- June 1998:   University of Natural Sciences and Mathematics; Zagreb, Croatia

B.S., Meteorology

September 2003- January 2006: Rutgers State University, New Brunswick, Graduate School- New Brunswick

M.S., Environmental Science

Work experience

April 2000- December 2002:   **Operational weather forecaster**, at the Department of Weather Analyses and Forecasting of the National Meteorological and Hydrological Service; Zagreb, Croatia

September 2003- May 2006:   **Research assistant**, at the Department of Environmental Sciences and Marine Sciences, Rutgers State University, New Brunswick, NJ.

September 2006- present: **Graduate assistant**, at the Department of Environmental Sciences and Marine Sciences, Rutgers State University, New Brunswick, NJ.

Publications:

1. Skific, N., J.A. Francis, and J.J. Cassano, 2009: Attribution of Projected Changes in Atmospheric Moisture Transport in the Arctic: A Self-Organizing Map Perspective, *Journal of Climate,* accepted.

2. Skific, N., J.A. Francis, and J.J. Cassano, 2009: Attribution of Seasonal and Regional Changes in Arctic Moisture Convergence, revised manuscript submitted to *Journal of Climate*.

3. Skific, N., and J.A. Francis: Changes of the Arctic moist static energy transport in the 21st century, in preparation.